NASA Technical Paper 1699

Crash Tests of Four Identical High-Wing Single-Engine Airplanes

Victor L. Vaughan, Jr., and Robert J. Hayduk

AUGUST 1980

NASA

NASA Technical Paper 1699

Crash Tests of Four Identical High-Wing Single-Engine Airplanes

Victor L. Vaughan, Jr., and Robert J. Hayduk
Langley Research Center
Hampton, Virginia

National Aeronautics
and Space Administration

**Scientific and Technical
Information Branch**

1980

SUMMARY

Four identical four-place, high-wing, single-engine airplane specimens with nominal masses of 1043 kg were crash tested at the Langley Impact Dynamics Research Facility under controlled free-flight conditions. These tests were conducted with nominal velocities of 25 m/sec along the flight path at various flight-path angles, ground-contact pitch angles, and roll angles. Three of the airplane specimens were crashed on a concrete surface; one was crashed on soil.

Crash tests revealed that on a hard landing, the main landing gear absorbed about twice the energy for which the gear was designed but sprang back, tending to tip the airplane up to its nose. On concrete surfaces, the airplane impacted and remained in the impact attitude. On soil, the airplane flipped over on its back. The crash impact on the nose of the airplane, whether on soil or concrete, caused massive structural crushing of the forward fuselage. The livable volume was maintained in both the hard-landing and the nose-down specimens but was not maintained in the roll-impact and nose-down-on-soil specimens. The pilot and copilot dummies impacted the instrument panel in the airplane specimens that lost cabin volume. Peak accelerations on the cabin floor were generally under -25g; for the nose-down-on-soil specimen, however, they were as high as -45g. The highest accelerations in the dummies' pelvises were in the normal direction and peaked as high as -65g in the nose-down-on-soil test. The dummies' heads that impacted the structure experienced accelerations as high as -60g, while non-impact accelerations were about -20g.

INTRODUCTION

With the rapid growth of private and commercial air traffic since World War II, increasing emphasis has been focused on the causes of passenger injuries and death in severe but potentially survivable crashes. The National Advisory Committee for Aeronautics (NACA) conducted a series of full-scale airplane crash tests with instrumented dummies in the 1950's (refs. 1 and 2). These tests were performed by accelerating the airplane along a horizontal guide rail and crashing it into an earthen mound. Later NACA studies on the dynamic response of seat structures to impact loads (ref. 3) resulted in a Civil Aeronautics Administration (CAA) update in static seat-strength requirements. The airplanes previously tested by NACA, however, were not structurally representative of current general-aviation airplanes.

In 1973, a general-aviation crash-test program was initiated jointly by the National Aeronautics and Space Administration (NASA) and the Federal Aviation Administration (FAA) (ref. 4). As part of this program, the NASA Langley Research Center has conducted a series of crash tests to obtain information on general-aviation airplane crashes under controlled free-flight conditions (refs. 5 to 8). Langley's studies are directed toward those crashes in which the airplane structure retains sufficient cabin volume and integrity for occupant survivability. The objectives of the studies are to determine the dynamic

response of the airplane structures, seats, and occupants during a simulated crash; to determine the effect of flight parameters at impact (i.e., flight speed, flight-path angle, pitch angle, roll angle, and ground condition) on the magnitude and pattern of structural damage; to determine the failure modes of the seats and occupant restraint systems; and to determine the loads imposed upon the occupants. This information is essential for predicting structural collapse and for designing safer seats, occupant restraint systems, and cabin structures.

The present tests were conducted to obtain a data base of crash information for four-place, high-wing, single-engine airplanes. This report describes the results of four airplane crash tests. Each airplane had a gross mass of 1043 kg and was impacted at a nominal flight-path velocity of 25 m/sec at various flight-path angles, ground-contact pitch angles, and roll angles. Three of the airplanes were crashed on a concrete surface and one on soil. The pilot and copilot were represented by anthropomorphic dummies. Effects of the flight parameters at impact are discussed in terms of structural damage, accelerations of the airplane structure and occupants, and loads in the passenger restraint system. These data can be used to assess future analytical predictions of stresses, strains, and motions of structural components and seat/occupant behavior. A motion-picture film supplement of these tests is available on loan. A request card form and a description of the film are given at the back of this paper.

TEST FACILITY AND PROCEDURES

Facility

The crash tests were performed at the Langley Impact Dynamics Research Facility shown in figure 1. The gantry is composed of truss elements arranged with three sets of inclined legs to give vertical and lateral support and another set of inclined legs to provide longitudinal support. The gantry is 73 m high and 122 m long. The supporting legs are spread 81 m apart at the ground and 20 m apart at the 66-m level. An enclosed elevator and a stairway provide access to the overhead work platforms, and catwalks permit safe traverse of the upper levels of the gantry. A movable bridge spans the gantry at the 66-m level and traverses the length of the gantry. Shown in figure 2 is a sketch of a full-scale airplane specimen suspended from the gantry in the position ready to be swung onto the impact surface. The reinforced concrete impact surface permits tests to be repeated and allows comparison between tests. A soil test bed approximately 12.1 m wide, 24.4 m long, and 1.2 m deep was placed on the concrete impact surface for one test. The test bed simulated a plowed field; that is, it was sufficiently firm to support a light tractor with pneumatic tires and soft enough for the aircraft to sink into the soil during the crash (ref. 9). Detailed information about the facilities used to carry out a successful aircraft crash test is reported in reference 10.

Crash-Test Technique

The test technique used to crash the airplane specimens is shown schematically in figure 3. The airplane specimen, suspended by two swing cables

attached to the top of the gantry, is drawn back and above the impact surface by a pullback cable to a height of about 49 m. The test sequence begins when the airplane specimen is released from the pullback cable. The airplane specimen swings pendulum style onto the impact surface. The swing cables are pyrotechnically separated from the airplane specimen when the airplane is about 1 m above the impact surface in order to free it from restraint during the crash impact. The umbilical cable remains attached during the impact for data acquisition and is pyrotechnically separated about 0.75 sec after swing-cable separation, which occurs about 1/2 sec after ground contact.

Airplane specimen attitude at impact can be adjusted prior to testing by changing the length of the cables in the suspension system. Adjustments up to about 30° can be made in angle of attack and roll angle. Only small adjustments can be made in yaw angle because of the small clearance between the pullback harness and empennage of the airplane. Additional yaw can be added by removing the stabilizers and simulating them with concentrated masses.

Airplane Suspension System

The airplane suspension system used to control the swing and impact attitude of this airplane specimen is shown in figure 4. The flight variables at impact, defined in figure 5, are flight-path angle γ, angle of attack α, pitch angle $\theta = \gamma + \alpha$, roll angle ϕ, and yaw angle ψ. The swing and pullback cables connect to the swing and pullback harnesses. The swing harness consists of two swing-cable extensions which attach to the wing hard points to support the airplane specimen and to control roll angle. There are two sets of pitch cables that connect to the swing-cable rings and to fuselage hard points fore and aft of the airplane center of gravity to control the angle of attack. The interaction of all cables in the harness system is involved in yaw control. The pullback harness consists of a pair of cables attached to the wing hard points, a pair of cables attached to the landing-gear struts, and a bar which spreads the cables to clear the airplane fuselage and empennage. The pullback cable attached to this harness is used to pull the airplane to the height necessary to produce the desired velocity at impact. An umbilical cable links the onboard instrumentation to a data-acquisition system located in a building adjacent to the gantry.

Test Parameters

The flight-path angles and attitude angles for the airplanes are identified in figure 5, along with the reference axes. Positive force directions coincide with the reference axes. The actual test parameters for the four tests reported here, along with photographs illustrating the impact attitude for each airplane test specimen, are presented in figure 6. For consistency and brevity, each test and airplane specimen will hereafter be identified by word descriptions (i.e., hard-landing, roll impact, nose-down impact, and nose-down-on-soil impact) for impact positions shown in figures 6(a) to 6(d) respectively. Detailed descriptions of these impact conditions are given in the individual "Results and Discussion" sections. The nominal flight-path velocity was 25 m/sec, which is approximately the stall speed for an airplane of this type.

The dynamics of the swing system caused the airplane to pitch around its own center of gravity after cable separation. However, this was a small effect and results in less than 1° of pitch variation at impact for all test conditions.

Airplane Test Specimen

Airplane specimens used for the tests were identical single-engine, high-wing, general-aviation airplanes having a nominal mass of 1043 kg with a capacity for four occupants (see fig. 7). The four airplane specimens were complete except for the upholstery and empennage. The mass and center of gravity of the empennage were simulated by two concentrated masses representing the fin-rudder and stabilizer-elevator combinations. The fuel tanks were filled with water to simulate the fuel mass. Spoilers were attached to the wings to minimize the aerodynamic lift. The exterior and interior of the airplane specimens were painted to enhance the photographic contrast, and black lines were painted over rivet lines to delineate the underlying structure.

The four airplanes carried the same basic equipment necessary for the tests. Anthropomorphic dummies, each with a mass of 102 kg, occupied the pilot's and copilot's seats (fig. 8). The seats were standard equipment for an airplane of this type. The restraint systems were standard for the pilot and copilot; they consisted of lap belts fastened to the airplane floor and single shoulder harnesses attached between the top of the fuselage and the lap belt. The passenger compartment (figs. 9, 10, and 11) contained additional equipment which brought the weight up to 1043 kg.

Instrumentation and Data Preparation

Onboard instrumentation for obtaining data pertaining to the dynamic behavior of the airplane structure, seats, and dummies consisted of dc accelerometers, high-speed motion-picture cameras, and load cells. Figure 10 shows a camera viewing the cabin from the rear of the luggage compartment. Figure 11 shows a camera mounted at the wing-spar junction which views the pilot through the port doorway (door removed). Figure 12 shows a camera mounted in the instrument panel for viewing the pilot and copilot dummies through a fish-eye lens.

External motion-picture coverage of the crash sequence at various film speeds was provided by tracking and fixed cameras located to the port side, front, back, and overhead of the test specimen (fig. 2). To obtain the horizontal velocity of the test specimen at impact, a Doppler radar unit was placed on the impact surface, approximately 60 m aft of the impact point, and the signal was recorded on one channel of an FM tape recorder.

The locations of the accelerometers onboard the airplanes are shown in figure 13. The accelerometers were oriented along the normal (Z), longitudinal (X), and transverse (Y) axes, as shown in figure 5. Each location is designated by its grid coordinates as follows: the first number indicates the longitudinal coordinate; the first letter indicates the normal coordinate (floor to roof); the second number indicates the transverse coordinate; and the second letter

indicates the accelerometer orientation with respect to the airplane body-axis system. For example, the normal accelerometer location on the floor nearest the pilot on the port side of the fuselage is designated 2D8N. The normal, longitudinal, and transverse orientations are designated as N, L, and T, respectively. The accelerometer locations and their orientation in the dummies are given in the table in figure 13. The orientations of the accelerometers are given in the dummy's body-axis system, and the locations are given in the airplane grid coordinate system.

Data signals were transmitted from the specimen through an umbilical cable to a junction box on top of the gantry, then through hardwire to the control room where they were recorded on FM tape recorders (fig. 2). To correlate the data signals on the FM recorders with the external motion-picture camera data, a time code was recorded simultaneously on the magnetic tape and on the film. There was also a time pulse generator onboard the airplane for the onboard cameras.

The raw data from the FM tape recorders were digitized and filtered with a 20-Hz digital filter to remove the higher frequencies that resulted from local structural vibrations. Calibration information was used to convert the results to engineering units from which acceleration curves were plotted. The analysis of the acceleration histories and the loads include time-event correlation from the corresponding motion-picture crash scenes, and these time events are superimposed on the data curves.

RESULTS AND DISCUSSION OF HARD-LANDING TEST

Crash Dynamics

A photographic sequence (fig. 14) illustrates the crash dynamics of the airplane test specimen during a simulated hard landing starting at initial ground contact. The airplane specimen contacted the concrete impact surface on the starboard landing gear with a velocity of 22.7 m/sec along a flight-path angle of -17° and at a pitch angle of 13.5°, a roll angle of 3.5°, and a yaw angle of -11.5°. The sink velocity of this airplane test was 6.64 m/sec, which is about twice the design sink velocity. The port landing gear contacted the impact surface 0.027 sec after initial ground contact, at which time the airplane had a pitch angle of 14.25°. At 0.037 sec into the impact, the nose gear contacted the impact surface, resulting in total collapse of the gear at 0.10 sec, while the airplane remained at a constant 13.25° pitch-up angle. The main landing gear reached its greatest deflection at 0.118 sec with the fuselage undersurface parallel with the impact surface. The spring steel landing gear started to spring back, imparting a forward (nose-down) pitching moment to the airplane which resulted in a -28.75° pitch attitude of the airplane with the collapsed nose gear in ground contact. The airplane then settled back onto its main landing gear as the airplane pitched up, deflecting the main gear and once again imparting a spring back that lifted the airplane off the impact surface in a nearly level attitude. It then settled onto the main gear and collapsed nose gear and rolled to a stop about 80 m from touch down. The pilot and copilot dummies remained relatively motionless during the impact.

Assessment of Damage

Postcrash photographs of the damage sustained by the airplane test specimen are presented in figure 15. The livable cabin volume (i.e., a volume sufficient in size to maintain space between the occupants and the structure) was maintained during the crash impact.

Figure 15(a) shows the airplane resting on the main landing gear, the collapsed nose gear, and the forward fuselage structure. There appeared to be little structural damage overall, and the occupants appeared to be sitting in a normal upright position in undamaged seats. A close-up view of the nose landing gear and the fuselage attachments are presented in figure 15(b). The composite wheel fairing was broken during impact. The lower attachment of the landing-gear strut was broken away from the fire wall and fuselage structure; the top attachment was torn away from the fire wall at the lower edge and rotated back into the fire wall at the top edge. During the impact, the wheel fairing rotated upward and damaged the engine air scoop.

The port main landing gear and wheel (fig. 15(b)) show a damaged brake disc caused by the disc contacting and scraping the concrete impact surface due to upward deflection of the main landing gear. An interior view of the control cable tunnel and fire wall inside the fuselage (fig. 15(c)) shows moderate damage in the form of buckling and a fracture as a result of lower fuselage and fire wall upheaval. Figure 15(d) presents a photograph showing wing-fuselage root damage in the form of panel buckling and fastener shear along the wing root. Both wings were damaged in the same manner as a result of the downward deflection of the wing during impact.

Acceleration Histories

The acceleration histories on the cabin floor and in the dummies as well as the loads in the restraint systems are presented in figure 16. The acceleration histories show that the main impulse lasted for about 0.12 sec as the main gear deflected to its fullest. The peak value of the normal acceleration on the cabin floor is about -5g, while the peak longitudinal accelerations are only about -2g. There was very little acceleration response due to the main gear spring back. The accelerations in the dummies' pelvic regions and heads (fig. 16(c)) were about ±10g maximum in both the normal and longitudinal directions. The loads experienced by the restraint harness system (fig. 16(d)) were extremely small, with the greatest level (600 N) occurring in the copilot's shoulder harness.

RESULTS AND DISCUSSION OF ROLL IMPACT TEST

Crash Dynamics

A photographic sequence (fig. 17) illustrates the crash dynamics of the airplane test specimen during a pitched-down, positive-roll (right wing down) crash starting at 0.022 sec before initial ground contact during the free-flight

stage after cable separation. The airplane specimen contacted the impact surface on the nose landing gear with a velocity of 25.9 m/sec along a flight-path angle of -34.5° and at a pitch angle of -39.0°, a roll angle of 18.6°, and a yaw angle of 3.2°. The nose gear started to collapse, and the engine cowling contacted the impact surface 0.028 sec after initial ground contact followed by the starboard wing tip at 0.035 sec. The windshield began to deflect and the fire wall started to penetrate the cabin at 0.06 sec. At the same time, the aft section of the fuselage began to deform and the starboard landing gear contacted the impact surface. The port landing gear contacted the impact surface at 0.13 sec into the impact, and the port wing immediately thereafter broke away from the fuselage at the aft spar and rotated forward around the front spar.

The approximate pitch attitude was retained during crash impact. At 0.15 sec, the aft cabin section pitched forward about 10° as a result of main landing-gear spring back. The airplane then settled back to about a 45° angle and continued to skid to a stop. The fuselage cabin remained at about the same pitch, roll, and yaw angles as the initial impact attitude.

The instrument panel began to move toward the occupants at 0.06 sec into the impact. The pilot dummy's head struck the instrument panel at about 0.11 sec followed by the head of the copilot dummy. The fuselage top caved in, causing the shoulder straps to go slack and allowing the occupants to move forward and rotate inside the harness as the seats came off the floor.

Assessment of Damage

Postcrash photographs of the damage sustained by the roll-impact airplane test specimen are presented in figure 18. The livable volume was not maintained during the crash impact.

Figure 18(a) shows the final resting position of the airplane and the overall structural damage viewed from the front. The slight S-shape of the fuselage (i.e., the nose to port of center line and the tail to starboard of center line) is apparent and resulted from the off-axis impact. The starboard wing is severely damaged near the tip where first wing contact occurred. The off-axis impact on the starboard wing and nose caused the port wing to break away from the fuselage. The impact was severe enough to buckle the starboard wing strut, which is a very stiff sructural element. Figure 18(b) again demonstrates the severity of the impact, since it shows the cabin top ripped apart. Encroachment of the fuselage, fire wall, and instrument panel section of the airplane into the cabin area and the reduced volume of the cabin due to folding of the structure is shown in figure 18(c), which is a view of the port side of the airplane. The off-axis impact is again apparent, as shown by the photograph in figure 18(d). The bottom leading edge of the door is against the impact surface, the door is folded outward, and the copilot and seat are resting in the deformed door. There was considerable loss of cabin volume on the starboard side of the fuselage. The interior view of the copilot's position (fig. 18(e)) shows the massive intrusion of the fuselage, fire wall, and instrument panel into the cabin. All seat legs are separated from the floor, and the floor-attached lap belt caused a severe binding of the dummy's pelvic region against the seat. The

control column and wheel are bent downward as a result of dummy impact. The slight indentation in the instrument panel in front of the copilot was caused when the dummy's head struck the panel.

Acceleration Histories

Time histories of the accelerations on the cabin floor and in the dummies and of the loads in the restraint systems are presented in figure 19. The normal, longitudinal, and transverse accelerations (figs. 19(a) and 19(b)) varied up to -20g except for the fire wall at the floor (0D8L). The fire wall contacted the impact surface and registered -35g at about the time structural penetration of the cabin began. The longitudinal accelerations extended over 0.10 sec, beginning about the time the engine cowling contacted the ground at 0.028 sec. The normal accelerations were somewhat delayed, did not start until cabin penetration had reached its maximum, and extended only over about 0.06 sec. The normal and transverse accelerations were also lower than the longitudinal acceleration, as would be expected because the airplane struck nose-on and stayed in that position during skidout. The airplane floor accelerations were low and resulted from the airplane structure absorbing much of the impact energy through structural crushing.

The greatest accelerations in the dummies occurred in the normal direction in the pilot's pelvis with about -40g. The dummy experienced higher accelerations than the floor, primarily because of the impact of the dummy with the instrument panel. All dummy accelerations started when cabin penetration started and peaked when the dummy came into full contact with the instrument panel. The longitudinal accelerations in the pelvic region were no more than -15g. The peak acceleration of 60g in the pilot's head occurred while the head was in contact with the instrument panel.

The loads experienced by the shoulder harnesses were considerably higher in the pilot (3400 N) than in the copilot (2000 N). The lap belts showed the same type of variation (2900 N to 2200 N). The shoulder harness loads peaked at the time the dummy impacted the instrument panel with the lap belt registering peak loads about 0.03 sec later. The higher loads in the pilot's restraint system may have occurred because the initial impact on the starboard side caused the copilot dummy to impact the structure first. The pilot dummy, therefore, had a longer time to develop loads in its restraint system before impact with the structure.

RESULTS AND DISCUSSION OF NOSE-DOWN IMPACT TEST

Crash Dynamics

A photographic sequence (fig. 20) illustrates the crash dynamics of the airplane test specimen during a negative-pitch (nose-down) crash starting at initial ground contact. The airplane contacted the concrete impact surface on the nose landing gear with a velocity of 24.7 m/sec along a flight path of -32°, a pitch angle of -30°, a roll angle of 7.5°, and a yaw angle of 0.7°. The fuselage nose contacted the impact surface 0.048 sec after initial ground contact.

There was a minor rebound; then the airplane slid to a stop in a pitch attitude of about -15°. The pilot and copilot dummies pitched forward but did not strike the instrument panel. The heads pivoted forward and downward and hit the control wheel.

Assessment of Damage

Postcrash photographs of the damage sustained by the nose-down test specimen are presented in figure 21. The livable volume was maintained during the crash impact in the pilot and copilot positions, but the volume maintained in the passengers' position was marginal.

Figure 21(a) shows the final position of the airplane and the overall structural damage. The slope of the lower section of the engine cowling is approximately the angle at which the airplane impacted the concrete. The major cabin damage was in the lower structure at the main landing-gear attachment, as shown in figure 21(b) and the close-up view in figure 21(c). This fuselage-buckling damage resulted from the combination of main landing-gear impact at a 30° angle and the downward inertia of the aft end of the fuselage. The interior damage occurred in the area of the passenger compartment with upheaval of the floor, as apparent in figure 21(d). The floor-mounted lap belt was very tight across the pelvic region of the dummy. The rear seat legs had separated from the rail, and the front legs were broken. These circumstances allowed the dummies to be thrown forward but not far enough to contact the instrument panel.

Acceleration Histories

Time histories of the accelerations on the cabin floor and in the dummies and of the loads in the restraint systems are presented in figure 22. The normal accelerations (fig. 22(a)) on the floor were about -20g on the port side and -25g on the starboard side. The difference can be attributed to the 7.5° starboard roll angle at initial impact; this roll caused higher accelerations on the starboard side. The same results were experienced in the longitudinal accelerations, which were about equal to the normal accelerations in the same location. These airplane floor accelerations were low and resulted from the airplane structure absorbing much of the impact energy through structural crushing. The acceleration values of the fire wall at 0F7N and 0F7L were both -25g. The fire wall accelerations at 0D8L were higher, and the traces resembled a sine wave. The nose landing gear broke away close to this location. The accelerations on the structure started about the time the engine propeller spinner contacted the ground and lasted about 0.06 sec, or until the structure started to collapse.

The greatest accelerations in the dummies occurred in the normal direction in the pelvis with about -25g in the pilot and about -40g in the copilot. The difference in accelerations again reflected the starboard roll impact. There were only about -5g accelerations noted in the copilot's pelvis in the longitudinal direction. The pilot's head experienced about ±20g in both the normal and longitudinal directions. Both the delayed response and the dual acceleration peaks of the dummy's head resulted from an input that caused the pilot to pitch forward and to suddenly decelerate at the lowest position of the head.

The loads experienced by the restraint system are presented in figure 22(d). There were two loads applied to the harness system. The first load occurred during the initial crash impulse and the second at the time the dummies had pitched forward to the farthest position. The pilot's lap belt shows two equal peaks of about 3900 N. The reason the copilot's lap belt did not experience the first peak is unknown. The shoulder harness maximum loads were nearly the same for both dummies. However, the loads first peaked at about 2000 N; the second peaks occurred at about 1600 N for the pilot and about 800 N for the copilot.

RESULTS AND DISCUSSION OF THE NOSE-DOWN-ON-SOIL TEST

Crash Dynamics

A photographic sequence (fig. 23) illustrates the crash dynamics of the airplane test specimen during a negative-pitch (nose-down) crash starting at initial ground (soil) contact. The airplane contacted the soil impact surface on the nose gear with a velocity of 25.3 m/sec along a flight-path angle of -32° and at a pitch angle of -34.5°, a roll angle of -1.5°, and a yaw angle of 2.0°. The nose gear began to fail immediately after initial ground contact followed by the fuselage nose (cowling) at 0.03 sec into the impact. The engine started to penetrate the soil impact surface at 0.067 sec, the same time that the fire wall and instrument panel started cabin penetration. The pitch angle of the airplane remained about constant during this period. Evidence of first buckling of the aft section of the fuselage occurred at 0.072 sec as the fuselage began to fold at the aft end of the baggage compartment. The airplane cabin section started to pitch over when the fire wall had moved into the cabin as far as the seats. At 0.212 sec, the cabin had pitched to a vertical position, while the aft section of the fuselage had pitched in the opposite direction to an angle of -17.0°. At this time, the airplane started an upward rebound which pulled the engine out of the ground. The aft section of the fuselage whipped over until it realigned itself with the cabin at 0.992 sec. The airplane then impacted the soil on its back at 1.21 sec into the crash. The pilot and copilot dummies contacted the instrument panel at 0.173 sec.

Assessment of Damage

Postcrash photographs of the damage sustained by the nose-down-on-soil test specimen are presented in figure 24. The livable volume was drastically reduced during the crash impact on soil.

Figures 24(a) and 24(b) show the final attitude of the airplane and the overall structural damage. The entire fire wall, engine mount, and fuselage structure in front of the pilot and copilot is collapsed to within a few centimeters of the airplane seats. The aft fuselage section is broken just aft of the luggage compartment. The engine is completely separated from the fuselage. Figure 24(c) is a close-up view of the forward section of the fuselage showing that the fire wall has moved back to form a plane between the leading edge of the wing and the fuselage-wing strut junction. The copilot's foot can be seen protruding through the fire wall. There is nothing left of the fuselage

forward of the leading edge of the wing. The aft section of the fuselage is shown in a close-up view in figure 24(d). The fuselage is broken at the luggage compartment rear bulkhead, and the luggage compartment volume has been greatly reduced. The final position of the pilot within the damaged airplane is shown in figure 24(e). The fuselage floor is displaced upward, pressing the dummy's head against the upper cabin with the shoulder level at the top of the door opening. The fire wall, fuselage forward floor, and instrument panel pushed the dummy's legs back to the front of the seat. The lap belt is attached to the floor and is tight around the dummy's pelvis. Figure 24(f) shows the pilot's station after the dummy had been removed. It is apparent that all structure in front of the pilot has been completely demolished. In addition, the pilot clearly contacted this structure head on during the impact. Figure 24(g) shows that the copilot's position was about the same as the pilot's; however, the forward fuselage structure shows more penetration into the cabin area on the copilot's side than on the pilot's side. The copilot dummy had both legs broken just below the knee as a result of the structural impact against the legs.

Acceleration Histories

Time histories of the accelerations on the cabin floor and in the dummies and of the loads in the restraint systems are presented in figure 25. The normal accelerations (fig. 25(a)) indicate a reversal of the expected load direction during the time that the fuselage cabin pitched up to a vertical position. There was little indication of the early part of the initial impact which ended at about 0.072 sec as a result of the massive crushing of the forward fuselage structure. Peak accelerations of about -45g longitudinally on the floor occurred at about 0.10 sec as all forward motion came to a stop. The fuselage had almost totally collapsed by this time.

There were negligible differences in the acceleration peak times for the dummies' pelvic regions and heads, since the entire front of the fuselage moved back to the seats. The greatest accelerations occurred in the pilot's and copilot's pelvises and averaged about -50g with a peak as high as 65g. The normal acceleration in the copilot's pelvis was only -25g; the low value cannot be explained. The copilot received the largest head accelerations (-60g) in the normal direction. All other accelerations in the heads were about -25g. The apparent instability in accelerations probably resulted from the dummies bouncing around in what was left of the cabin.

The loads in the restraint harness systems ranged from about 1500 N to 3400 N. The front fuselage structure had moved back into the cabin and may have caused a reduction in the restraint system loading due to body impact, since the harness loads peaked at that time.

CONCLUDING REMARKS

Four identical four-place, high-wing, single-engine airplane specimens with nominal masses of 1043 kg were crash tested at the Langley Impact Dynamics Research Facility under controlled free-flight conditions. These tests were

conducted with nominal velocities of 25 m/sec along the flight path at various flight-path angles, ground-contact pitch angles, and roll angles. One test simulated a hard landing; another represented a pitched-down, positive roll (right wing down) crash; and, the third simulated a negative pitch (nose-down) crash. These three airplane specimens were crashed on concrete. A fourth specimen was crashed at the same flight attitude as the third, but impacted on soil instead of concrete.

The livable volume (i.e., a volume sufficient in size to maintain space between the occupants and the structure) in the cabin of the hard-landing and nose-down specimens was maintained, although there was some intrusion of the floor structure, over the main landing gear, into the cabin of the nose-down specimen. The livable volume in the cabin of the roll-impact and nose-down-on-soil specimens was significantly reduced by structural penetration into the cabin. The pilot and copilot dummies impacted the instrument panel in both the latter specimens during impact. All specimens, except the hard-landing specimen, sustained massive damage in the form of structural crushing in the forward section of the fuselage. The nose-down-on-soil specimen sustained massive structural damage throughout the entire airplane.

The accelerations on the floor of the roll-impact and nose-down specimens were nominally -20g to -25g. These airplane floor accelerations were low and resulted from the airplane structure absorbing much of the impact energy through structural crushing. The longitudinal accelerations on the floor of the nose-down-on-soil specimen were higher (-45g) as a result of the almost complete collapse of the fuselage and the very sudden stop in the longitudinal direction. The hard-landing airplane specimen experienced very small accelerations on the floor.

The accelerations experienced by the dummies' pelvises in the roll-impact and nose-down specimens were about -40g in the normal direction and no more than -15g in the longitudinal direction. The dummies in the nose-down-on-soil specimen experienced accelerations as high as -65g in the pelvic region. The accelerations in the dummies' heads in the roll-impact and nose-down-on-soil specimens peaked at about -60g as a result of head-structure impact. The accelerations in the heads of the dummies in the nose-down specimen were about ±20g, since they did not impact the structure.

The loads experienced by the restraint systems in the hard-landing specimen were only about 600 N. The shoulder harness and lap belts in the roll-impact and nose-down-on-soil specimens experienced average loads of about 3400 N and 2600 N, respectively. The nose-down specimen experienced loads in the opposite order of the other specimens, about 2000 N on the shoulder and about 3900 N in the lap belt. The absence of impact between the dummy and structure in the nose-down specimen probably caused this difference.

Langley Research Center
National Aeronautics and Space Administration
Hampton, VA 23665
July 11, 1980

REFERENCES

1. Preston, G. Merritt; and Moser, Jacob C.: Crash Loads. NACA Conference on Airplane Crash-Impact Loads, Crash Injuries and Principles of Seat Design for Crash Worthiness (Cleveland, Ohio), Apr. 1956, pp. 2-1 - 2-47. (Available as NASA TM X-60777.)

2. Eiband, A. Martin; Simpkinson, Scott H.; and Black, Dugald O.: Accelerations and Passenger Harness Loads Measured in Full-Scale Light-Airplane Crashes. NACA TN 2991, 1953.

3. Pinkel, I. Irving; and Rosenberg, Edmund G.: Seat Design for Crash Worthiness. NACA Rep. 1332, 1957. (Supersedes NACA TN 3777.)

4. Hayduk, Robert J.; Thomson, Robert G.; and Carden, Huey D.: NASA/FAA General Aviation Crash Dynamics Program - An Update. Forum, vol. 12, no. 3, Winter 1979, pp. 147-156.

5. Alfaro-Bou, Emilio; and Vaughan, Victor L., Jr.: Light Airplane Crash Tests at Impact Velocities of 13 and 27 m/sec. NASA TP-1042, 1977.

6. Castle, Claude B.; and Alfaro-Bou, Emilio: Light Airplane Crash Tests at Three Flight-Path Angles. NASA TP-1210, 1978.

7. Castle, Claude B.; and Alfaro-Bou, Emilio: Light Airplane Crash Tests at Three Roll Angles. NASA TP-1477, 1979.

8. Vaughan, Victor L., Jr.; and Alfaro-Bou, Emilio: Light Airplane Crash Tests at Three Pitch Angles. NASA TP-1481, 1979.

9. Cheng, Robert Y. K.: Soil Analyses and Evaluations at the Impact Dynamics Research Facility for Two Full-Scale Aircraft Crash Tests. NASA CR-159199, 1977.

10. Vaughan, Victor L., Jr.; and Alfaro-Bou, Emilio: Impact Dynamics Research Facility for Full-Scale Aircraft Crash Testing. NASA TN D-8179, 1976.

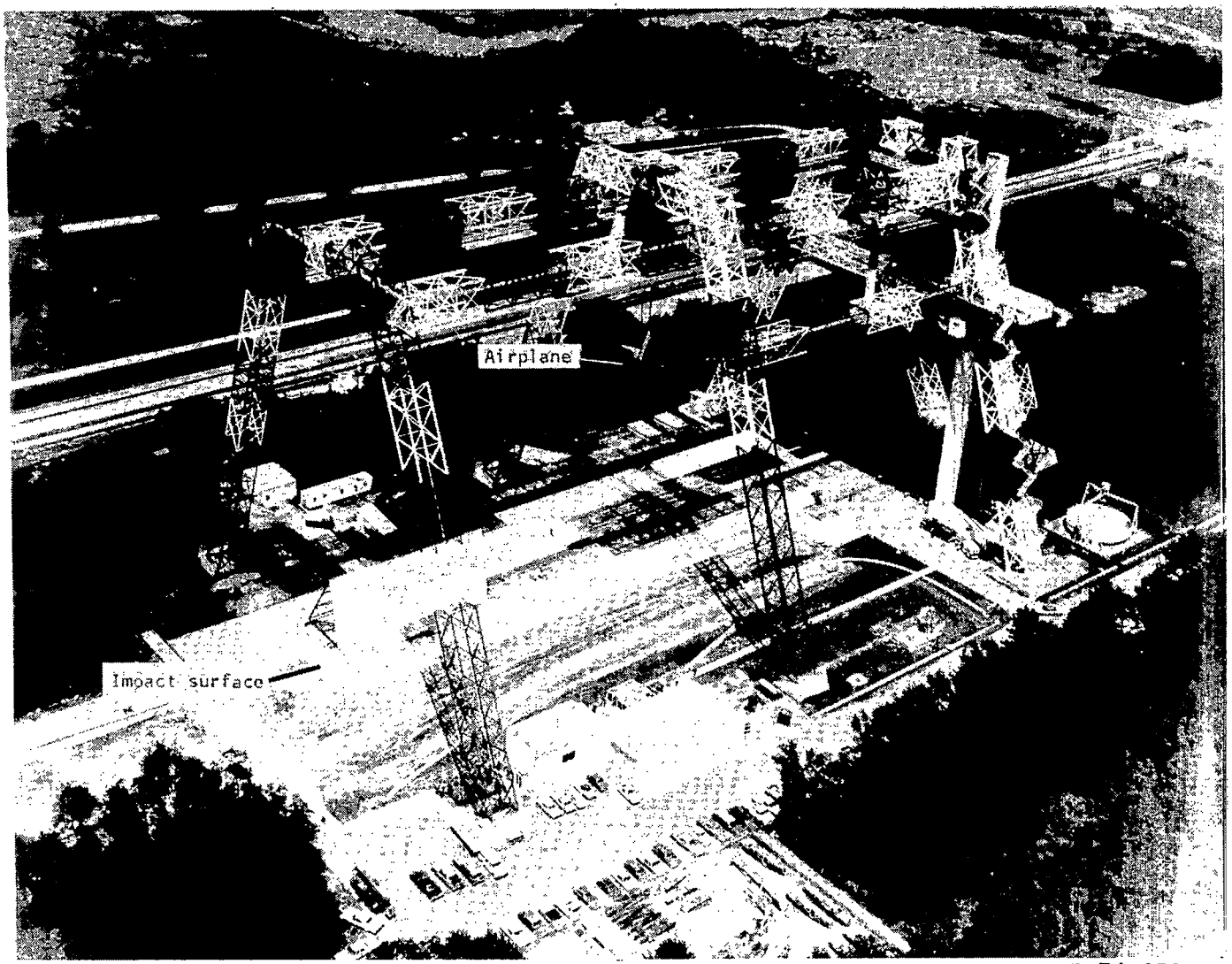

L-74-2505.5

Figure 1.- Langley Impact Dynamics Research Facility.

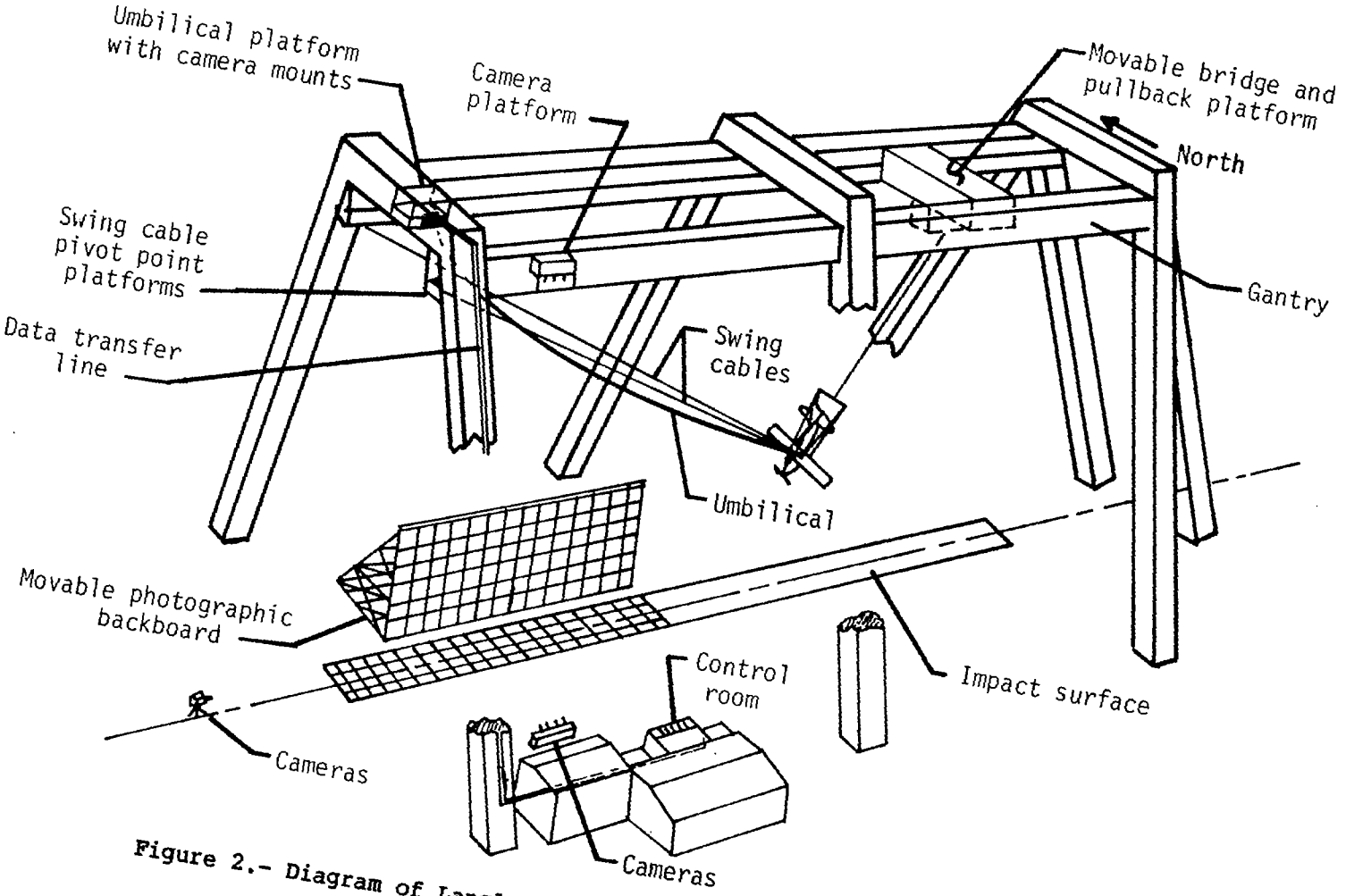

Figure 2.- Diagram of Langley Impact Dynamics Research Facility.

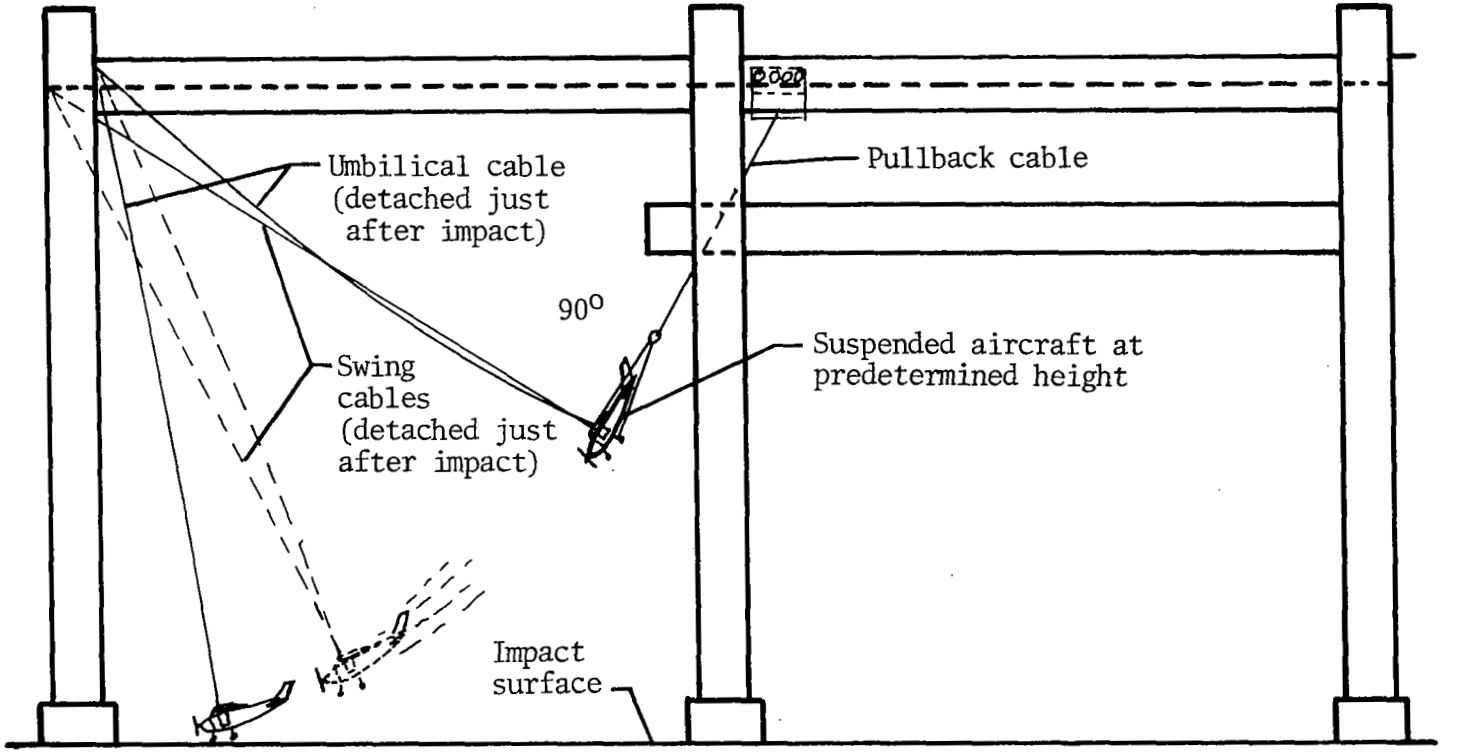

Figure 3.- Full-scale airplane crash-test technique.

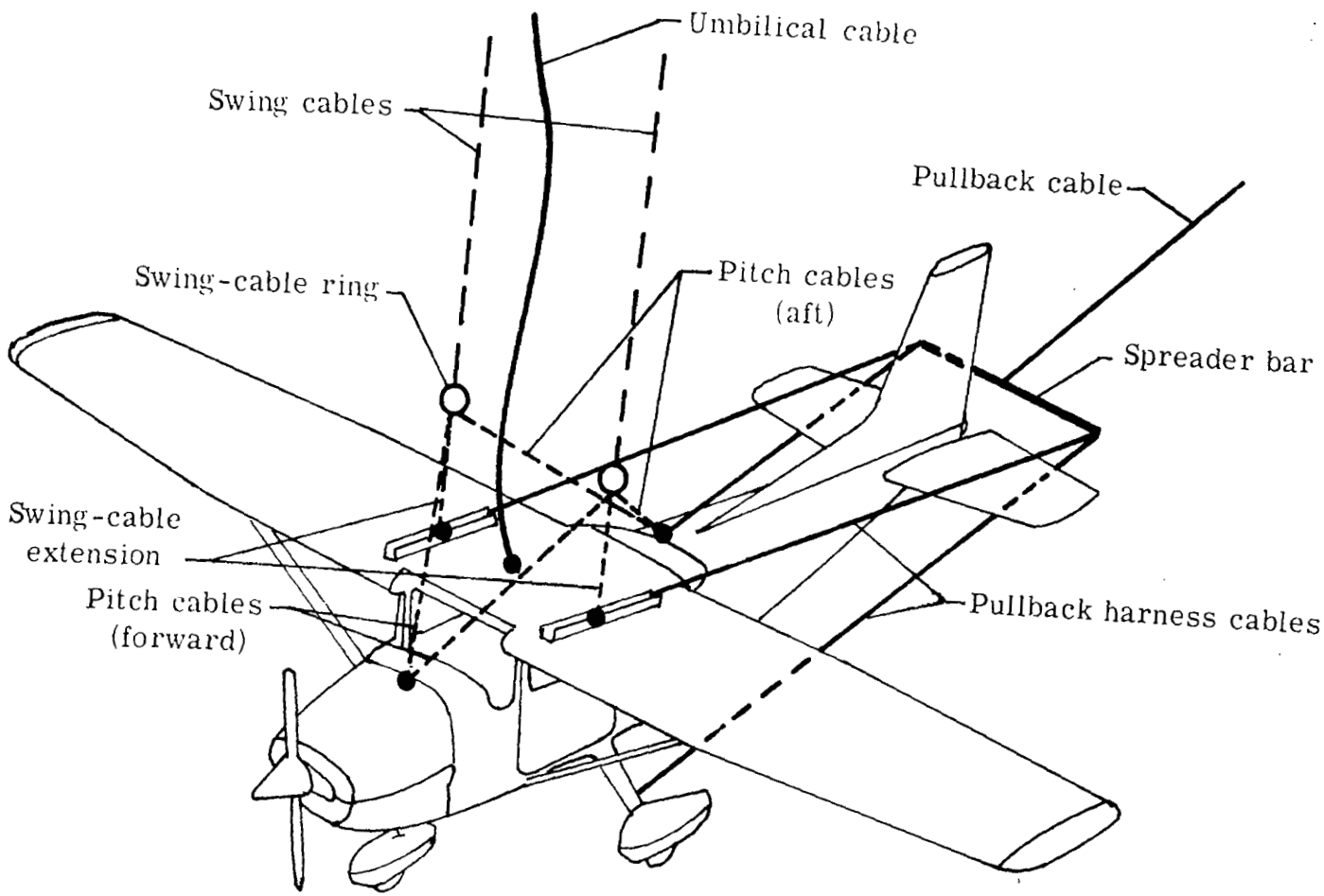

Figure 4.- Aircraft suspension system.

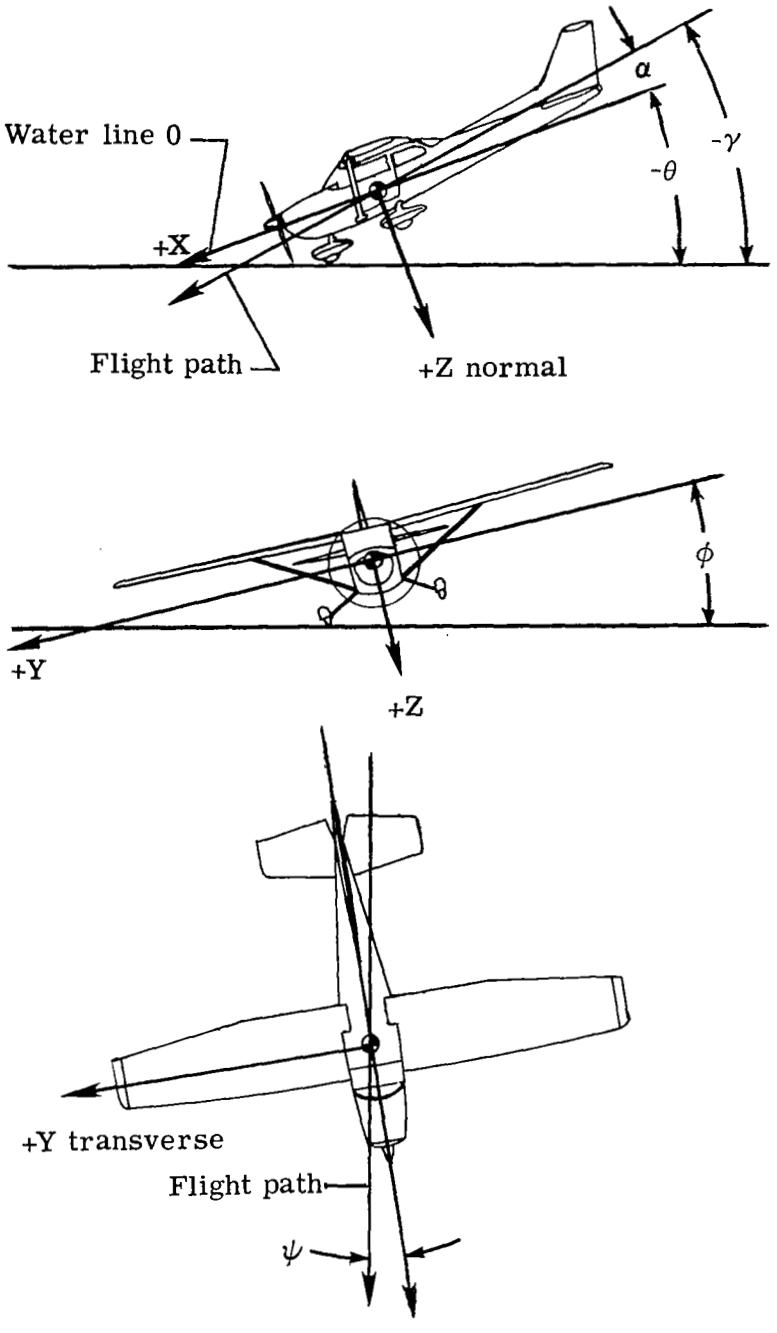

γ Flight-path angle
α Angle of attack
θ Pitch angle,
$\theta = \gamma + \alpha$

ϕ Roll angle

ψ Yaw angle

Figure 5.- Definition of flight path, crash attitudes, axes, and force directions.

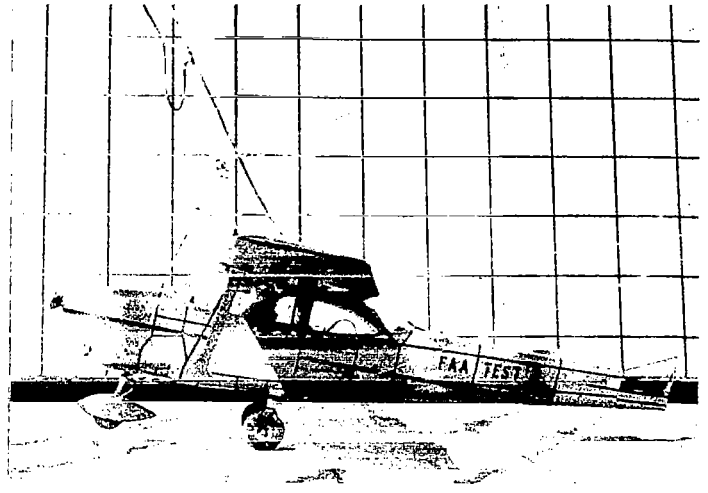

(a) Hard-landing test.

Flight-path angle, γ	-17.0°
Angle of attack, α	30.5°
Pitch angle, θ	13.5°
Roll angle, ϕ	3.5°
Yaw angle, ψ	-11.5°
Flight-path velocity	22.7 m/sec
Pitching velocity	0.43 rad/sec

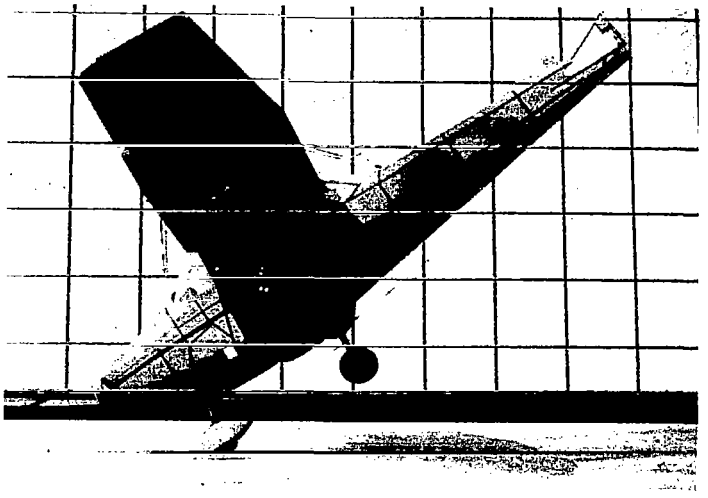

(b) Roll-impact test.

Flight-path angle, γ	-34.5°
Angle of attack, α	-4.5°
Pitch angle, θ	-39.0°
Roll angle, ϕ	18.6°
Yaw angle, ψ	3.2°
Flight-path velocity	25.9 m/sec
Pitching velocity	0.79 rad/sec

L-80-176

Figure 6.- Airplane pretest photographs and crash-test attitudes and parameters.

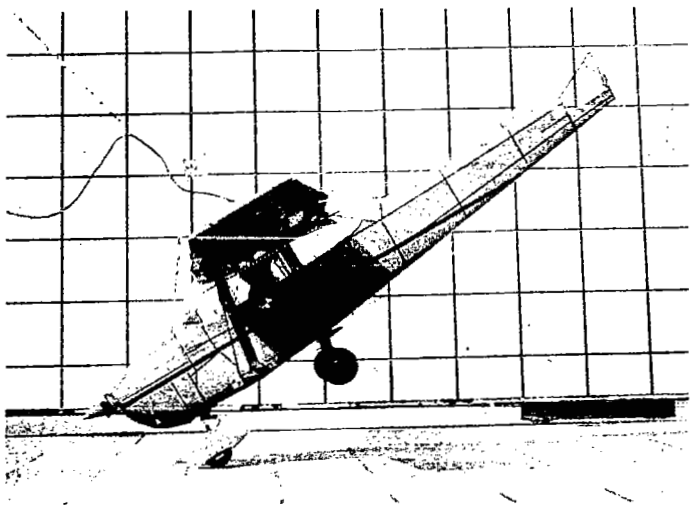

(c) Nose-down test.

Flight-path angle, γ	-32.0°
Angle of attack, α	2.0°
Pitch angle, θ	-30.0°
Roll angle, ϕ	7.5°
Yaw angle, ψ	0.7°
Flight-path velocity	24.7 m/sec
Pitching velocity	0.61 rad/sec

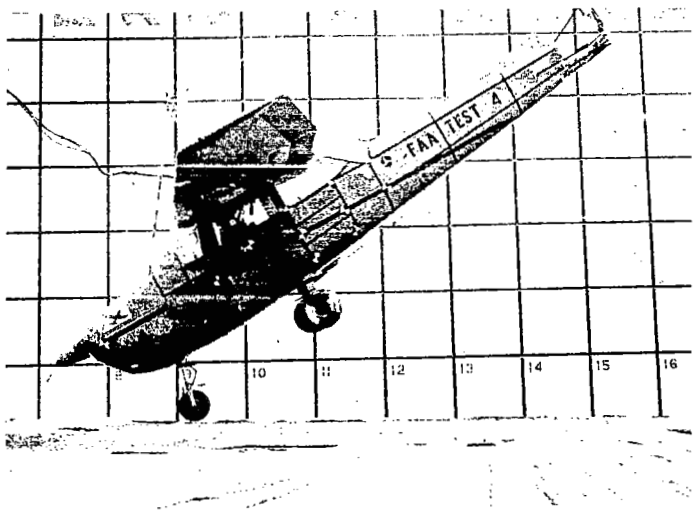

(d) Nose-down-on-soil test.

Flight-path angle, γ	-32.0°
Angle of attack, α	2.5°
Pitch angle, θ	-34.5°
Roll angle, ϕ	-1.5°
Yaw angle, ψ	2.0°
Flight-path velocity	25.3 m/sec
Pitching velocity	0.35 rad/sec

L-80-177

Figure 6.- Concluded.

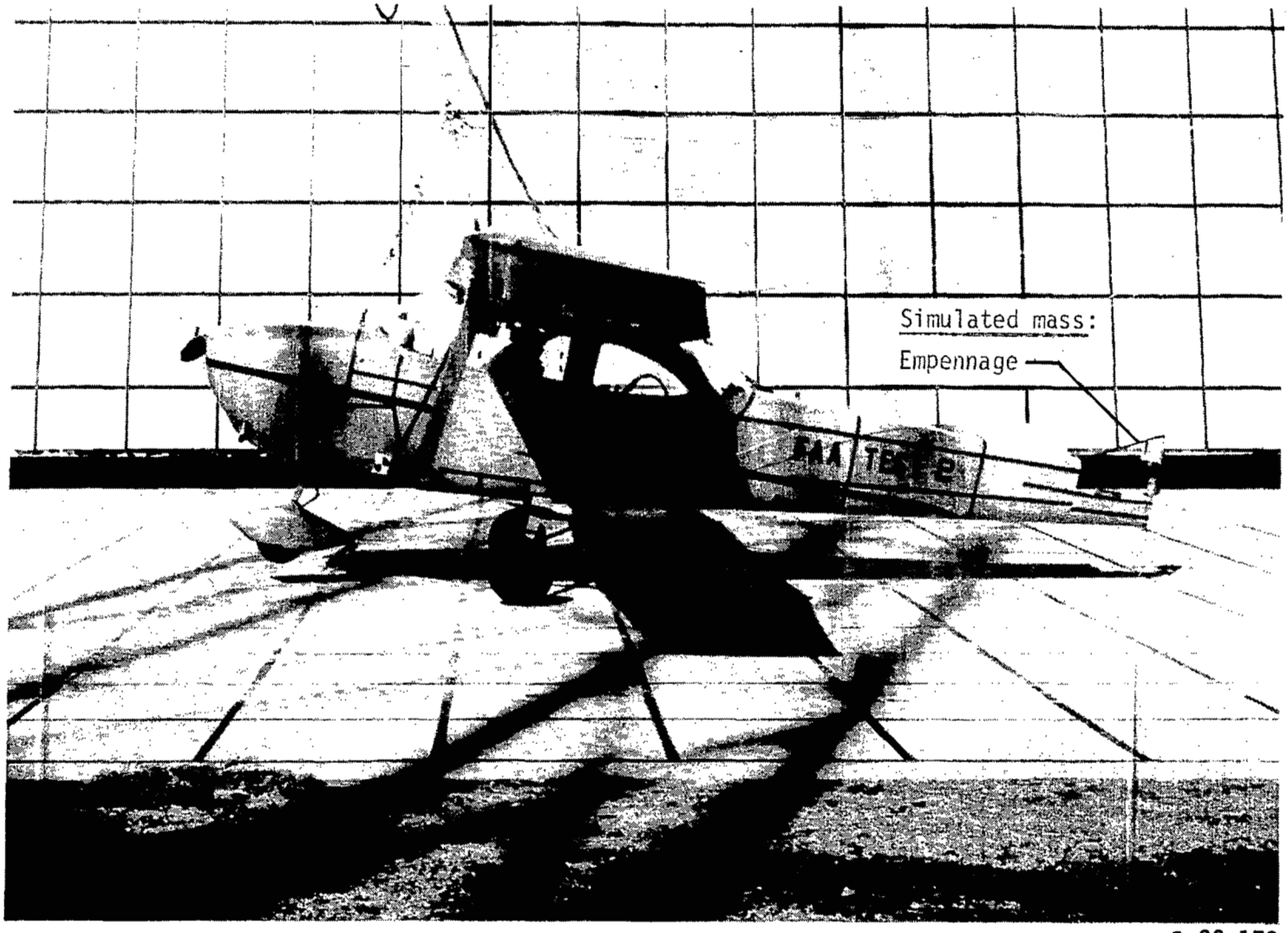

L-80-178

Figure 7.- Typical airplane test specimen in crash-test preparation.

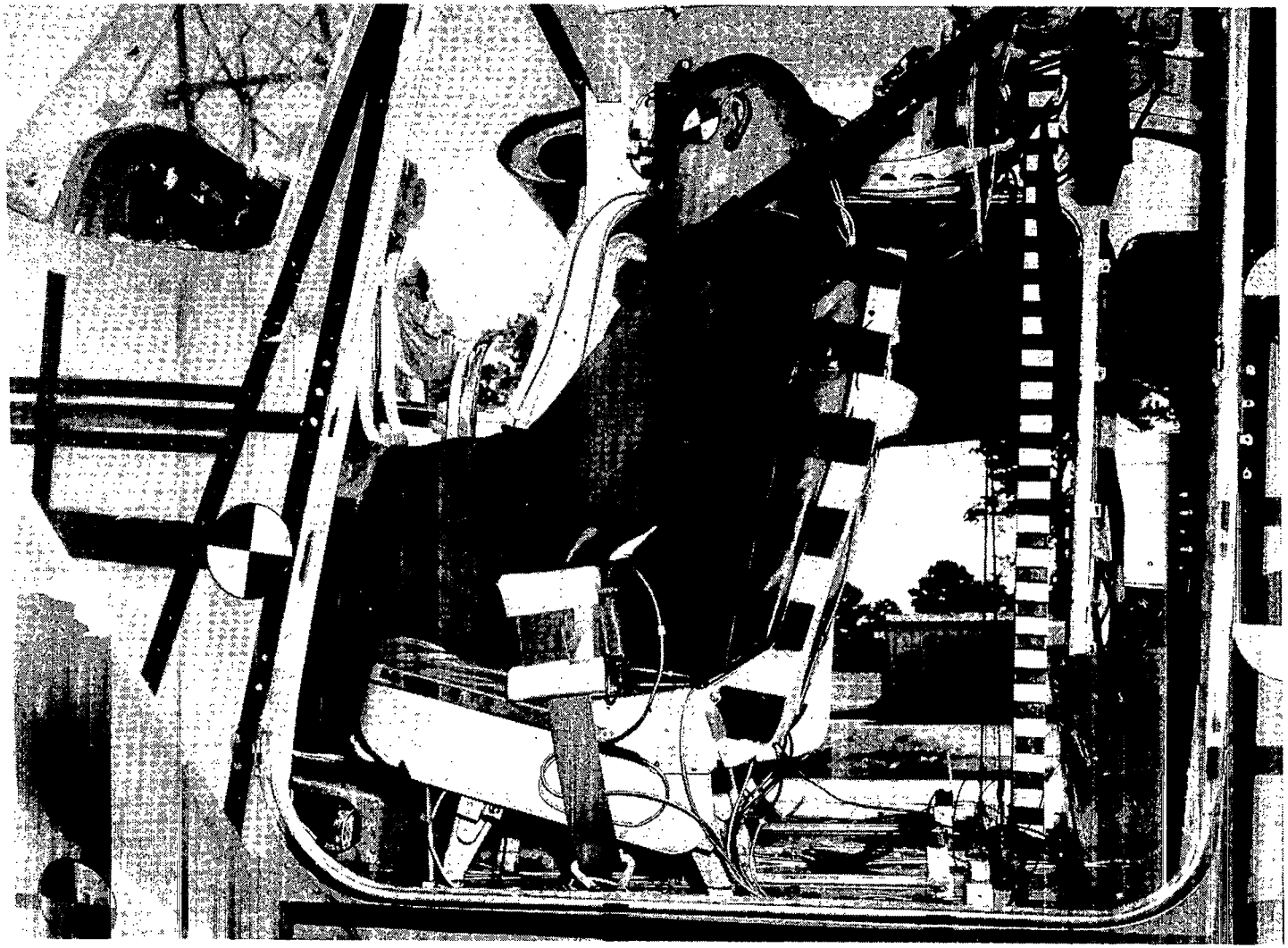

L-77-4464

Figure 8.- General configuration of airplane interior, seats, dummies, and restraint system before test.

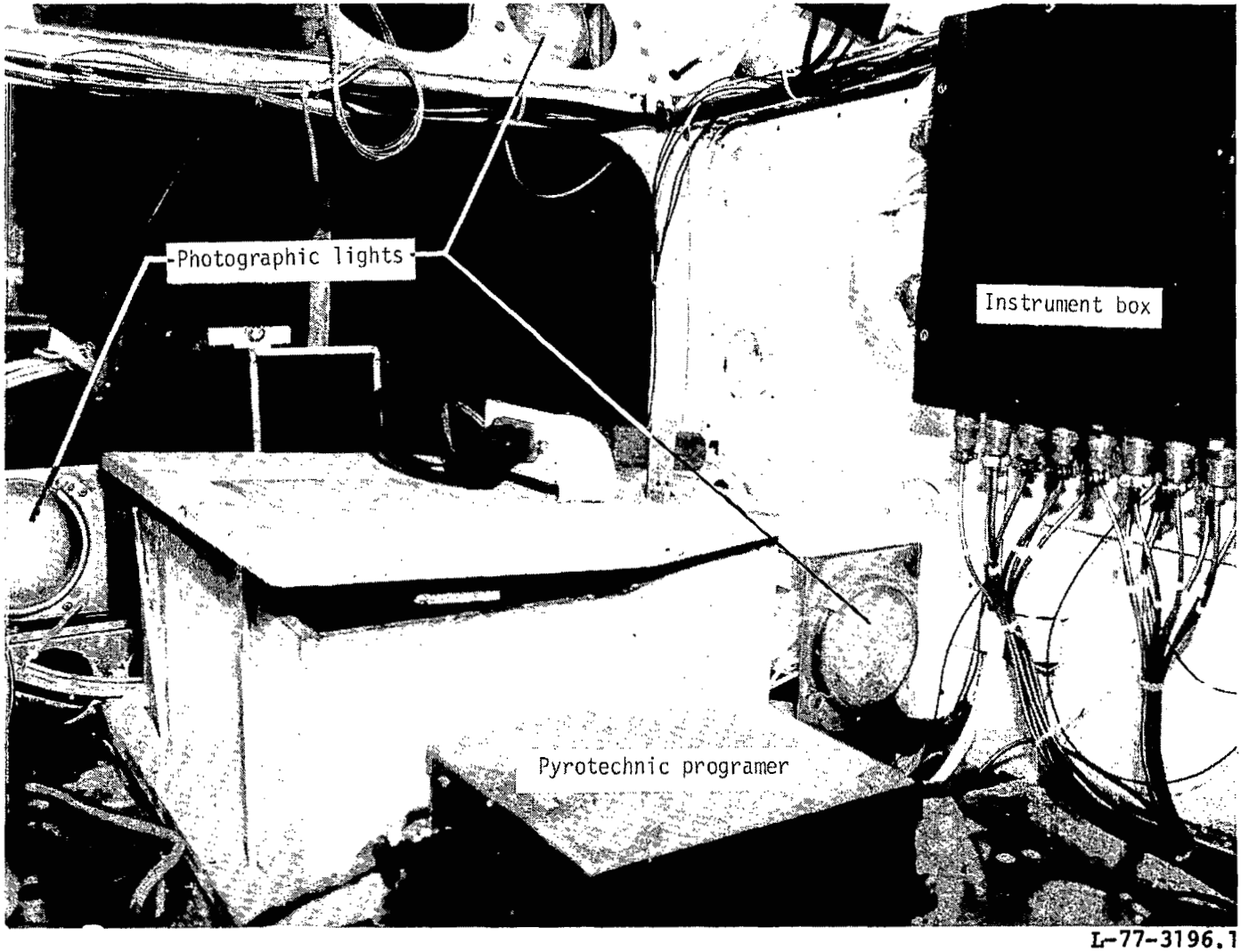

L-77-3196.1

Figure 9.- General configuration of port side of airplane interior before test.

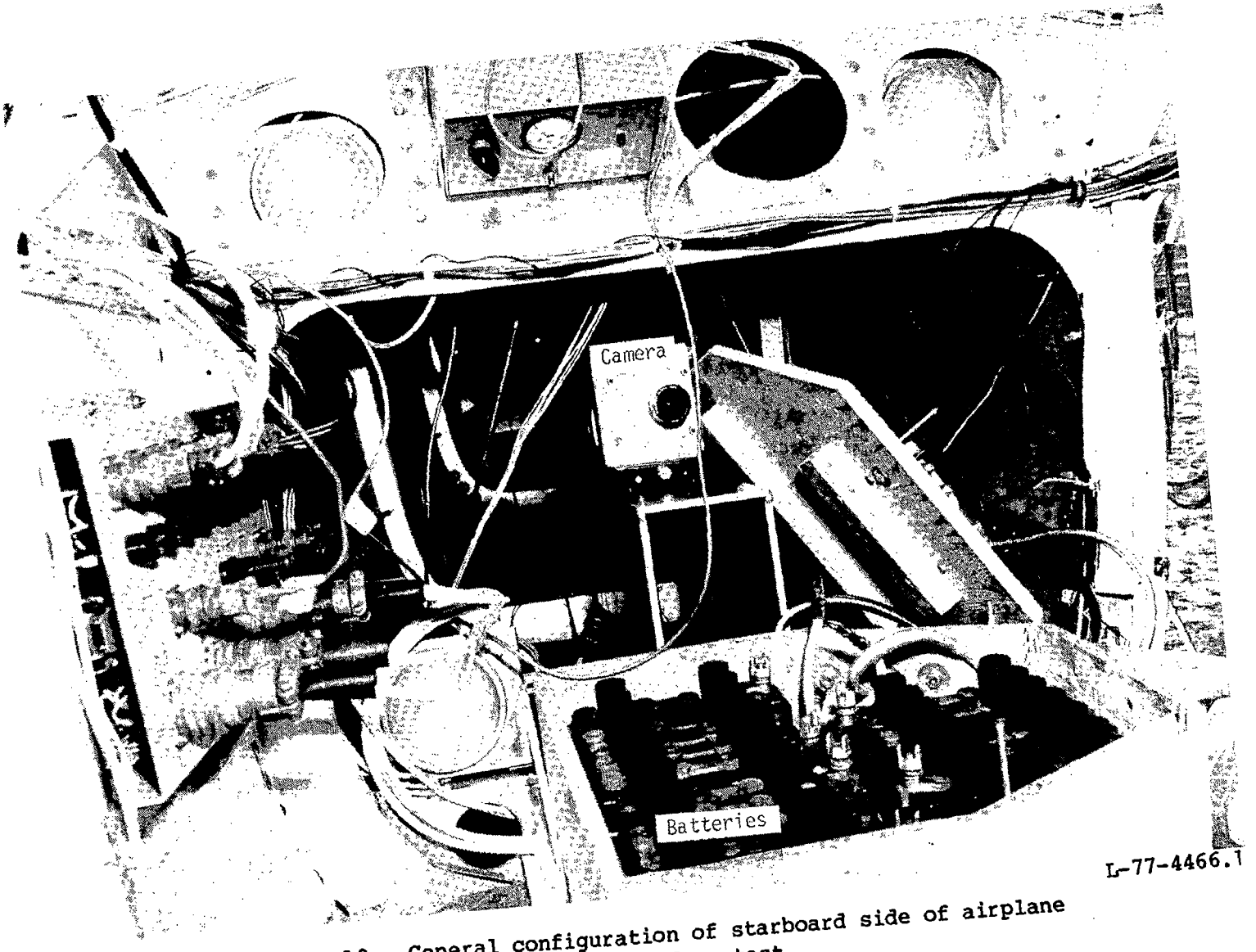

Figure 10.- General configuration of starboard side of airplane interior before test.

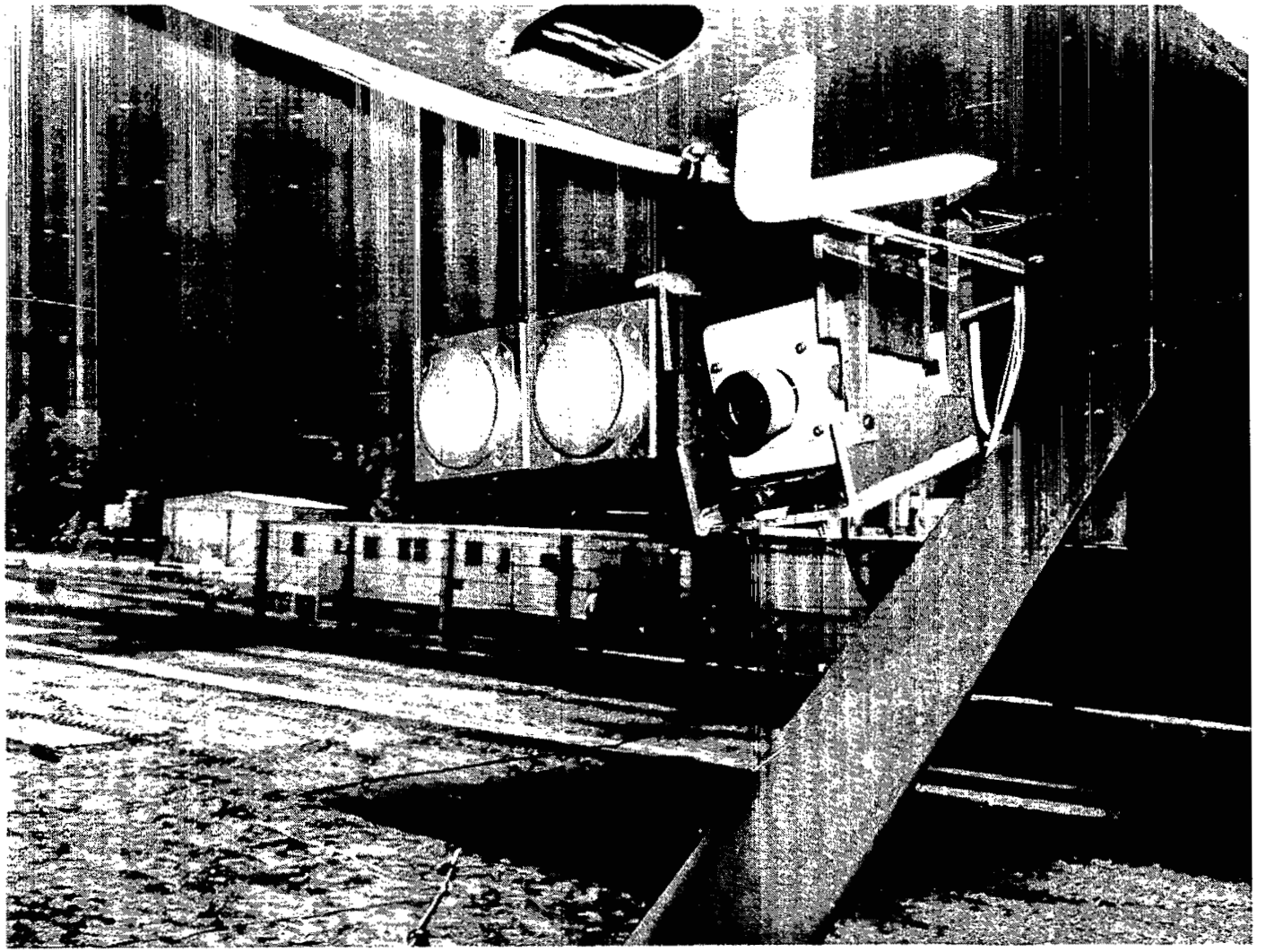

L-77-4463

Figure 11.- Camera and light mounted on port wing for viewing the pilot's position.

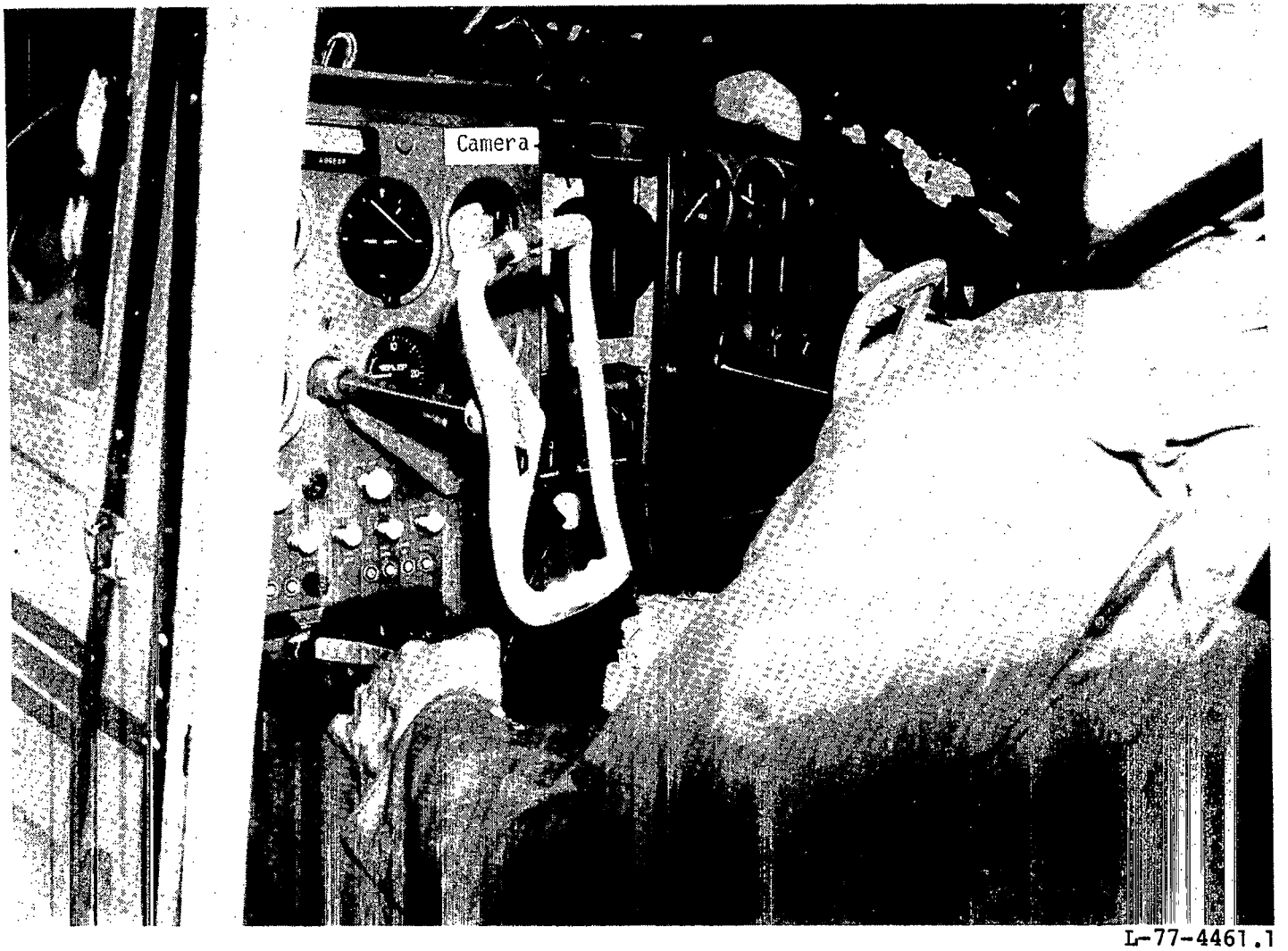

L-77-4461.1

Figure 12.- Camera mounted in instrument panel for viewing pilot and copilot dummies.

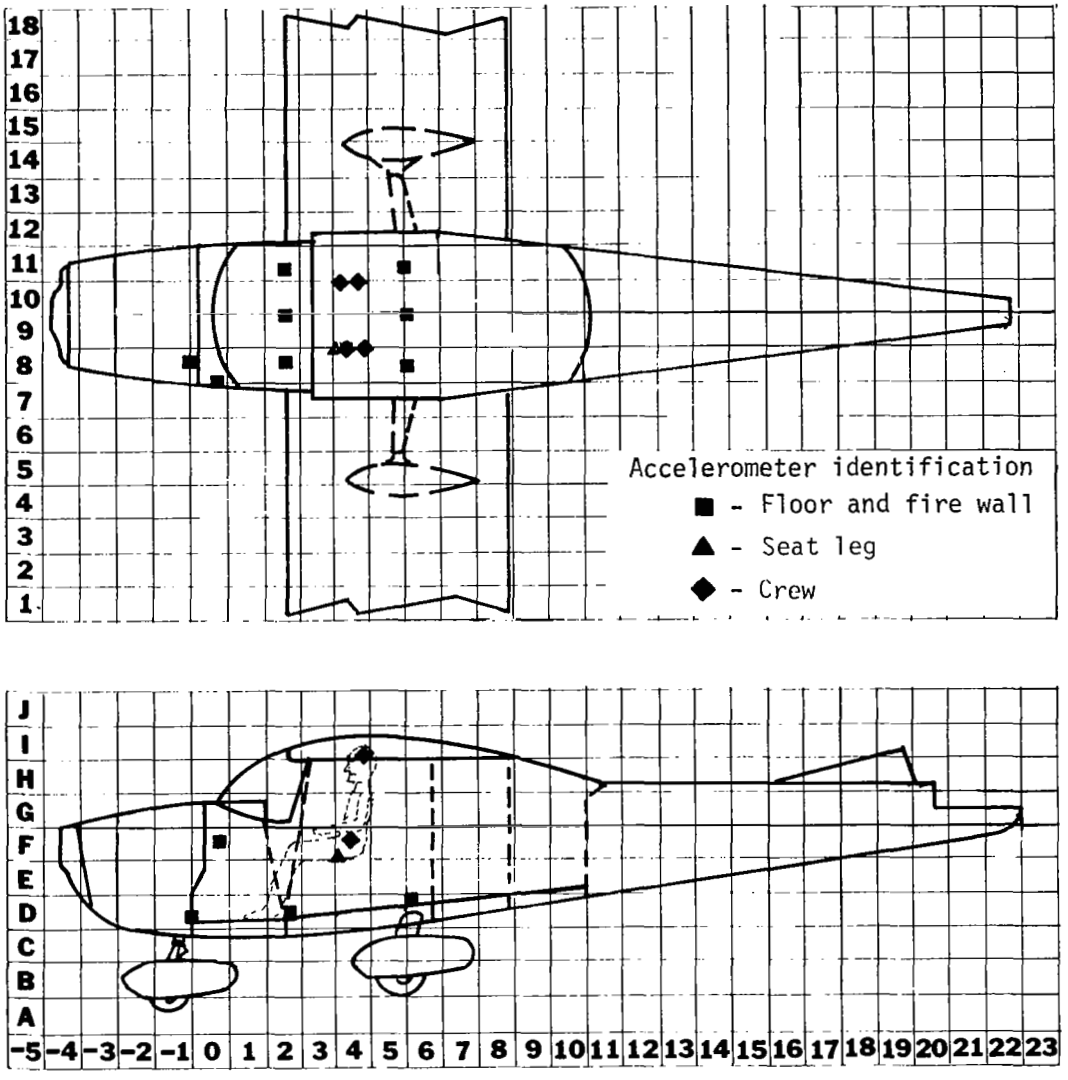

Accelerometers in dummies

Pilot, pelvic, normal*	4F8N	Copilot, pelvic, normal	4F11N
Pilot, pelvic, longitudinal**	4F8L	Copilot, pelvic, longitudinal	4F11L
Pilot, head, normal	4I8N	Copilot, head, normal	4I11N
Pilot, head, longitudinal	4I8L	Copilot, head, longitudinal	4I11L

* Along spine.
** Perpendicular to spine.

Figure 13.- Diagram of accelerometer locations on airplane structure and in dummies.

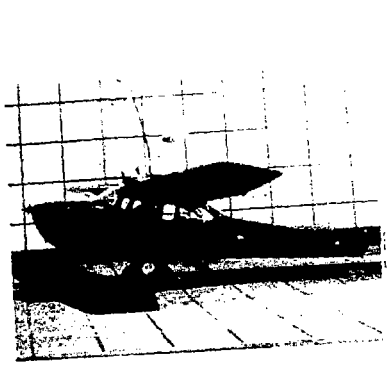

Time = 0.00 sec

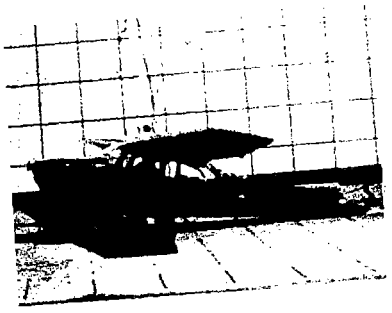

Time = 0.05 sec

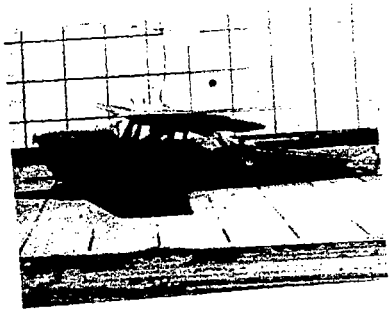

Time = 0.10 sec

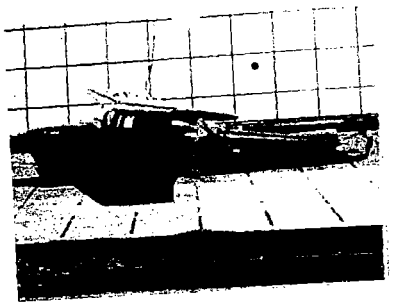

Time = 0.15 sec

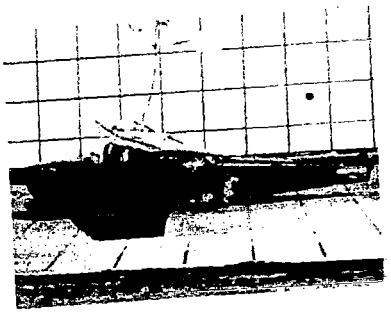

Time = 0.20 sec

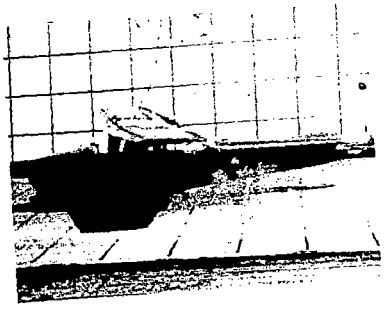

Time = 0.25 sec

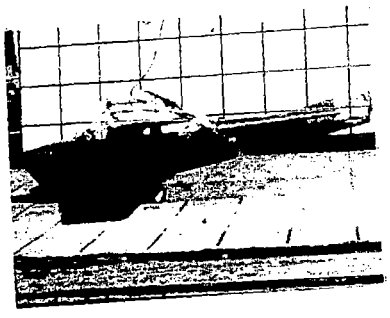

Time = 0.30 sec

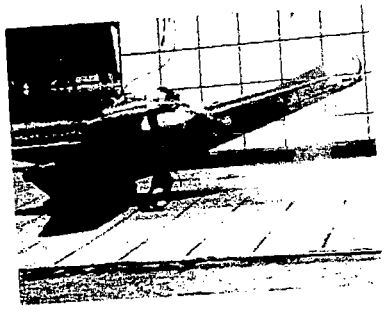

Time = 0.40 sec

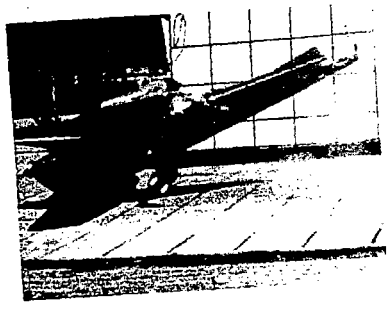

Time = 0.50 sec

L-77-2206

Figure 14.- Crash sequence photographs of hard-landing test.

L-77-1841

(a) View of front of airplane.

Figure 15.- Postcrash damage of hard-landing test.

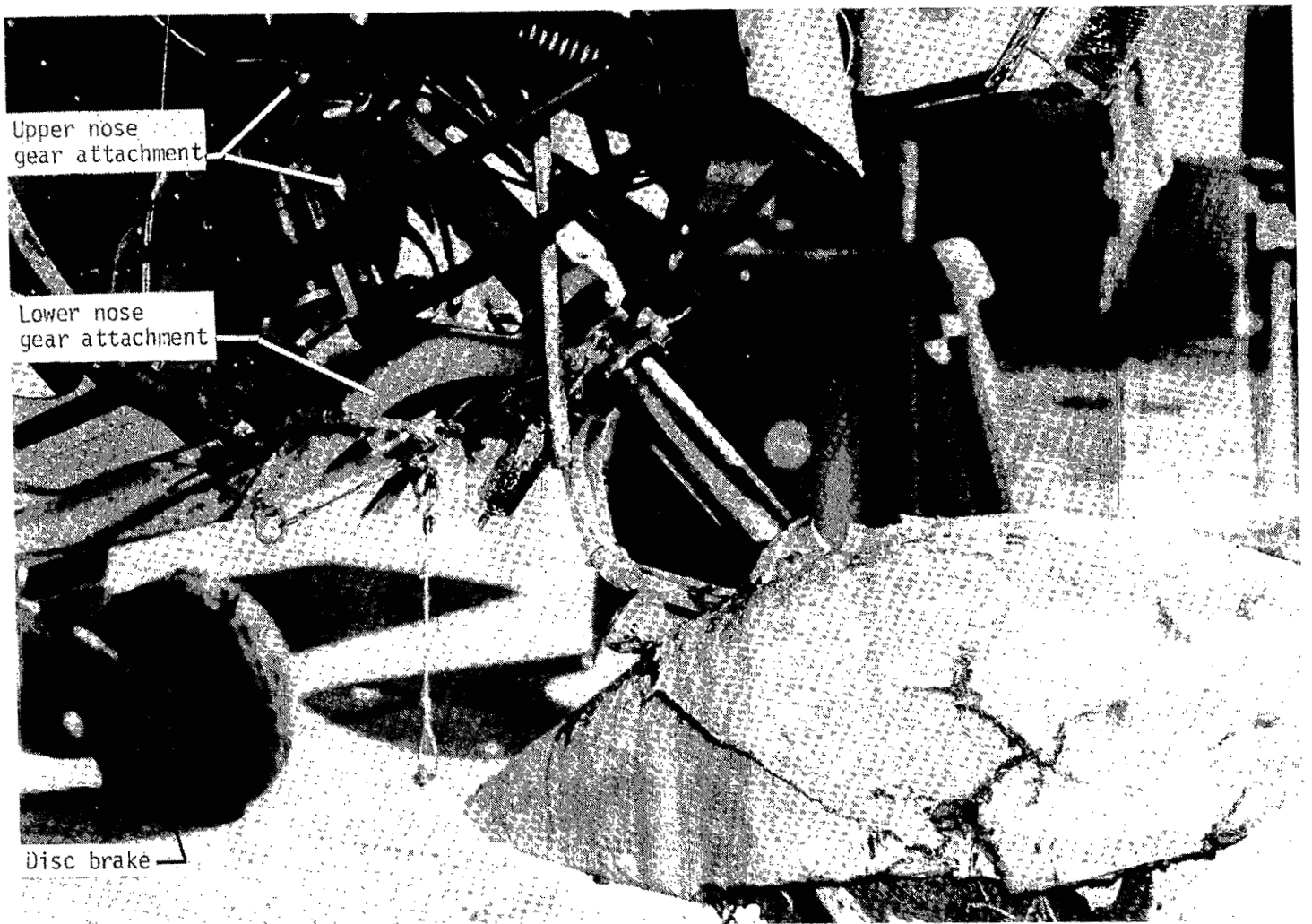

(b) View of nose landing gear and fire wall.

Figure 15.- Continued.

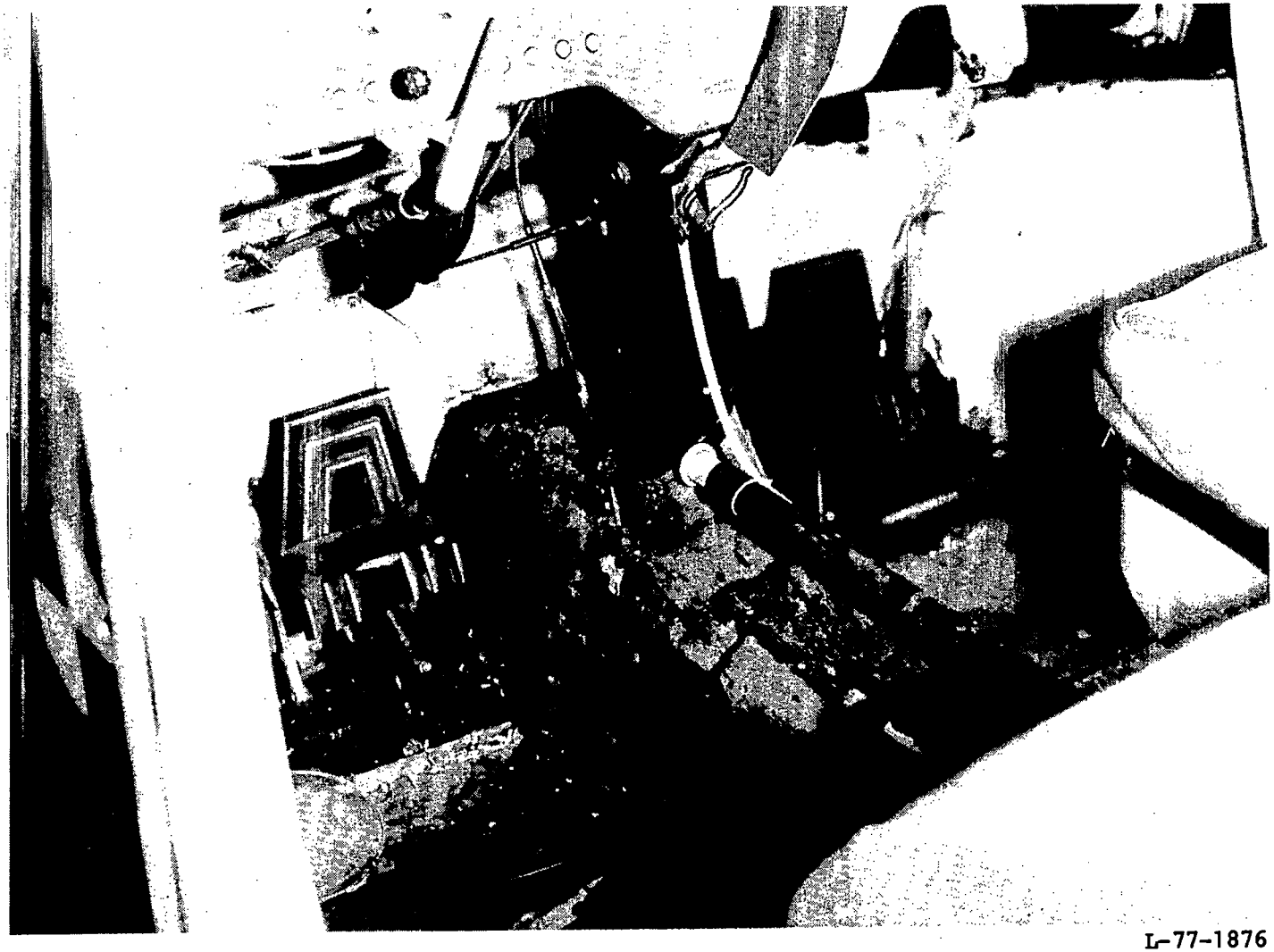

L-77-1876

(c) View of control line tunnel inside airplane.

Figure 15.- Continued.

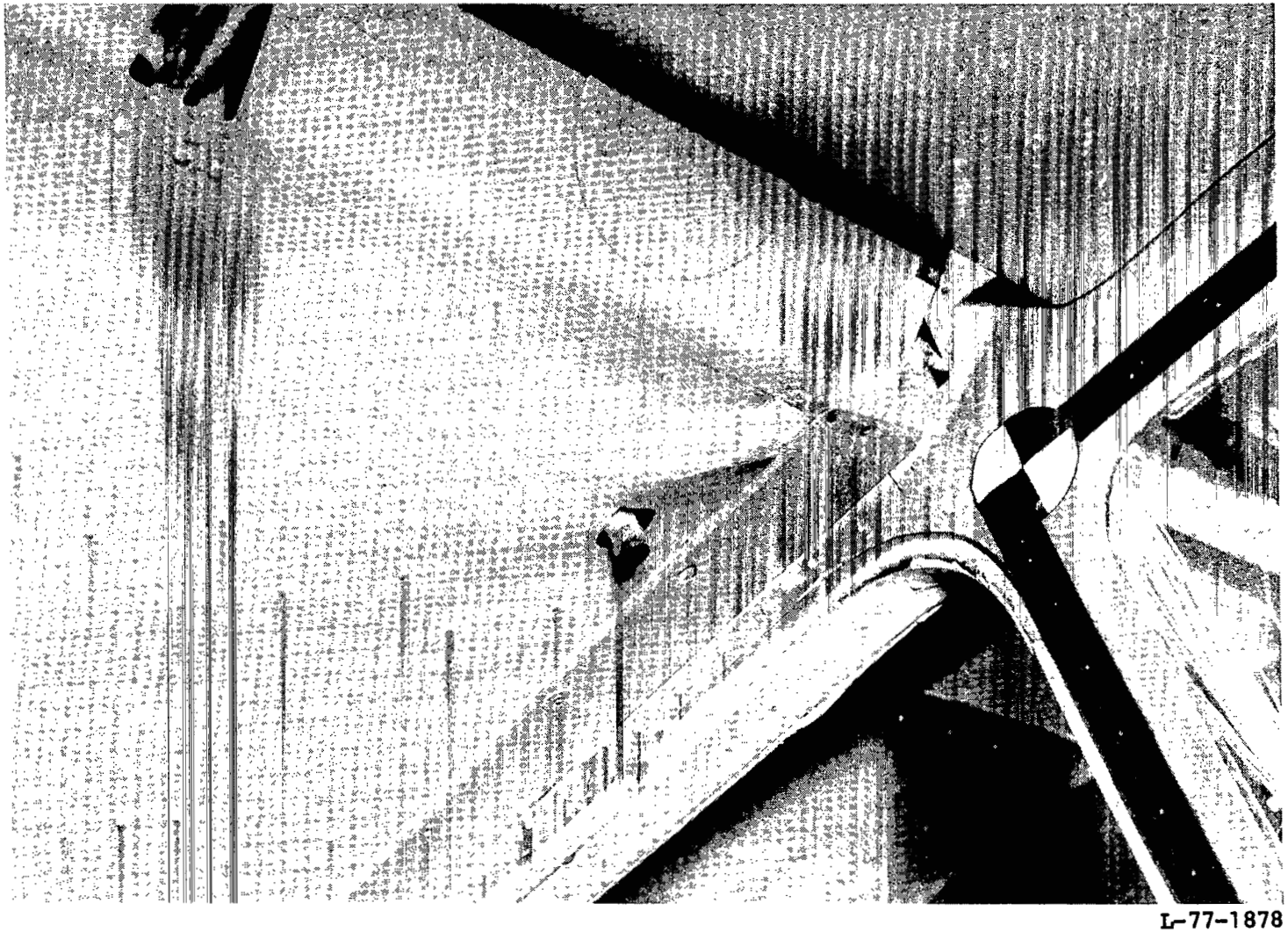

L-77-1878

(d) View of trailing edge of wing at fuselage junction.

Figure 15.- Concluded.

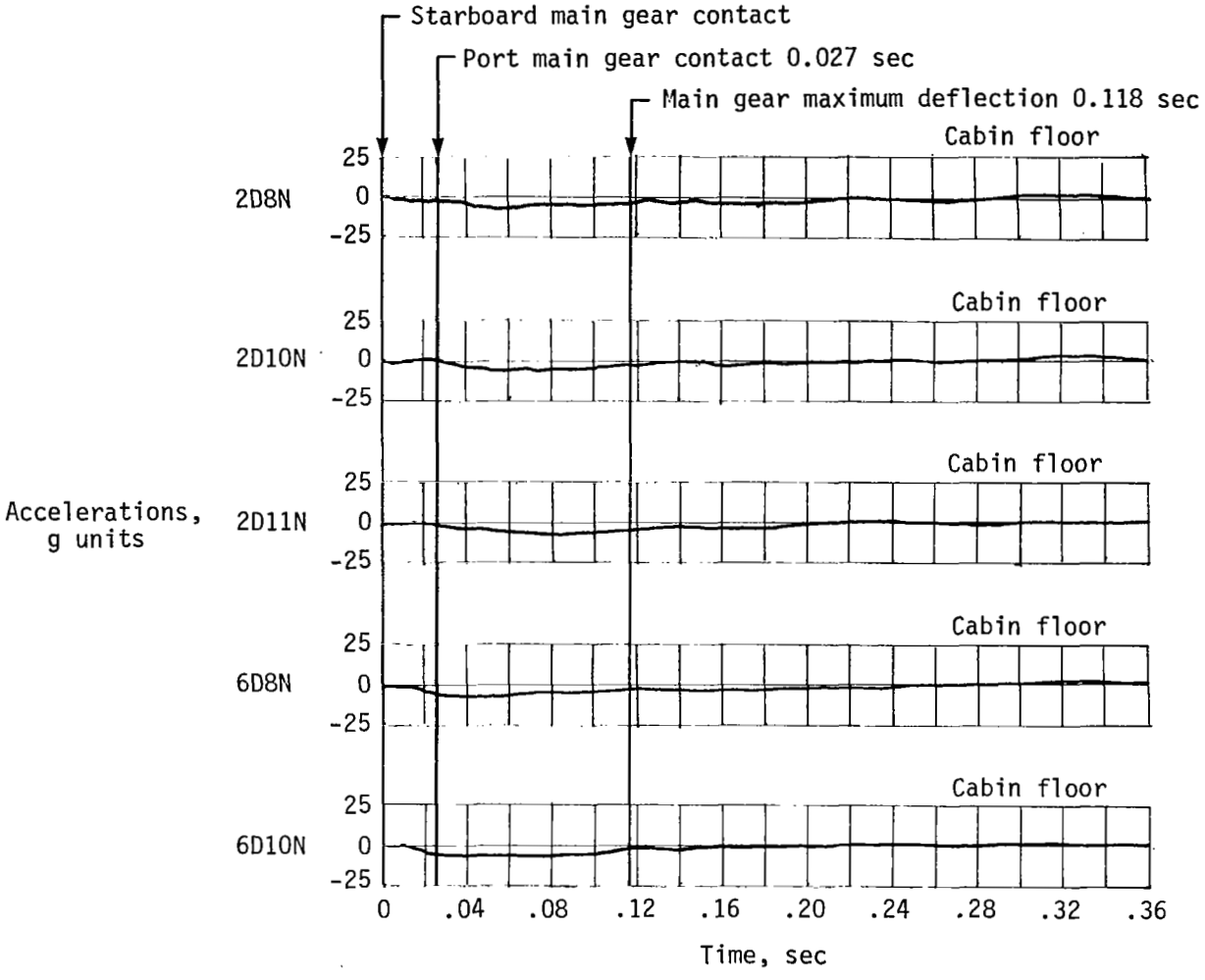

(a) Normal accelerations of cabin floor.

Figure 16.- Acceleration and load histories on board hard-landing test specimen.

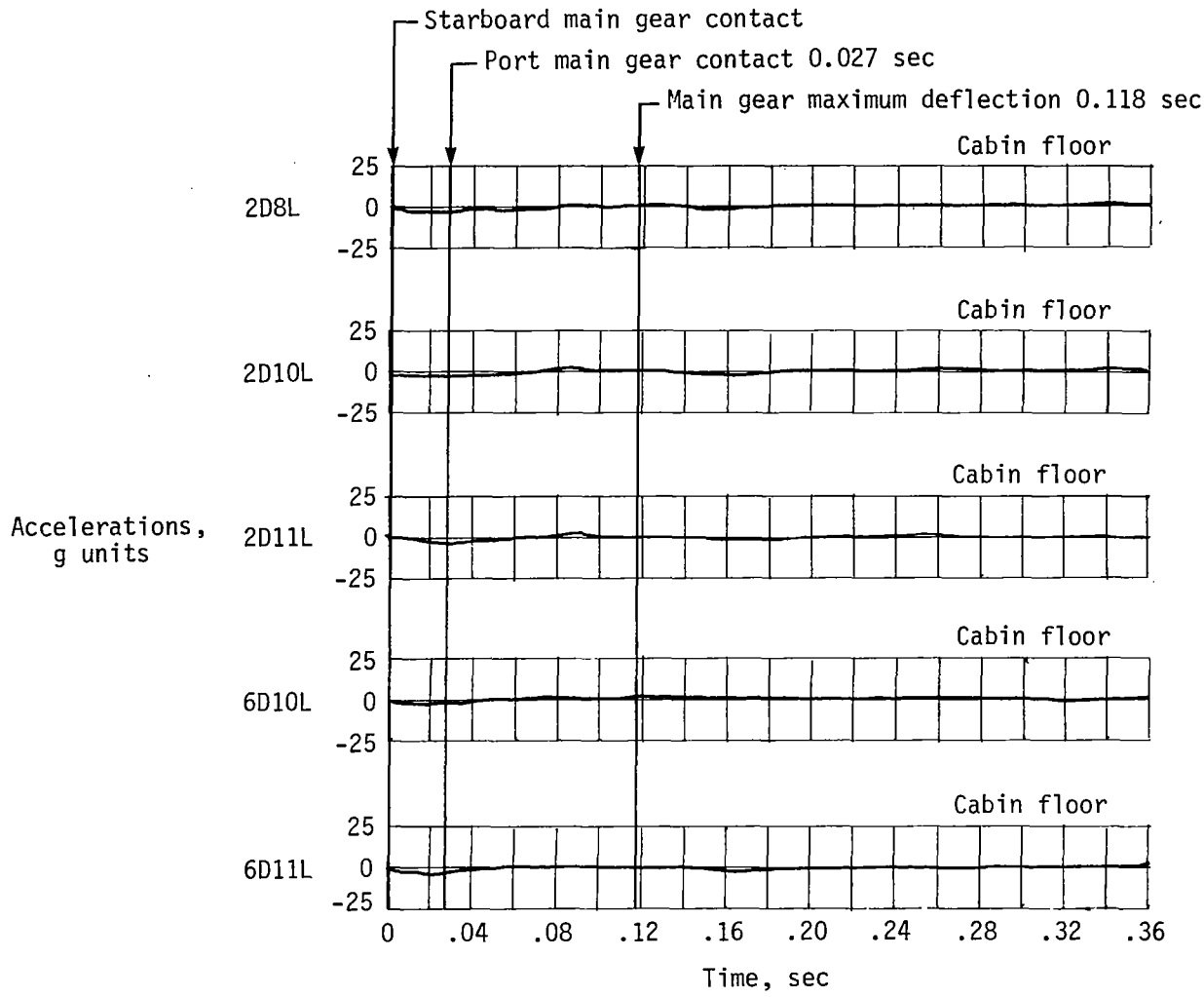

(b) Longitudinal accelerations of cabin floor.

Figure 16.- Continued.

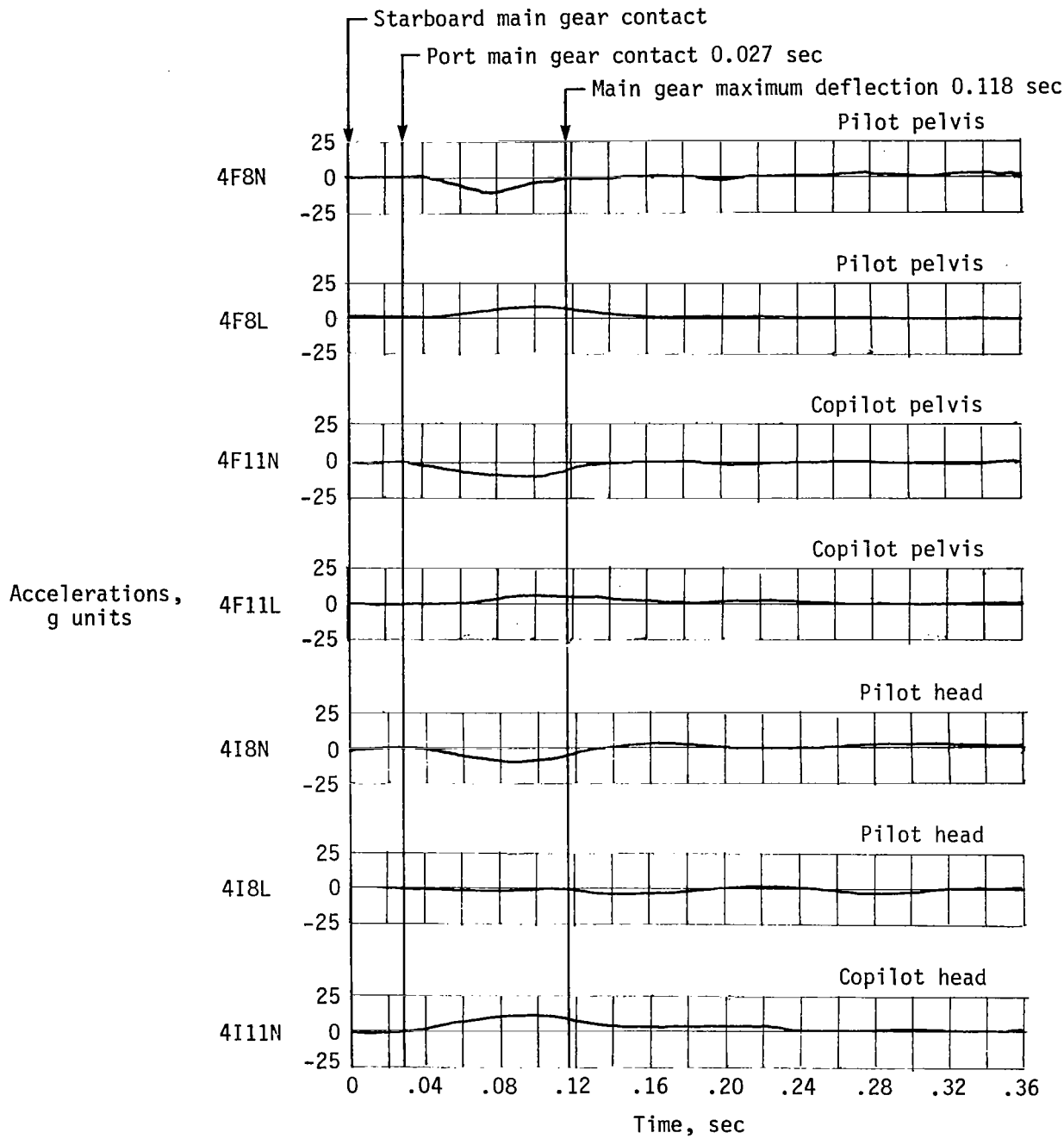

(c) Accelerations in pilot and copilot dummies.

Figure 16.- Continued.

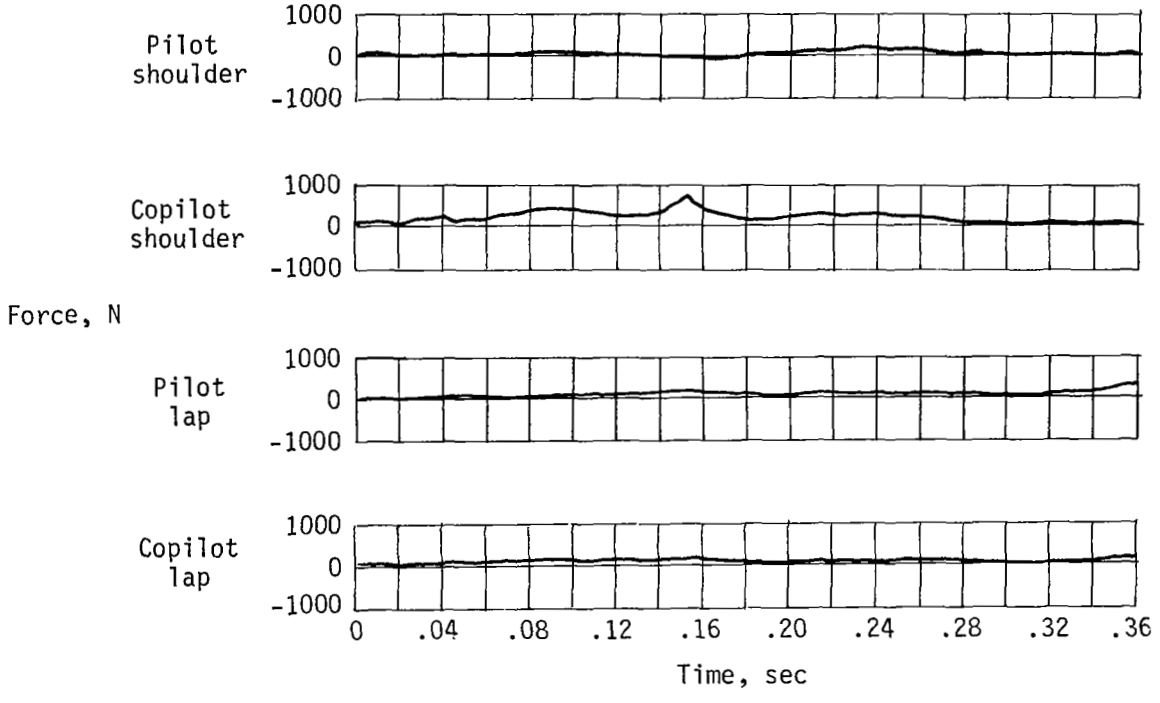

(d) Loads in restraint harness system.

Figure 16.- Concluded.

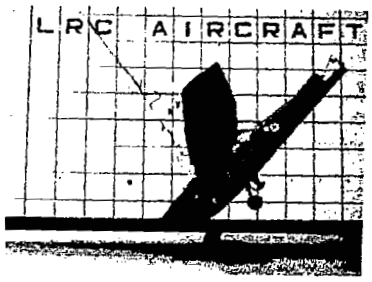

Time = -0.022 sec

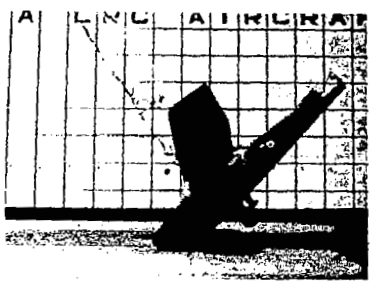

Time = 0.028 sec

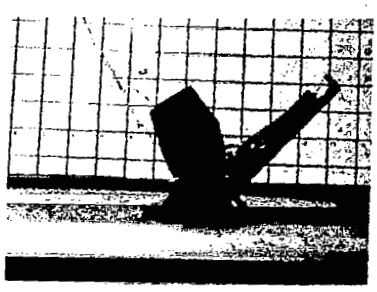

Time = 0.078 sec

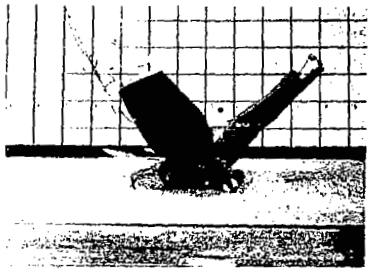

Time = 0.128 sec

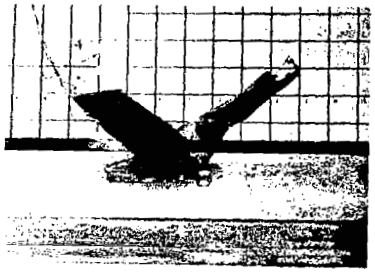

Time = 0.178 sec

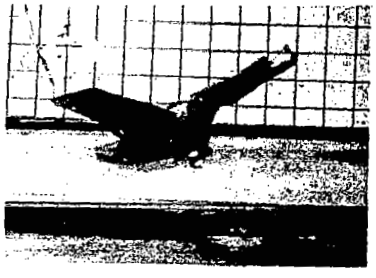

Time = 0.228 sec

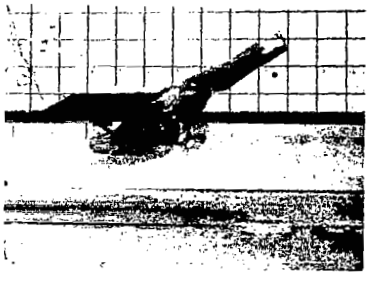

Time = 0.278 sec

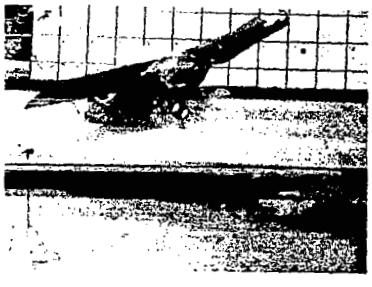

Time = 0.328 sec

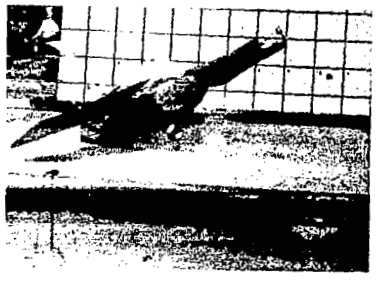

Time = 0.378 sec

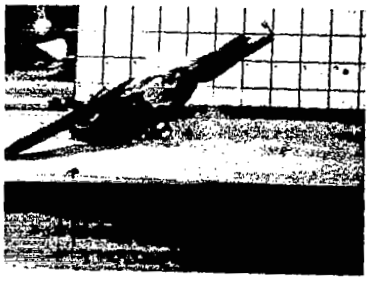

Time = 0.428 sec

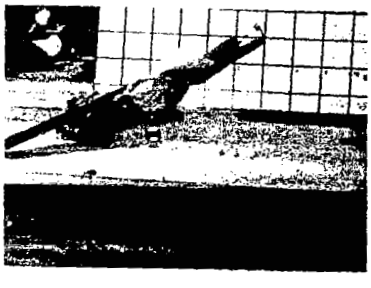

Time = 0.478 sec

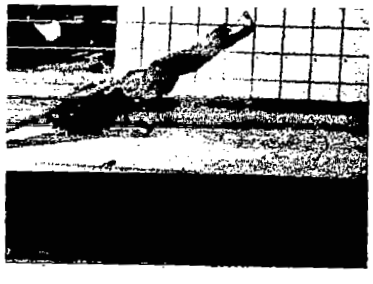

Time = 0.528 sec

Figure 17.- Crash sequence photographs of roll-impact test. L-80-179

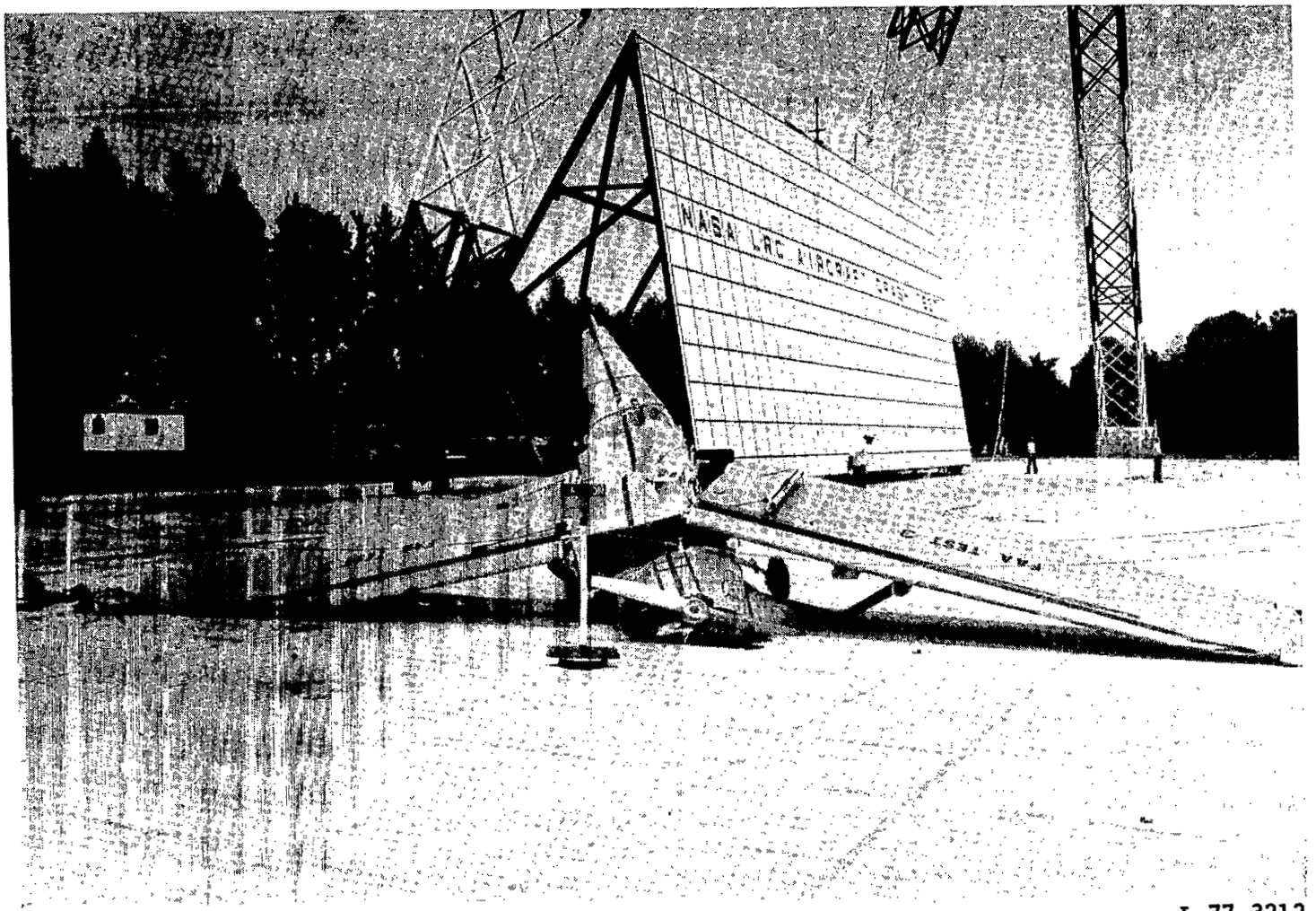

L-77-3212

(a) View of front of airplane.

Figure 18.- Postcrash damage of roll-impact test.

L-77-3168

(b) View of top of fuselage and wing junction.

Figure 18.- Continued.

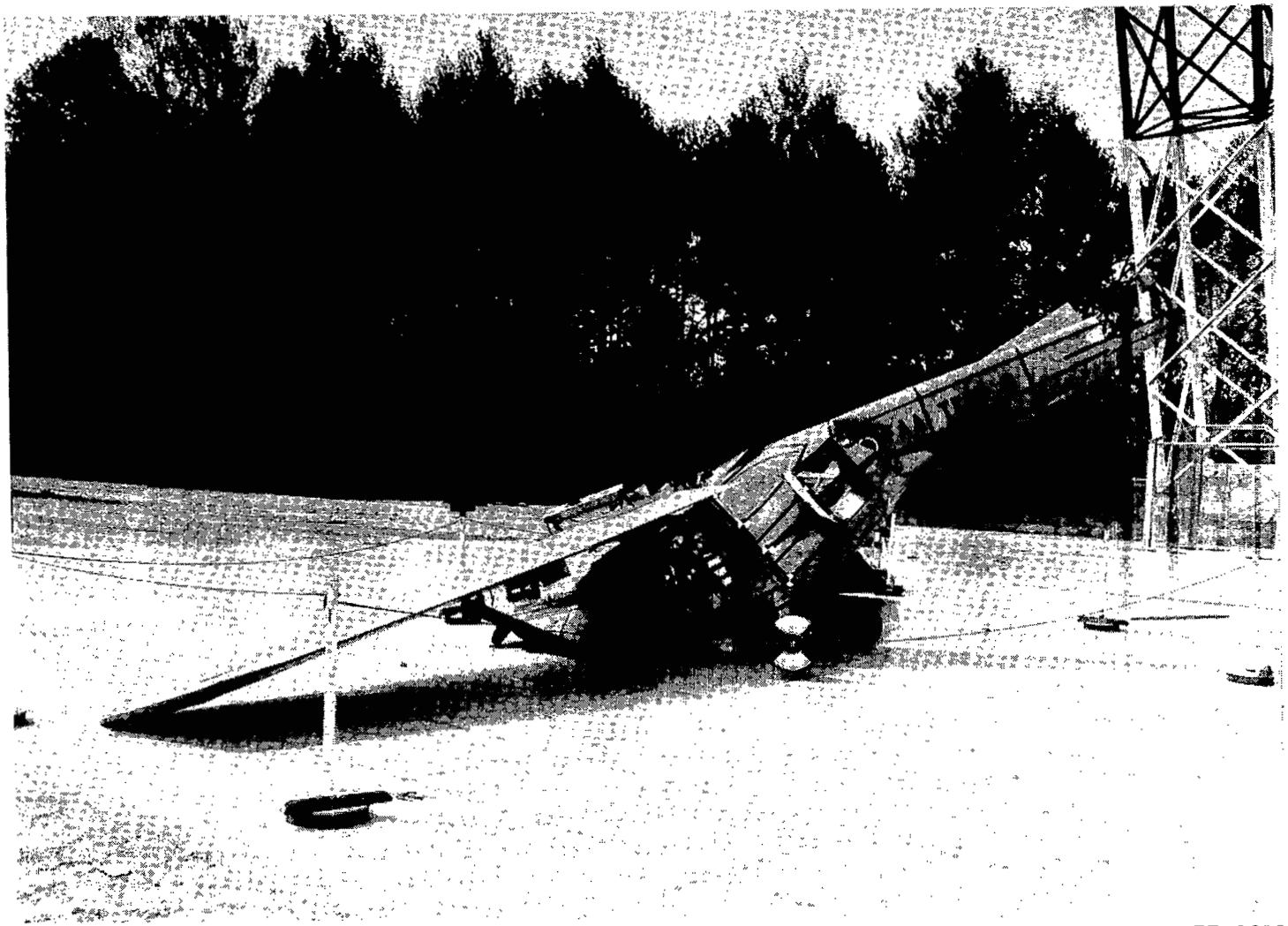

L-77-3211

(c) View of port side of airplane.

Figure 18.- Continued.

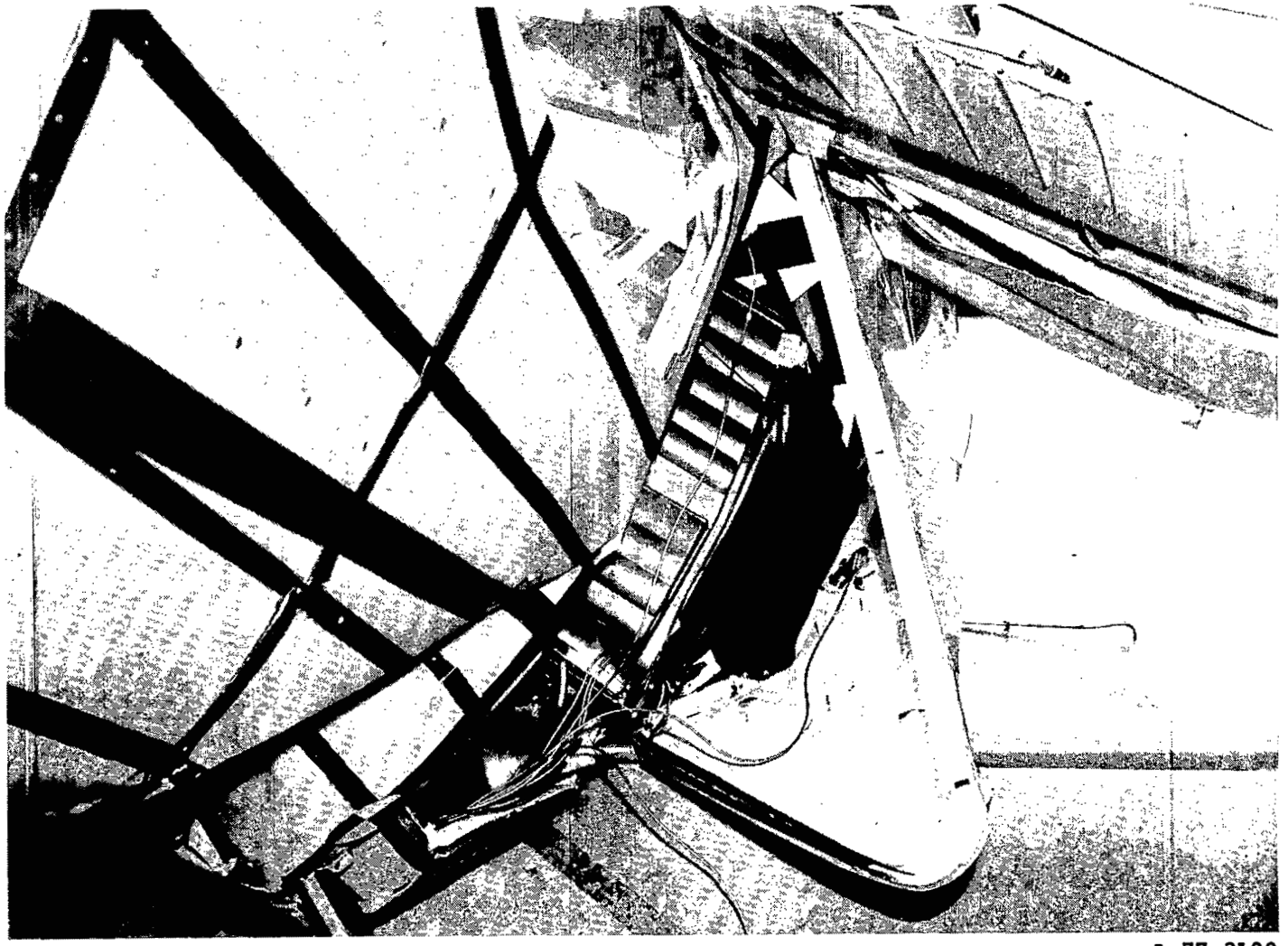

L-77-3199

(d) Close-up view of starboard side door.

Figure 18.- Continued.

(e) View of copilot dummy and interior of airplane.

Figure 18.- Concluded.

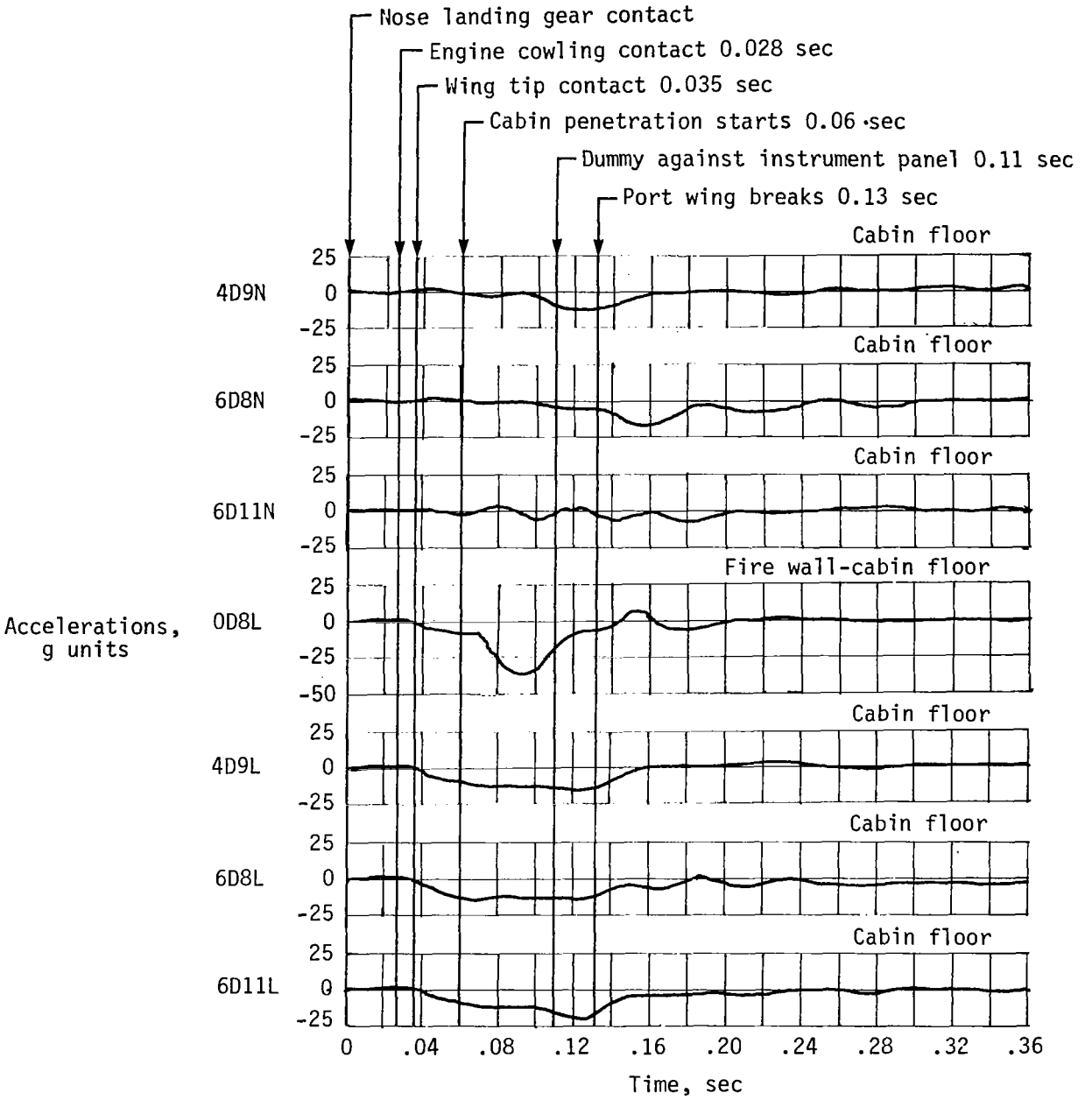

(a) Accelerations on cabin floor and fire wall at floor.

Figure 19.- Acceleration and load histories onboard roll-impact test specimen.

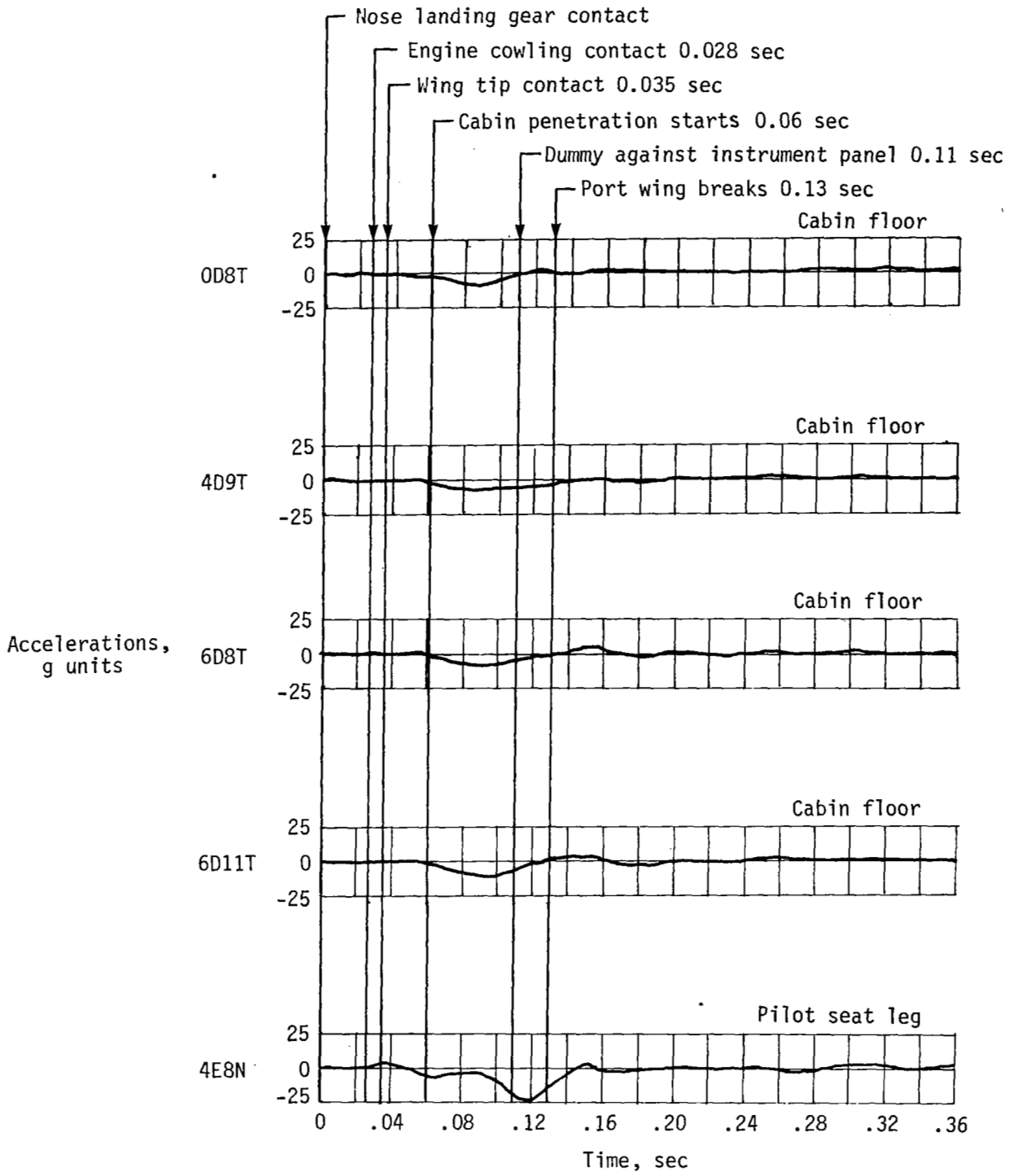

(b) Transverse accelerations on cabin floor and normal accelerations of pilot's seat leg.

Figure 19.- Continued.

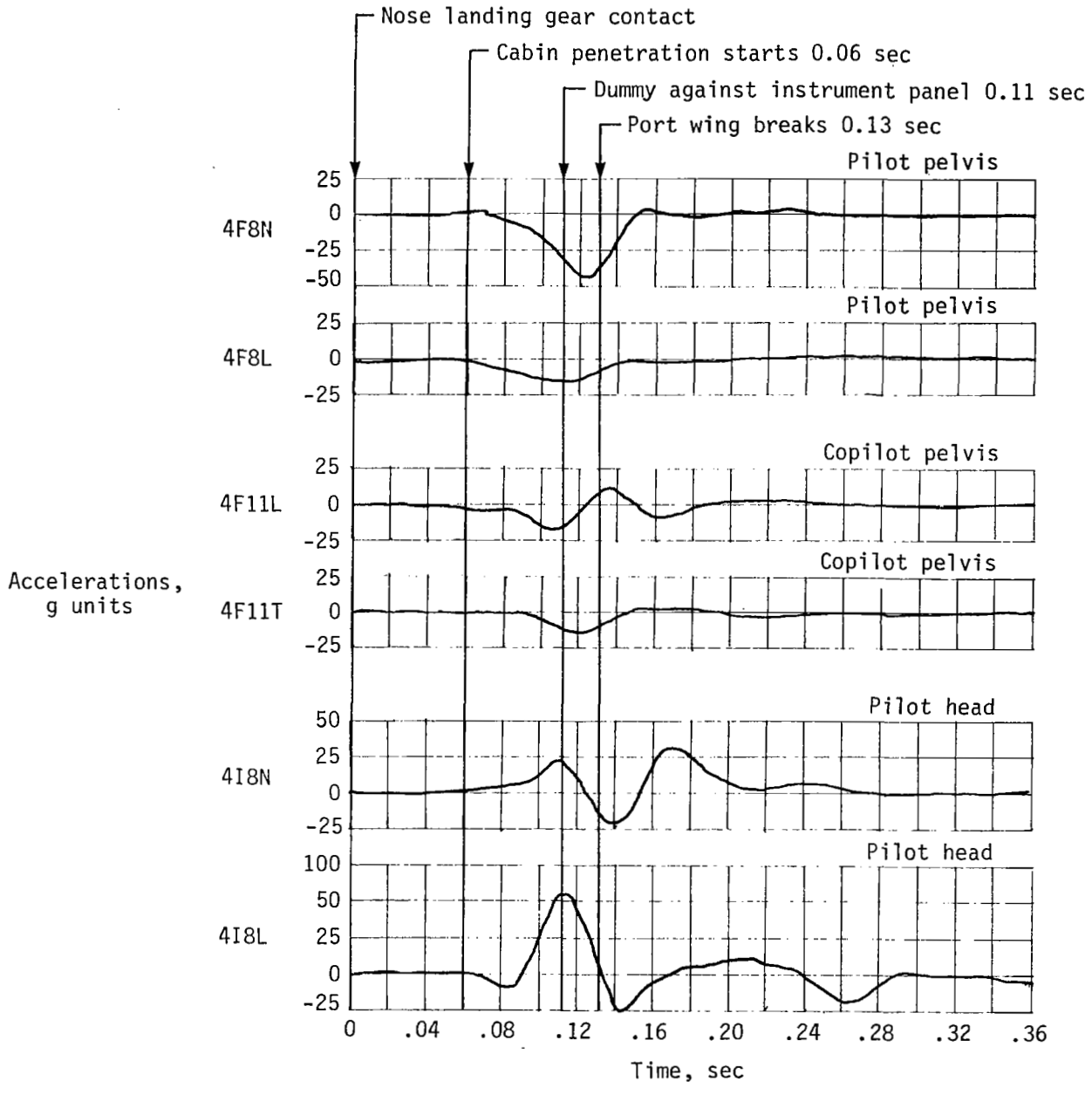

(c) Accelerations in pilot and copilot dummies.

Figure 19.- Continued.

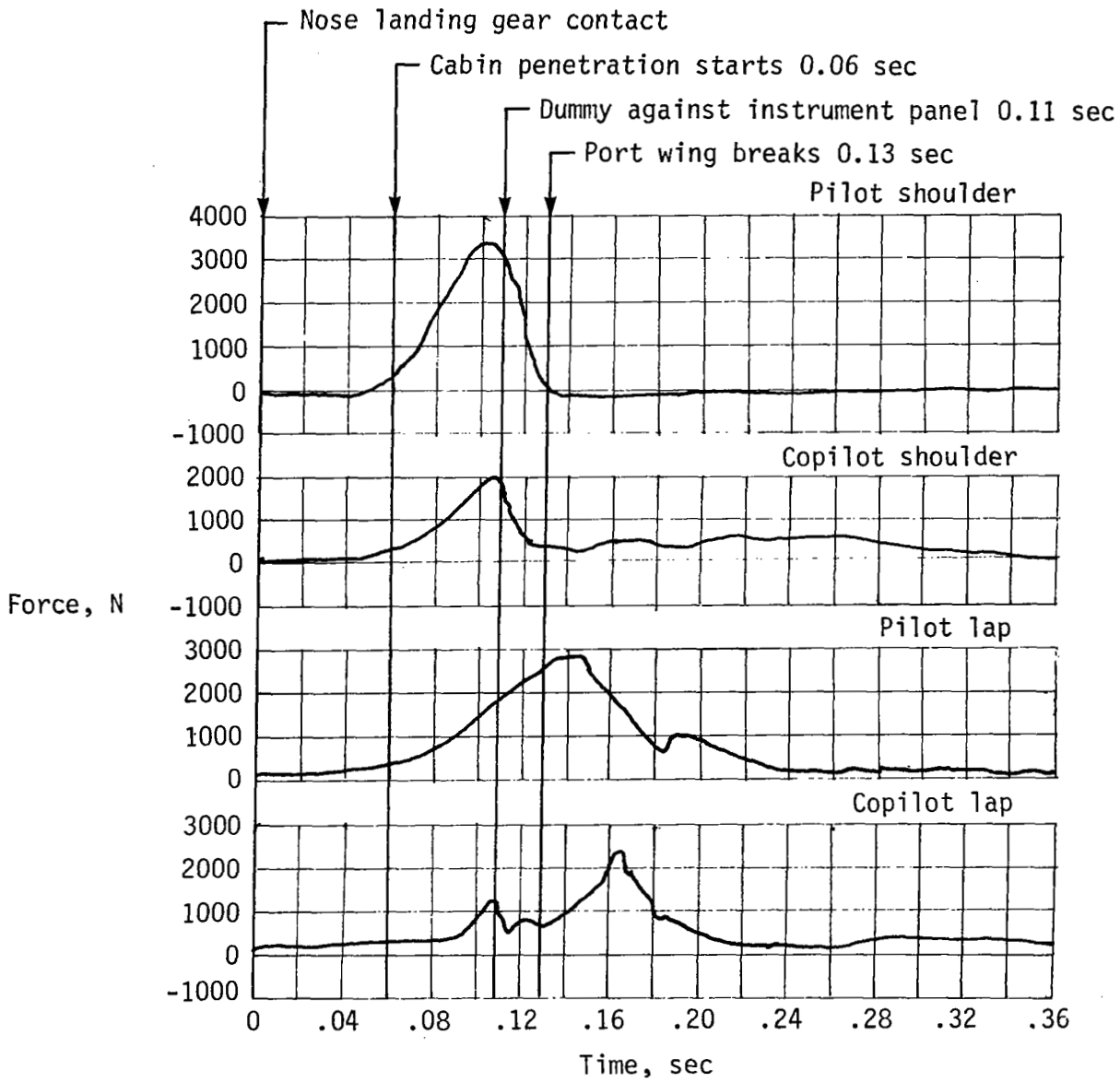

(d) Loads in restraint harness system.

Figure 19.- Concluded.

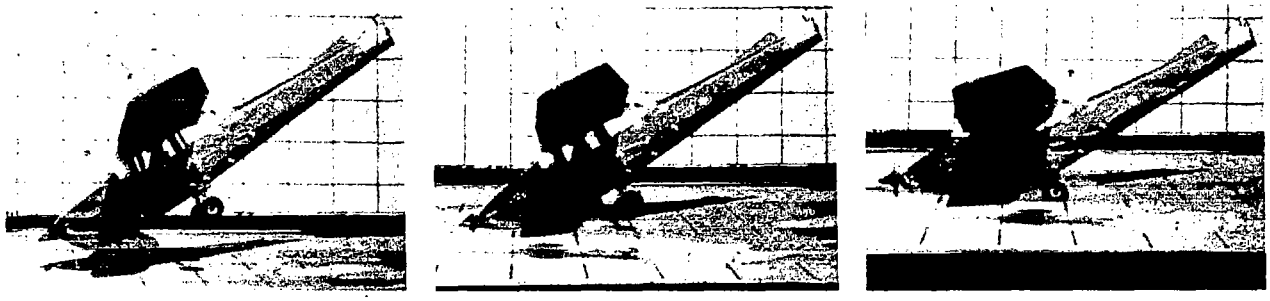

Time = 0.00 sec | Time = 0.05 sec | Time = 0.10 sec

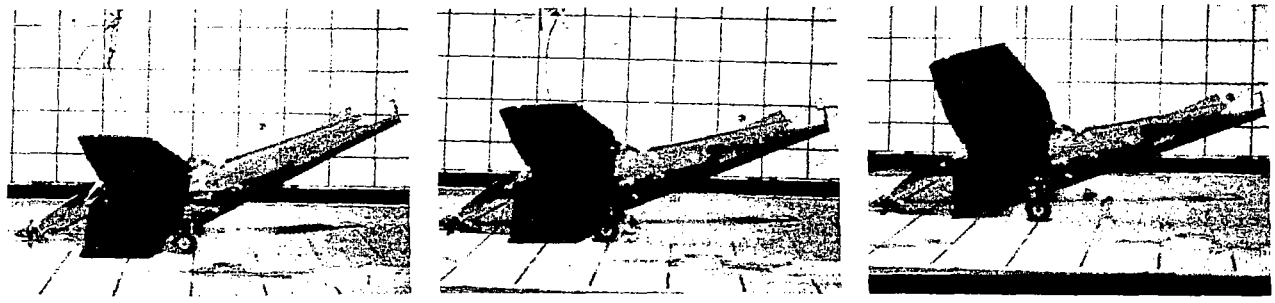

Time = 0.15 sec | Time = 0.20 sec | Time = 0.25 sec

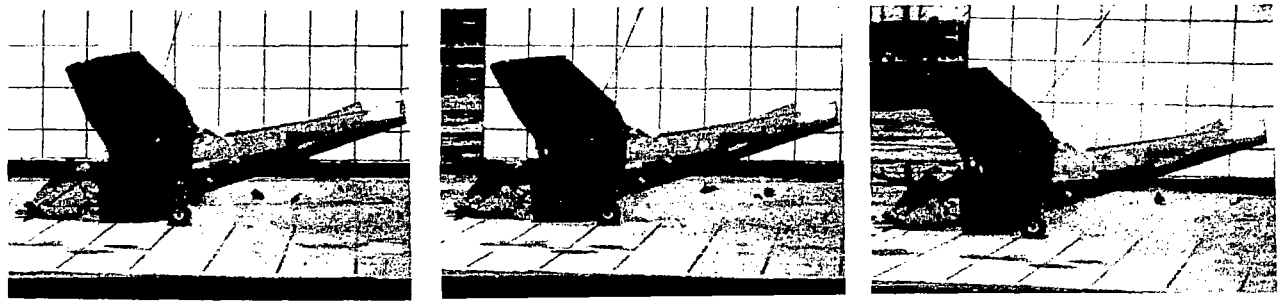

Time = 0.30 sec | Time = 0.35 sec | Time = 0.40 sec

L-77-1023

Figure 20.- Crash sequence photographs of nose-down test.

L-77-778

(a) View of front and port side of airplane.

Figure 21.- Postcrash damage of nose-down test.

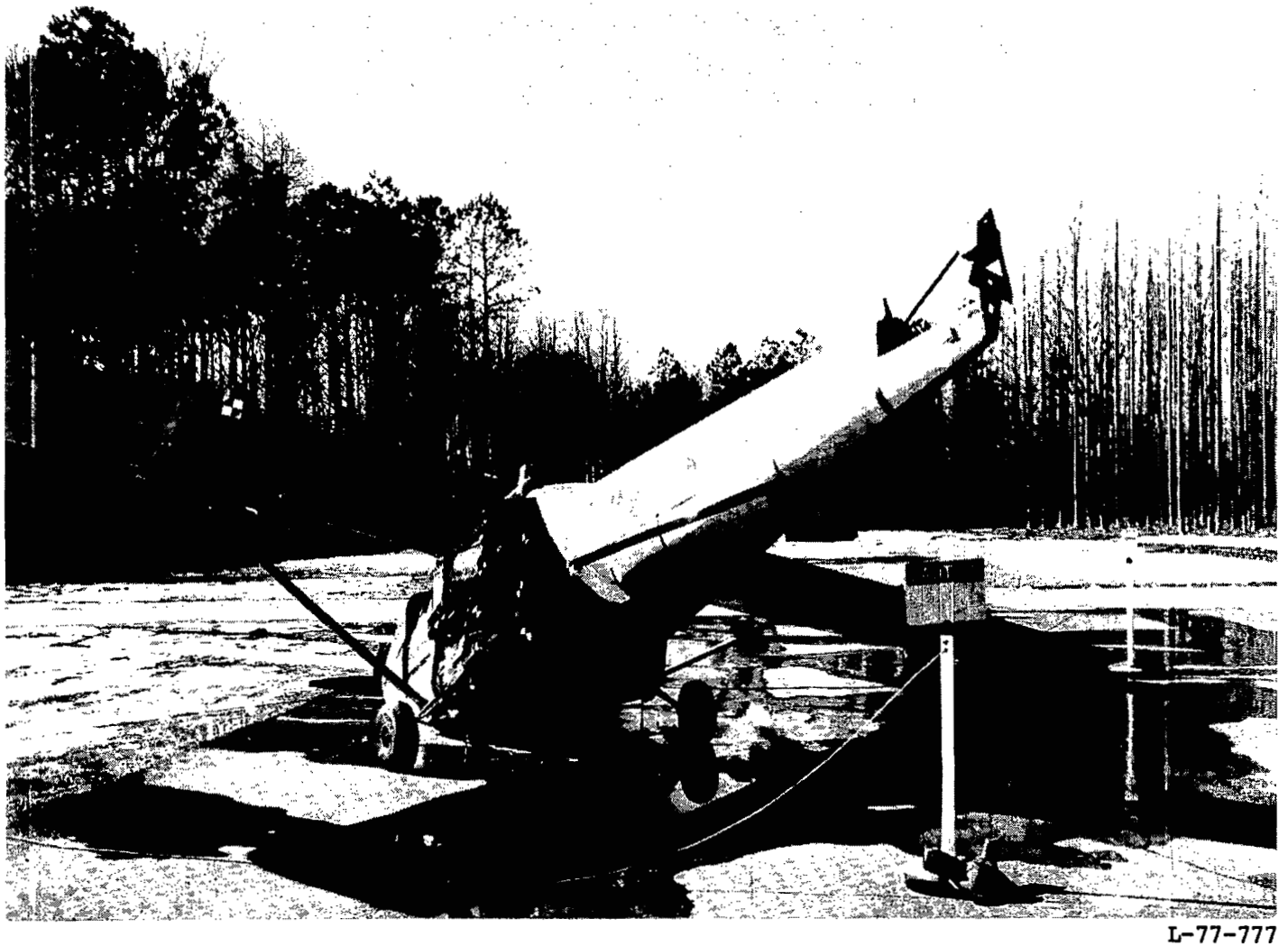

L-77-777

(b) View of aft section of airplane.

Figure 21.- Continued.

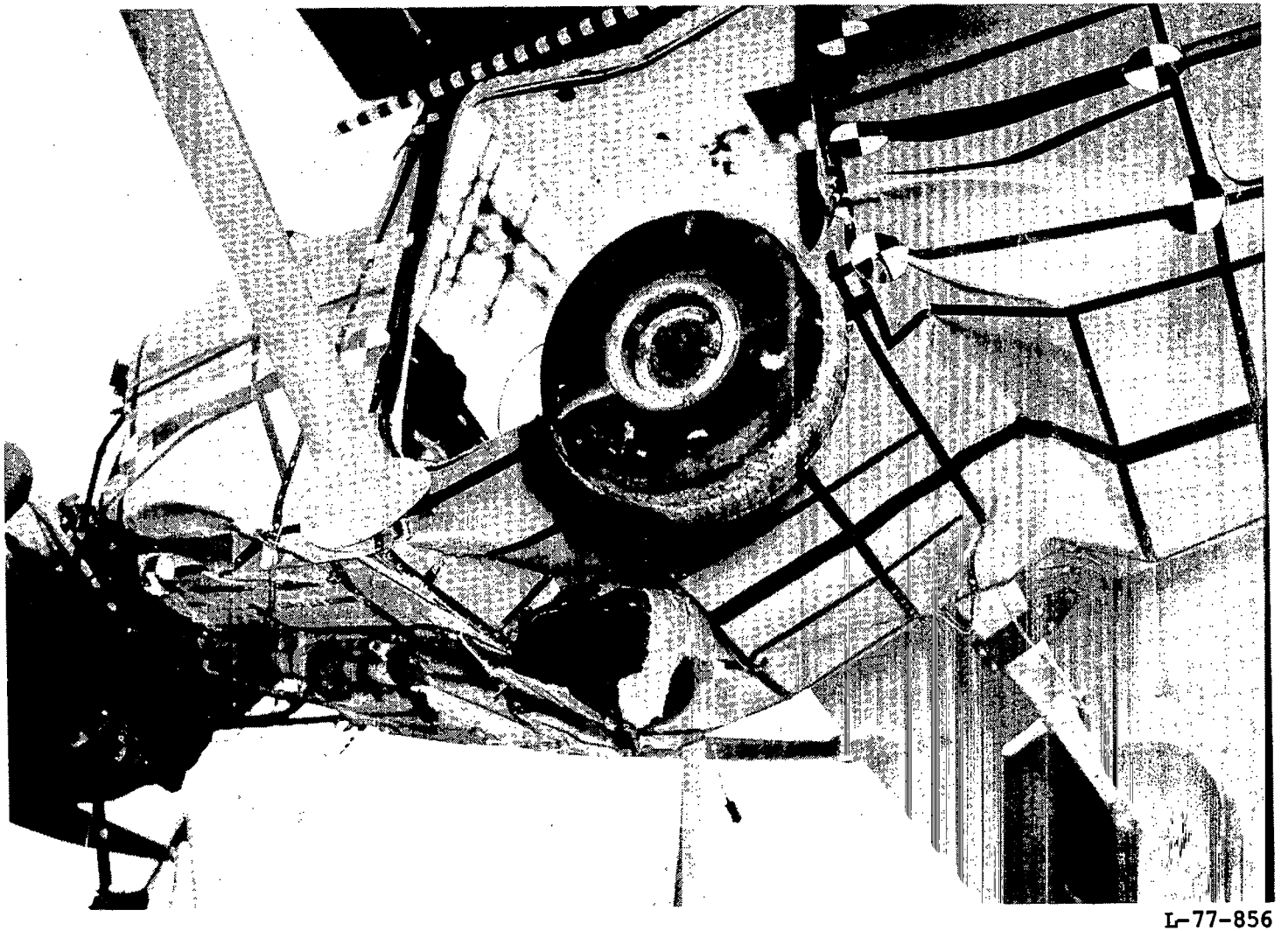

L-77-856

(c) View of bottom of airplane fuselage.

Figure 21.- Continued.

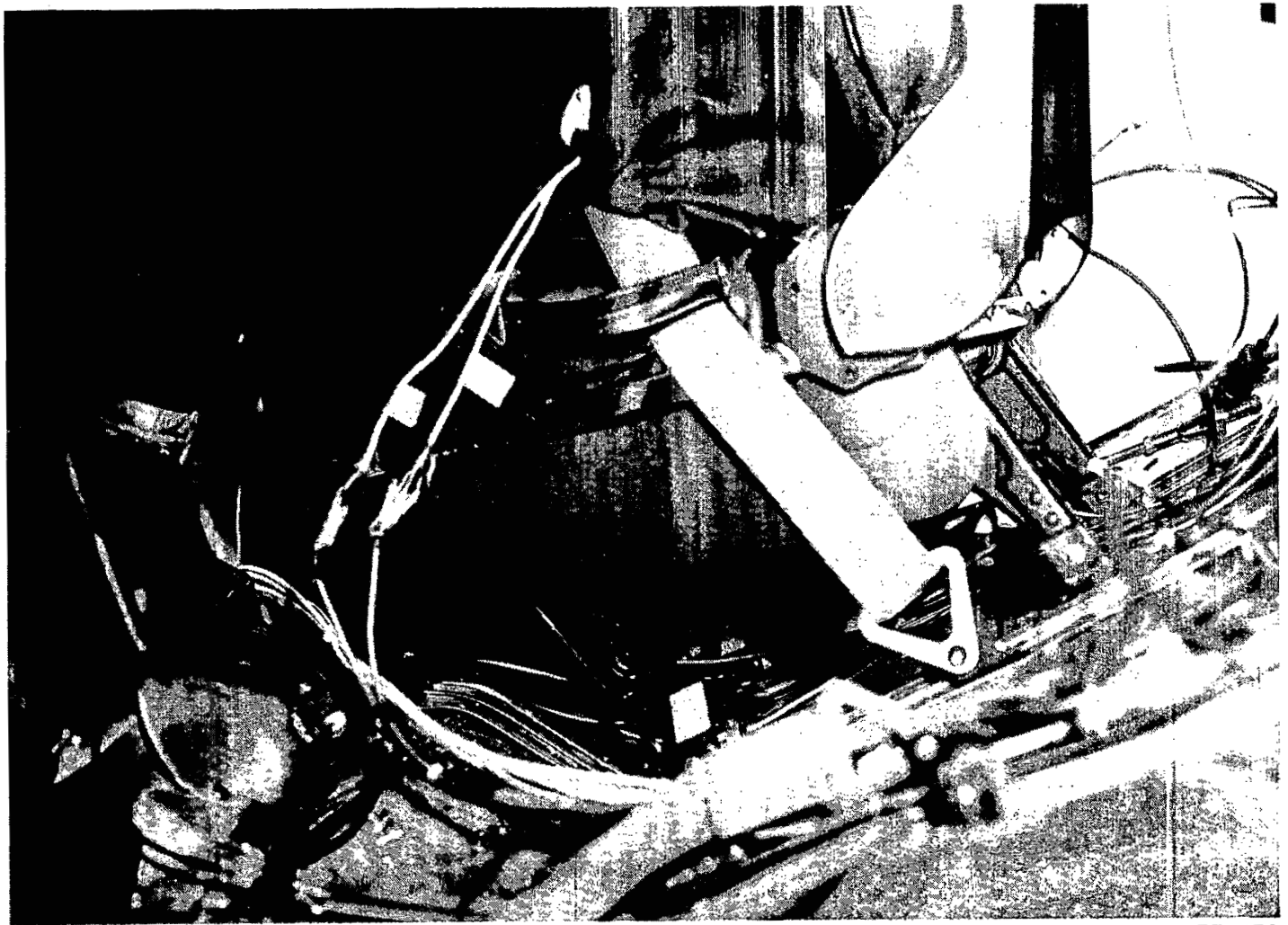

L-77-873

(d) View of copilot's seat and interior of airplane.

Figure 21.- Concluded.

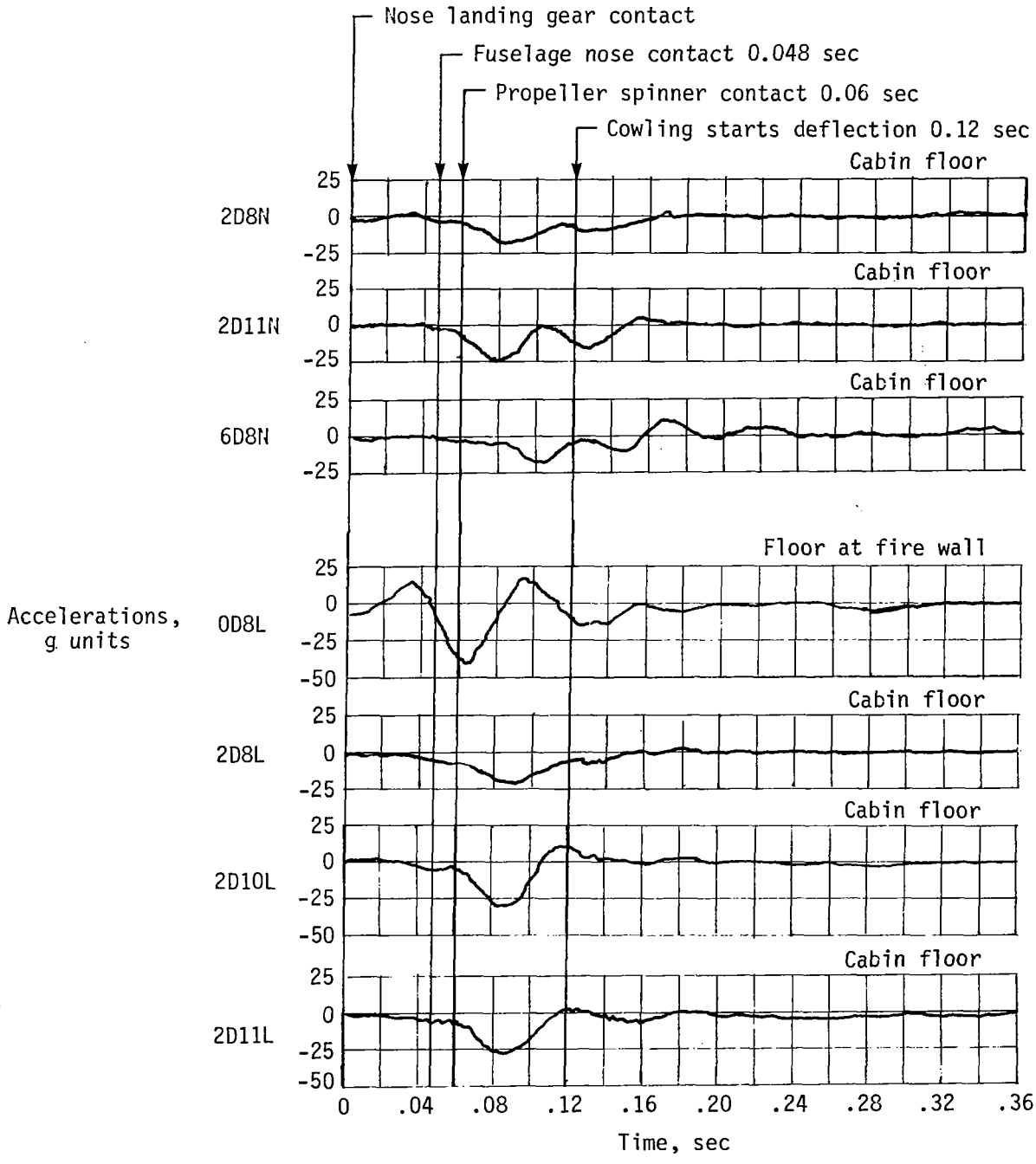

(a) Acceleration on cabin floor and fire wall at floor.

Figure 22.- Acceleration and load histories onboard nose-down test specimen.

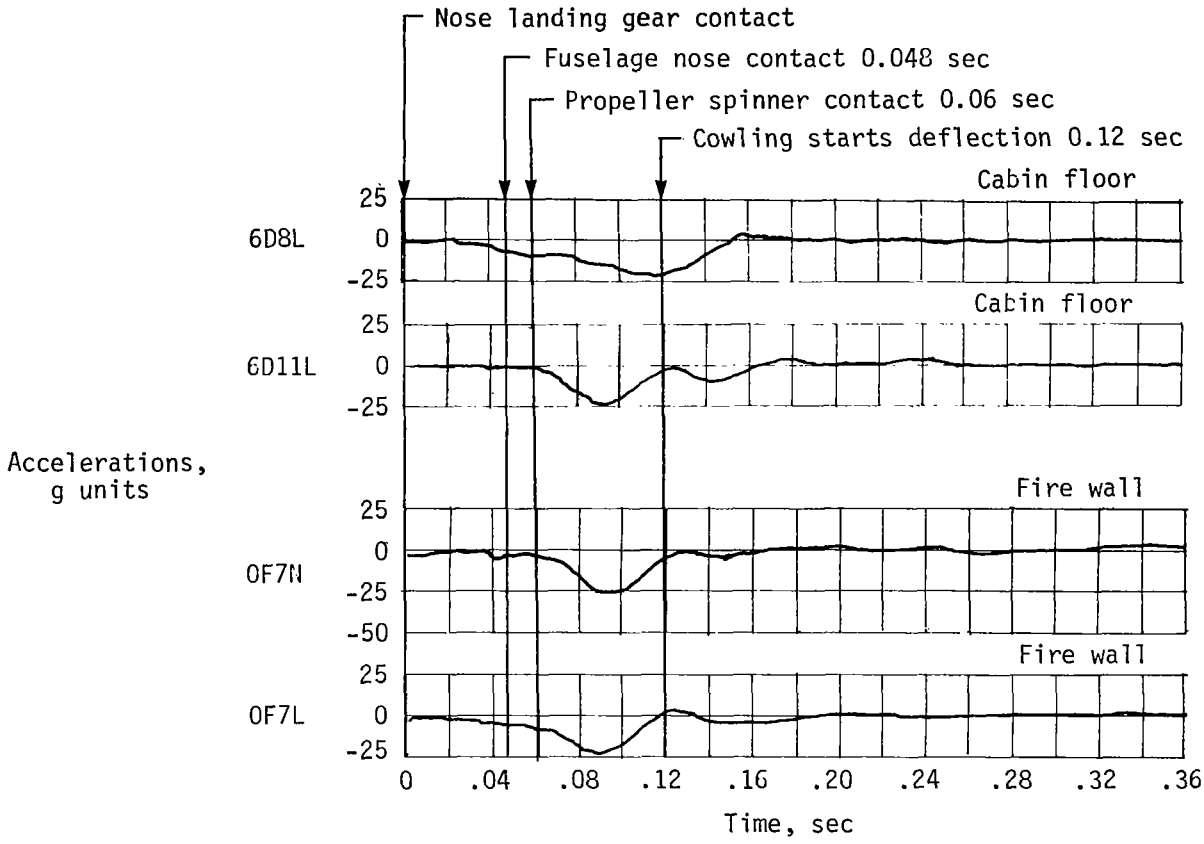

(b) Accelerations on cabin floor and on fire wall.

Figure 22.- Continued.

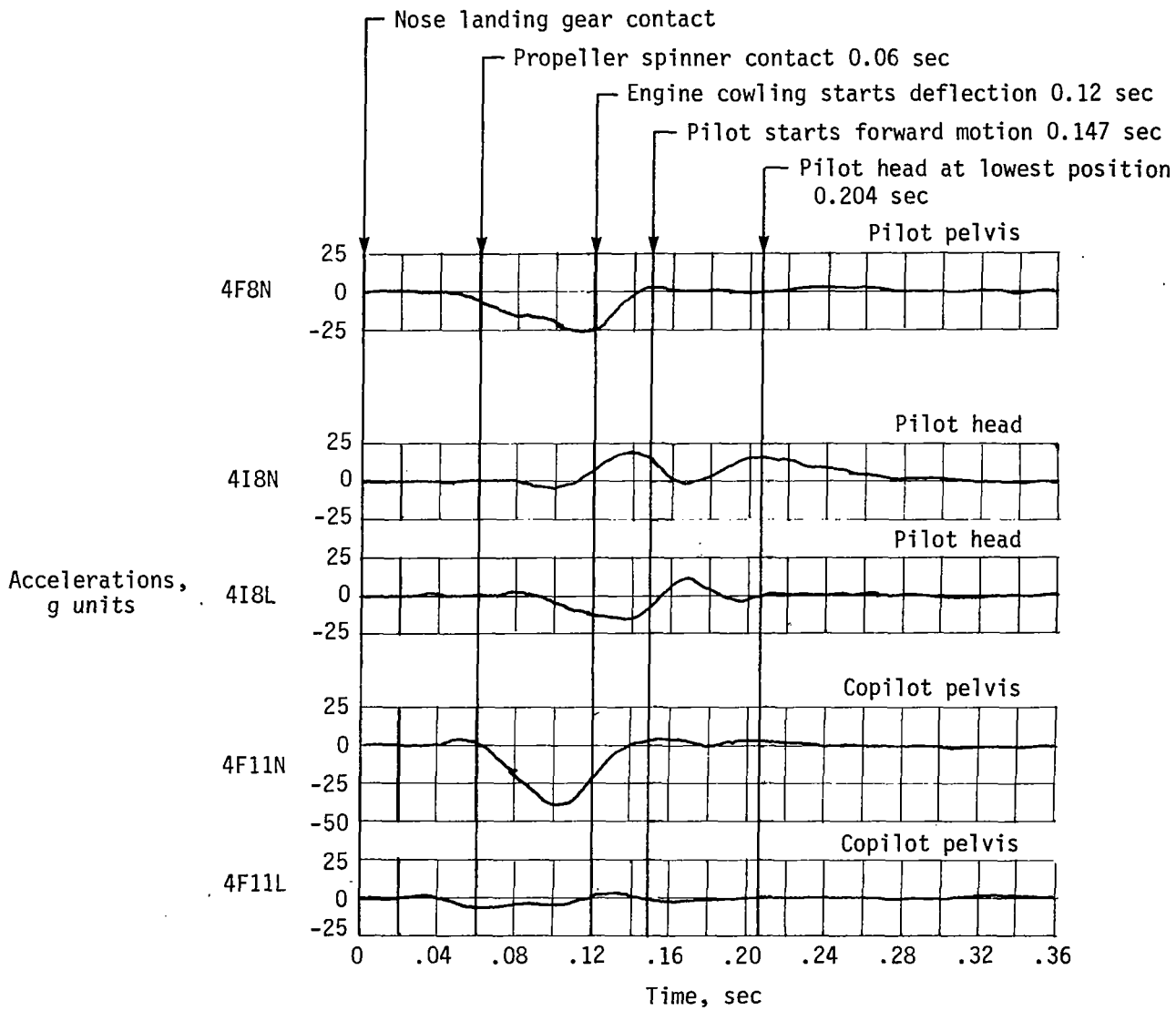

(c) Accelerations in the pilot and copilot dummies.

Figure 22.- Continued.

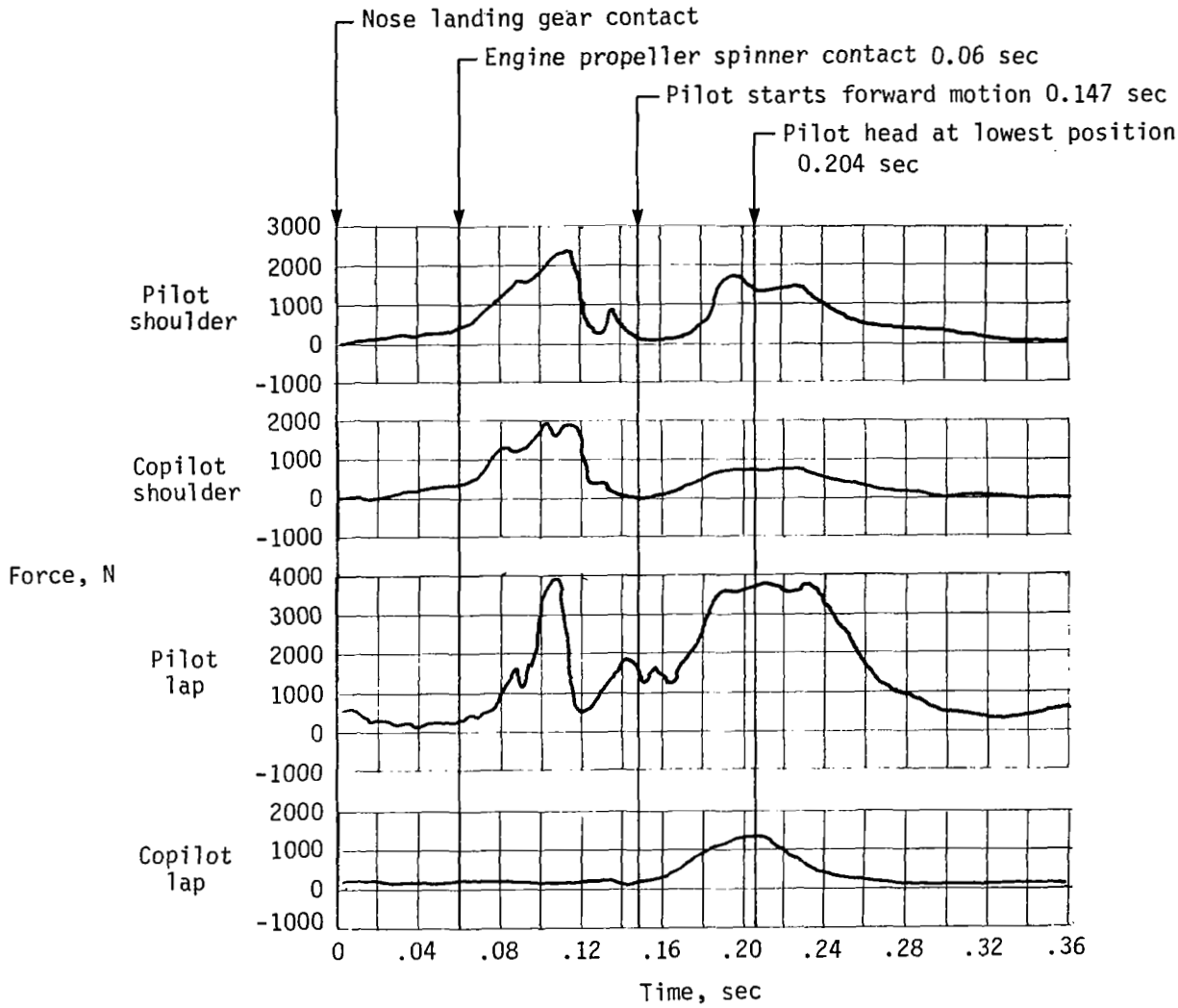

(d) Loads in restraint harness system.

Figure 22.- Concluded.

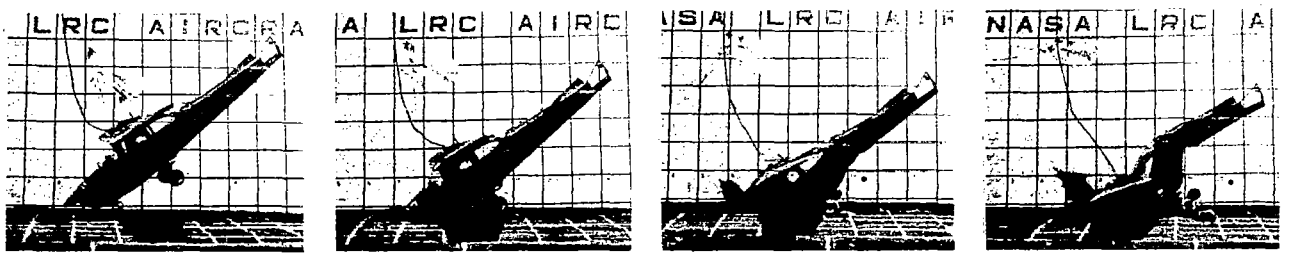

Time = 0.00 sec | Time = 0.05 sec | Time = 0.10 sec | Time = 0.15 sec

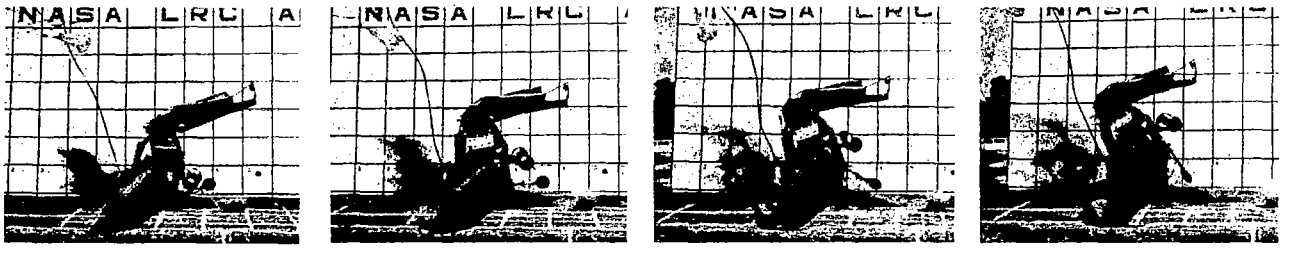

Time = 0.20 sec | Time = 0.25 sec | Time = 0.30 sec | Time = 0.35 sec

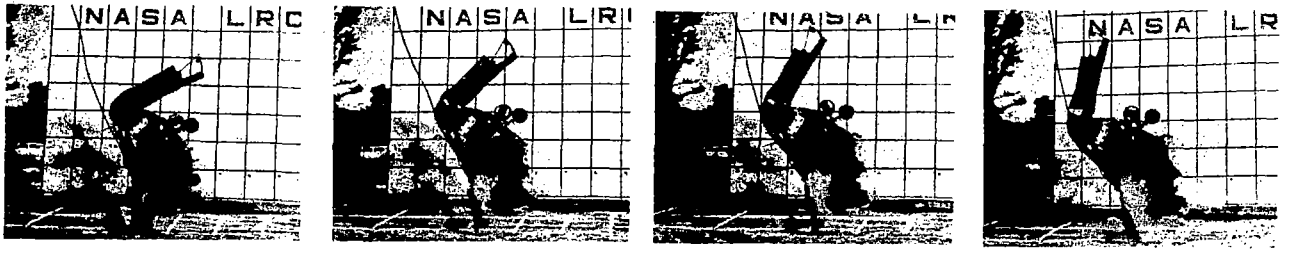

Time = 0.40 sec | Time = 0.45 sec | Time = 0.50 sec | Time = 0.55 sec

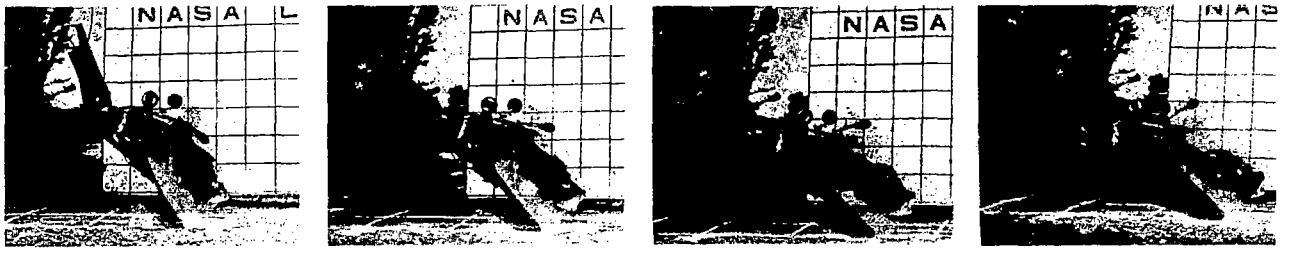

Time = 0.65 sec | Time = 0.75 sec | Time = 0.85 sec | Time = 0.95 sec

L-77-4648

Figure 23.- Crash sequence photographs of nose-down-on-soil test.

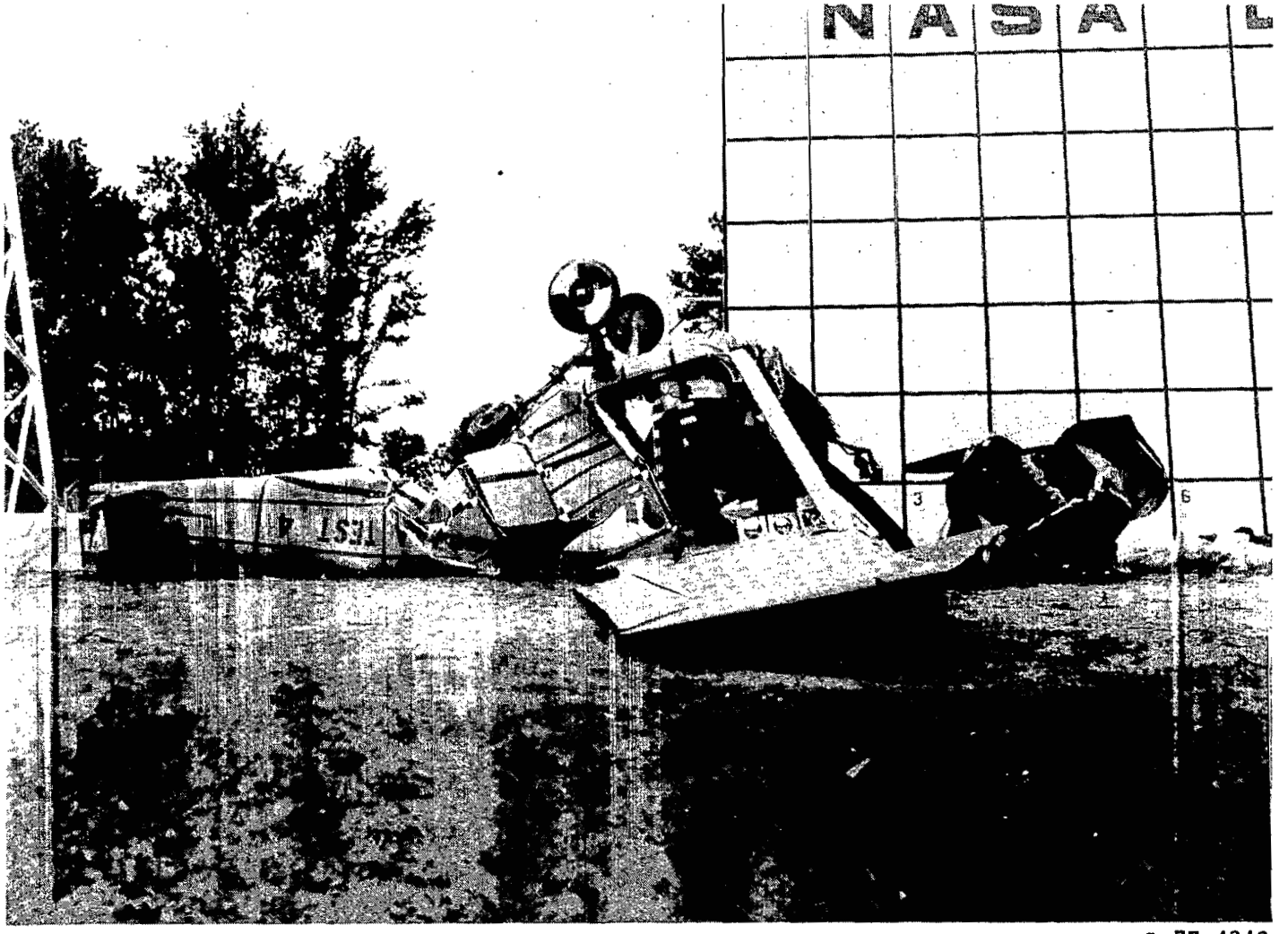

L-77-4342

(a) View of port side of airplane.

Figure 24.- Postcrash damage of nose-down-on-soil test.

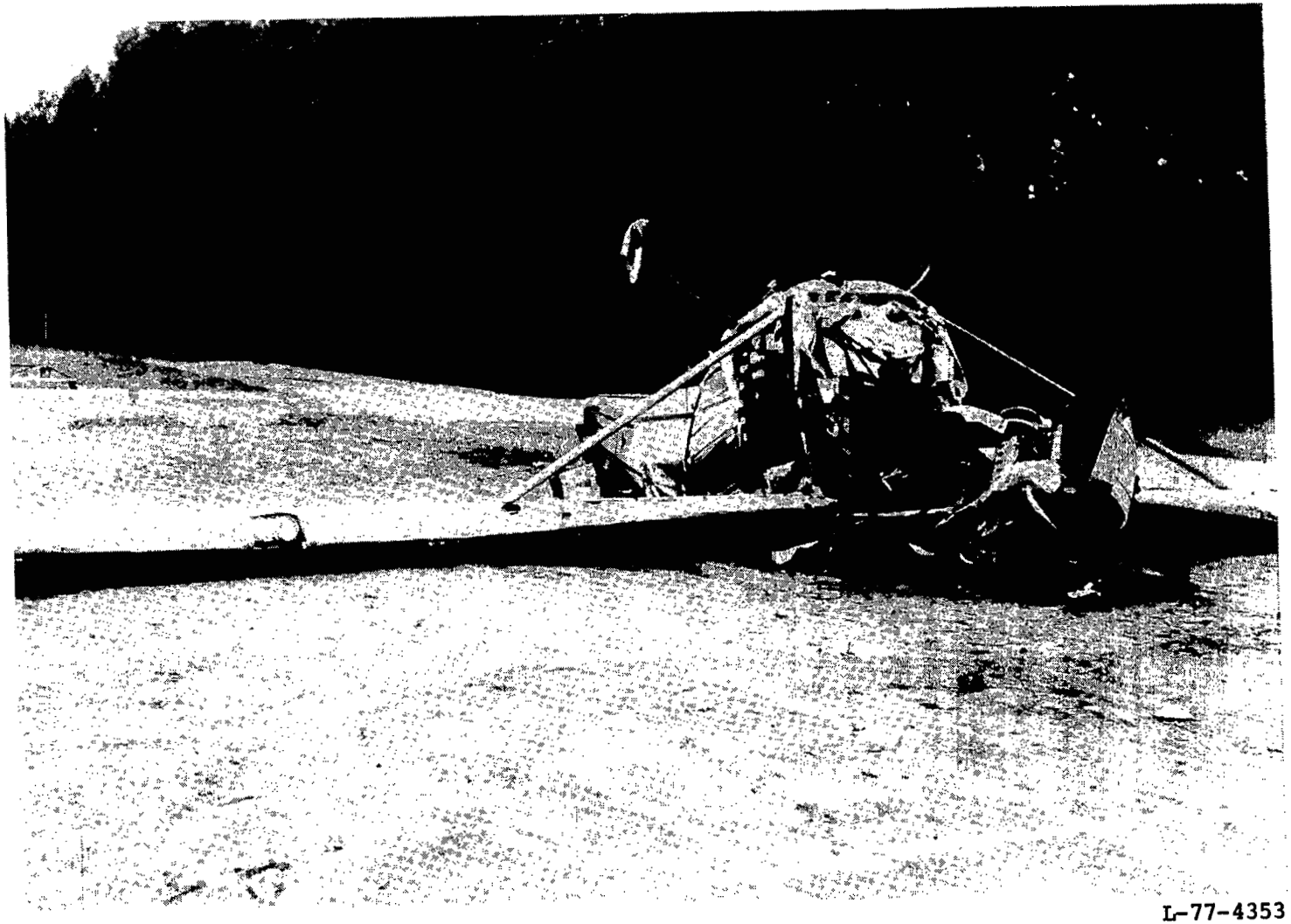

L-77-4353

(b) View of front of airplane.

Figure 24.- Continued.

L-77-4352.1

(c) Close-up view of front of fuselage and fire wall.

Figure 24.- Continued.

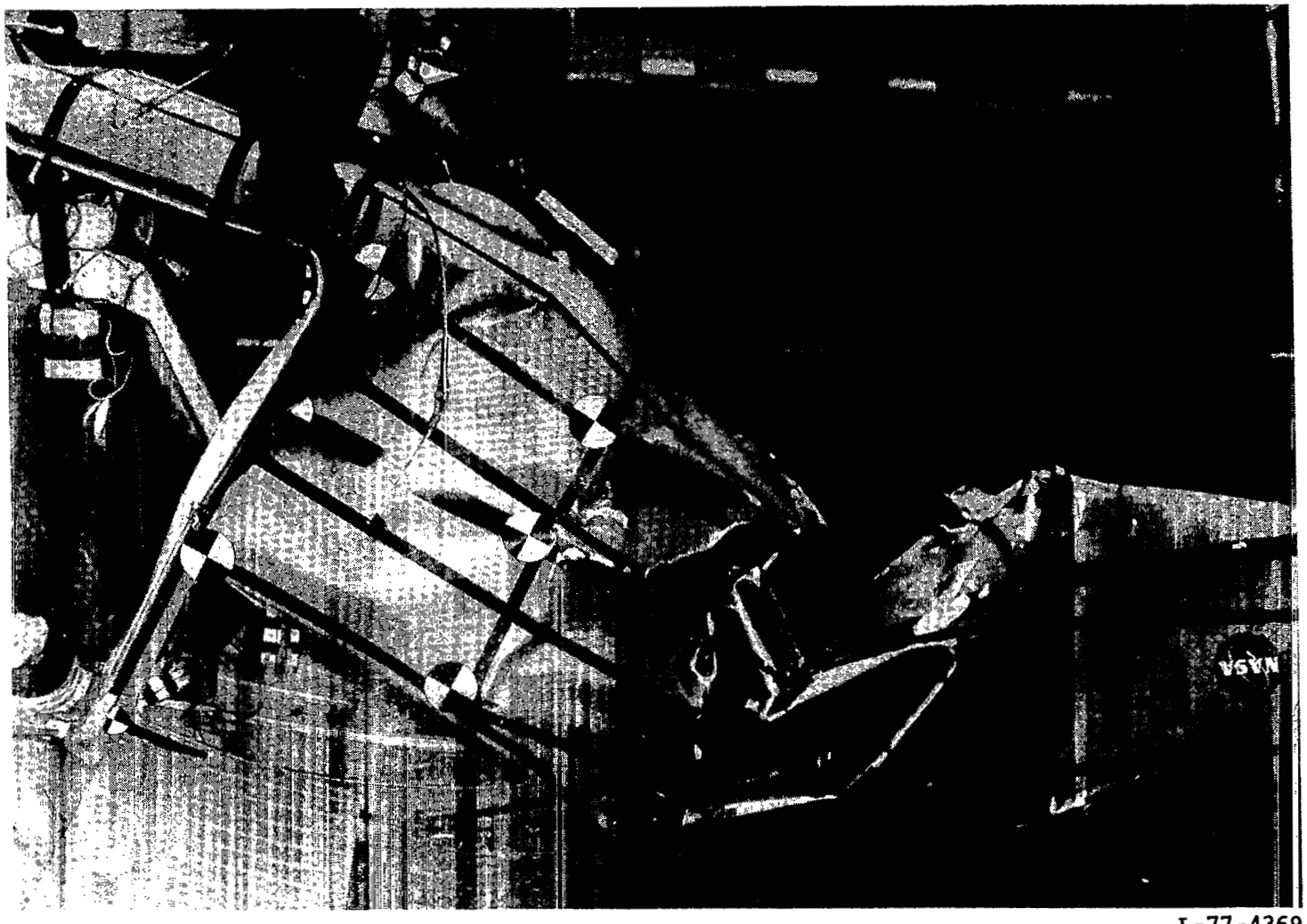

L-77-4369

(d) Close-up view of aft section of airplane.

Figure 24.- Continued.

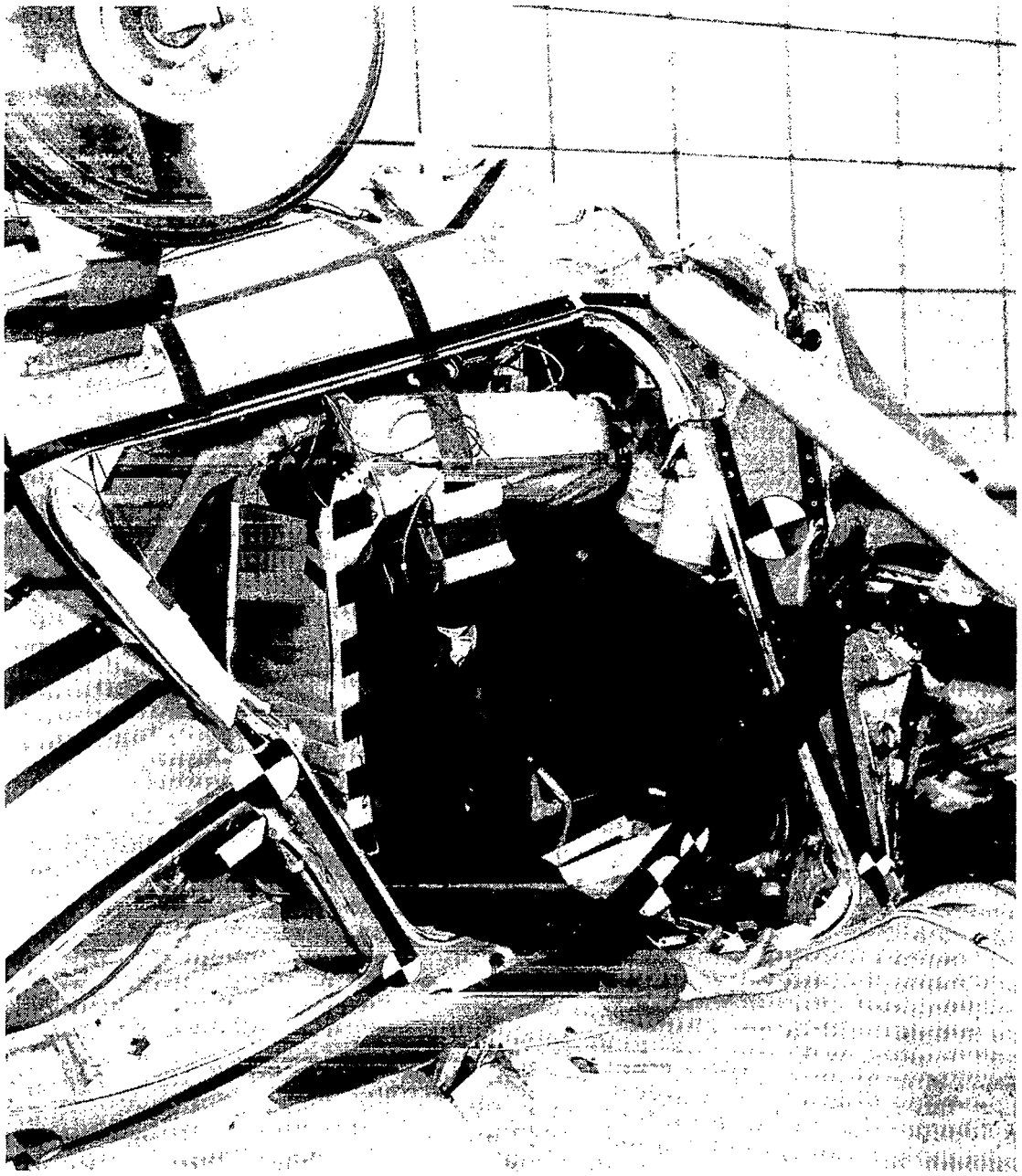

L-77-4354

(e) Close-up view of pilot's position in crashed airplane.

Figure 24.- Continued.

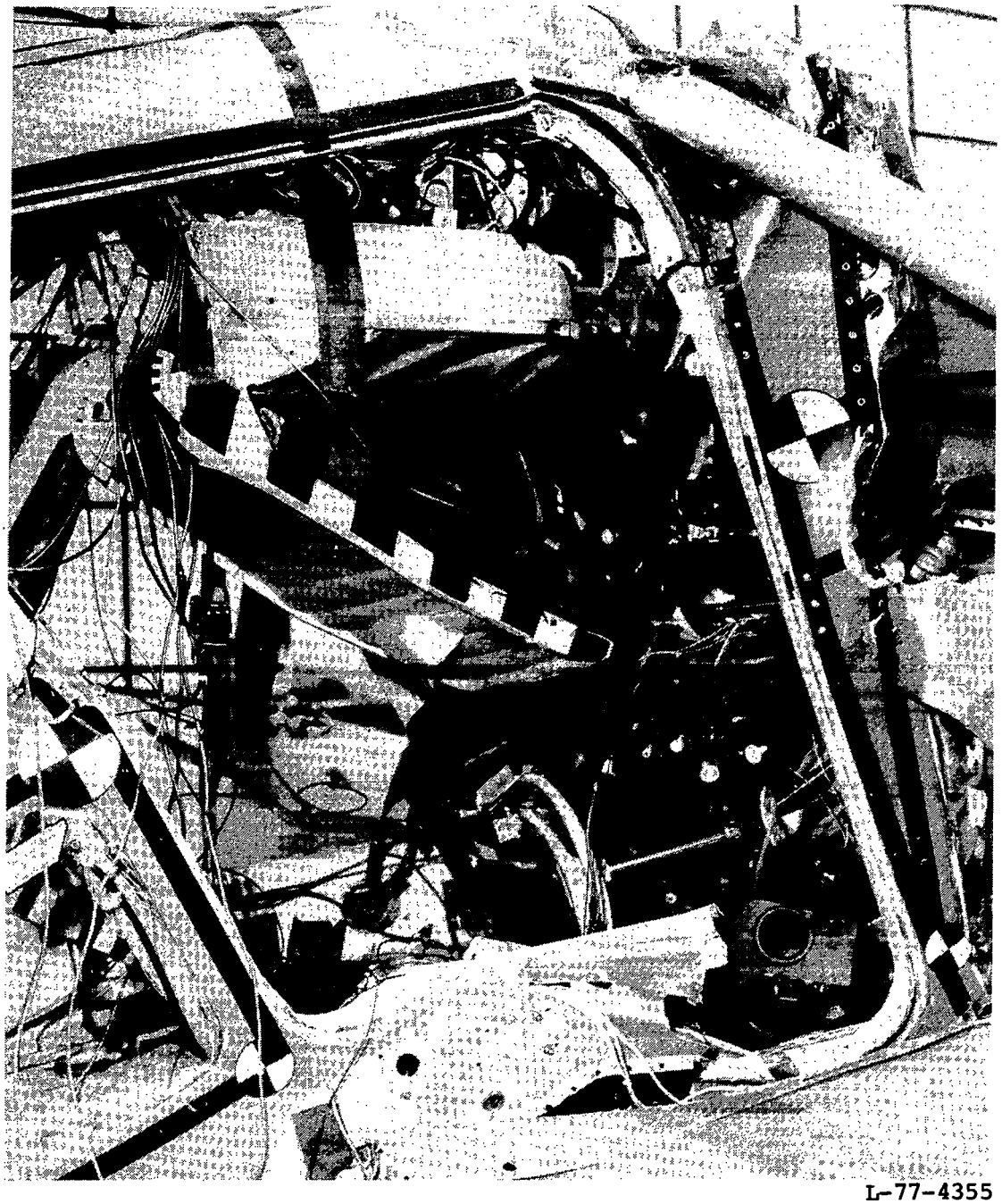

L-77-4355

(f) Close-up view of pilot's station with dummy removed.

Figure 24.- Continued.

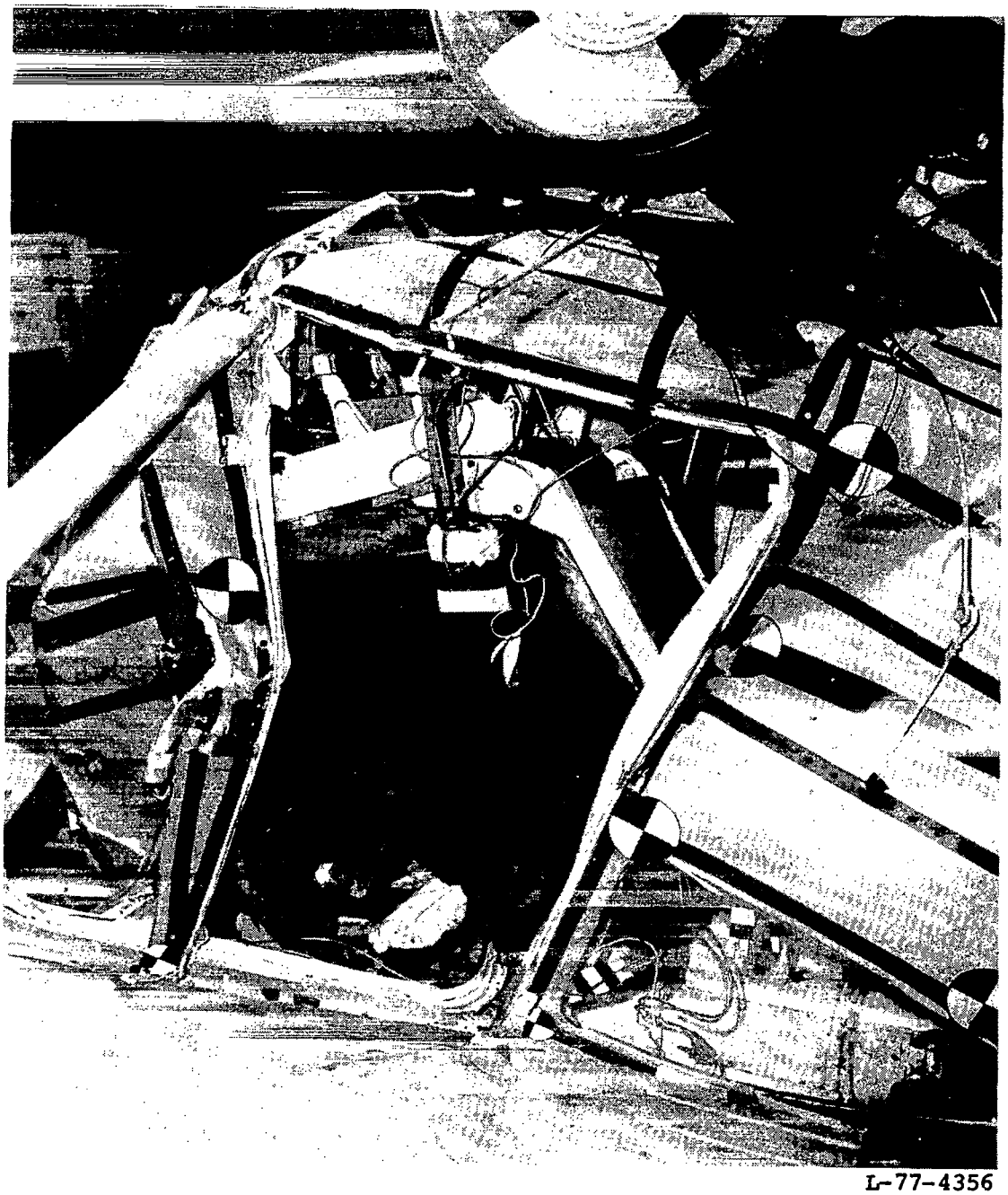

L-77-4356

(g) Close-up view of copilot's position in crashed airplane.

Figure 24.- Concluded.

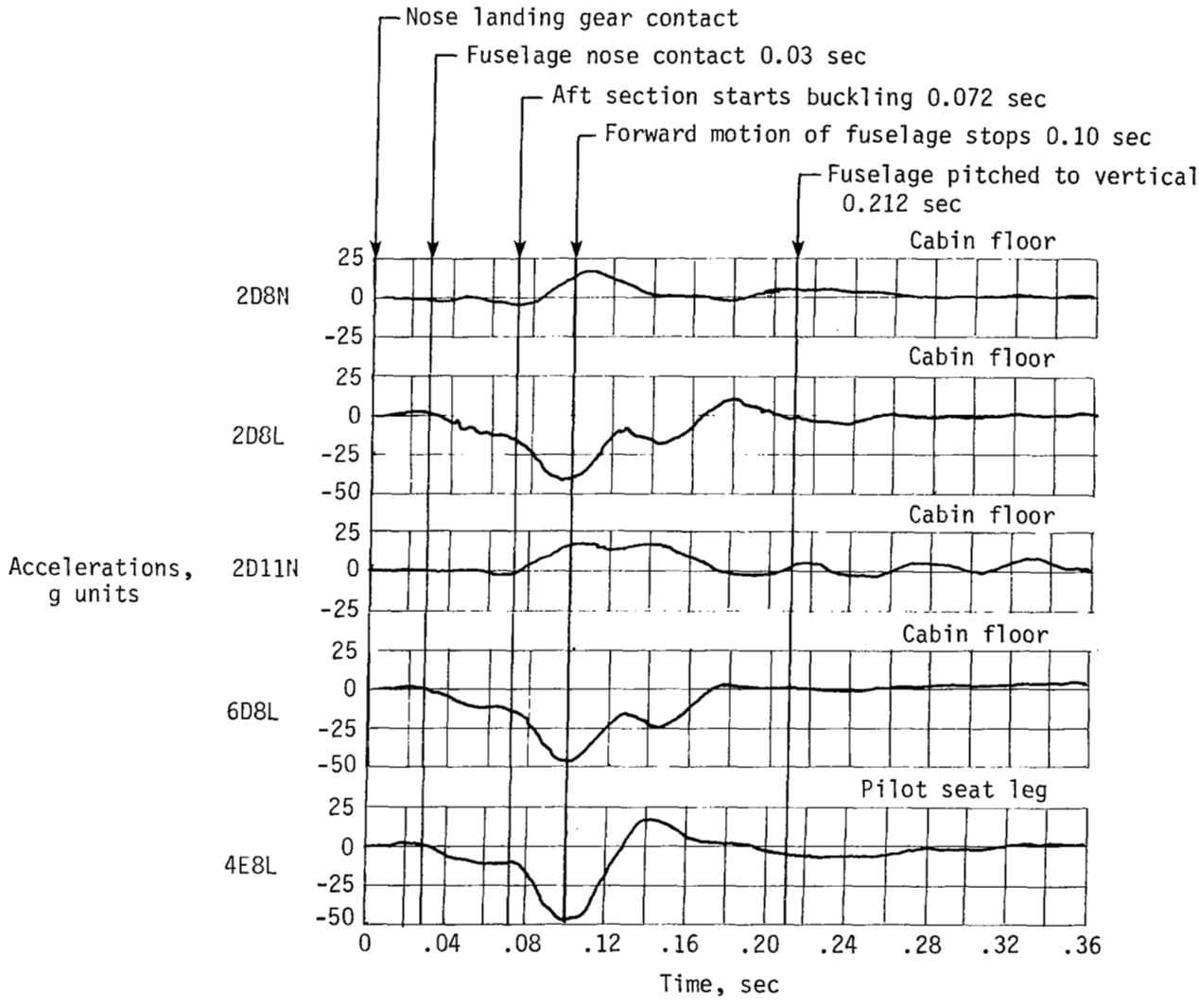

(a) Accelerations on cabin floor and pilot's seat leg.

Figure 25.- Acceleration and load histories onboard nose-down-on-soil test specimen.

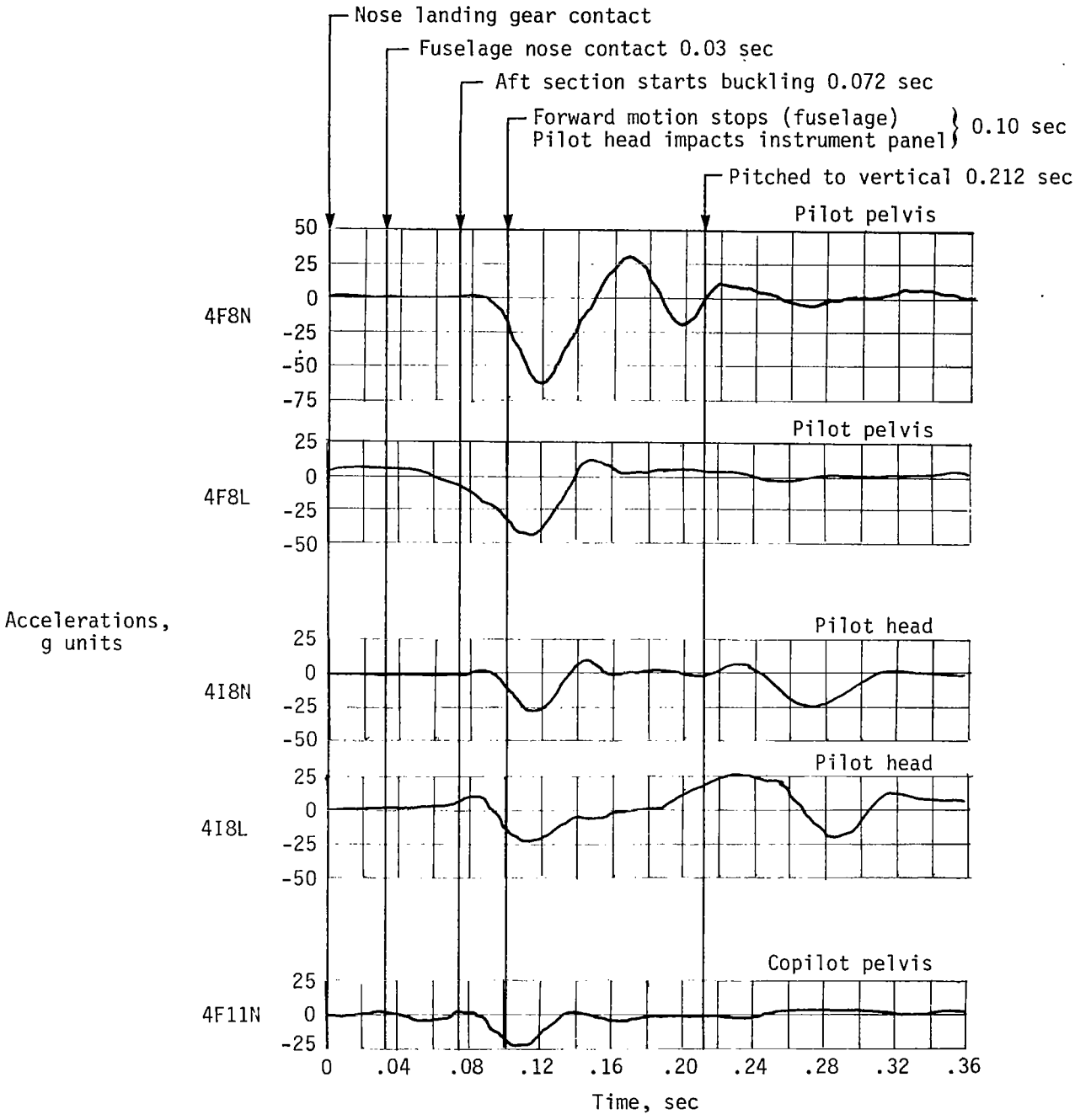

(b) Accelerations in pilot and copilot dummies.

Figure 25.- Continued.

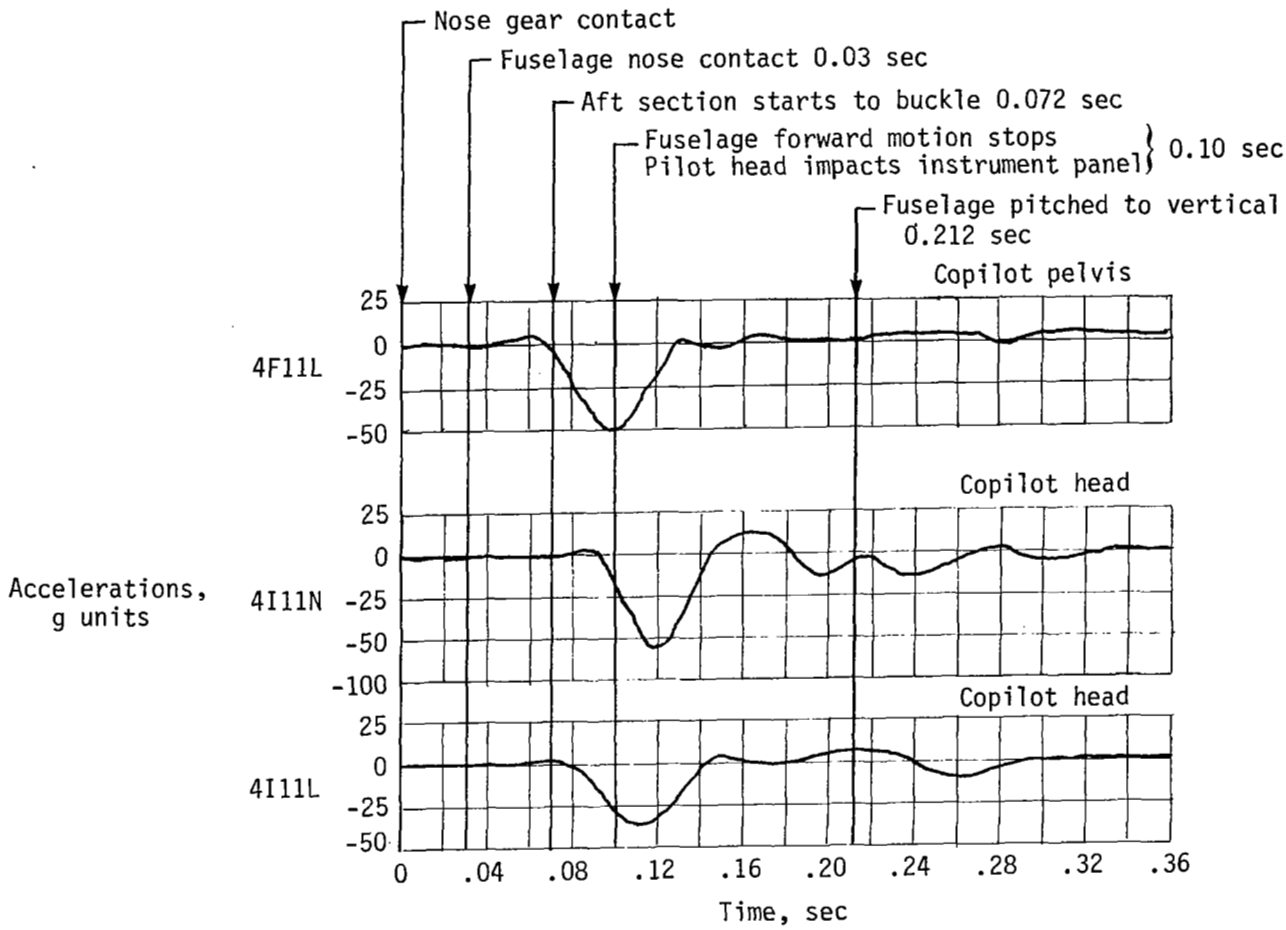

(b) Concluded.

Figure 25.- Continued.

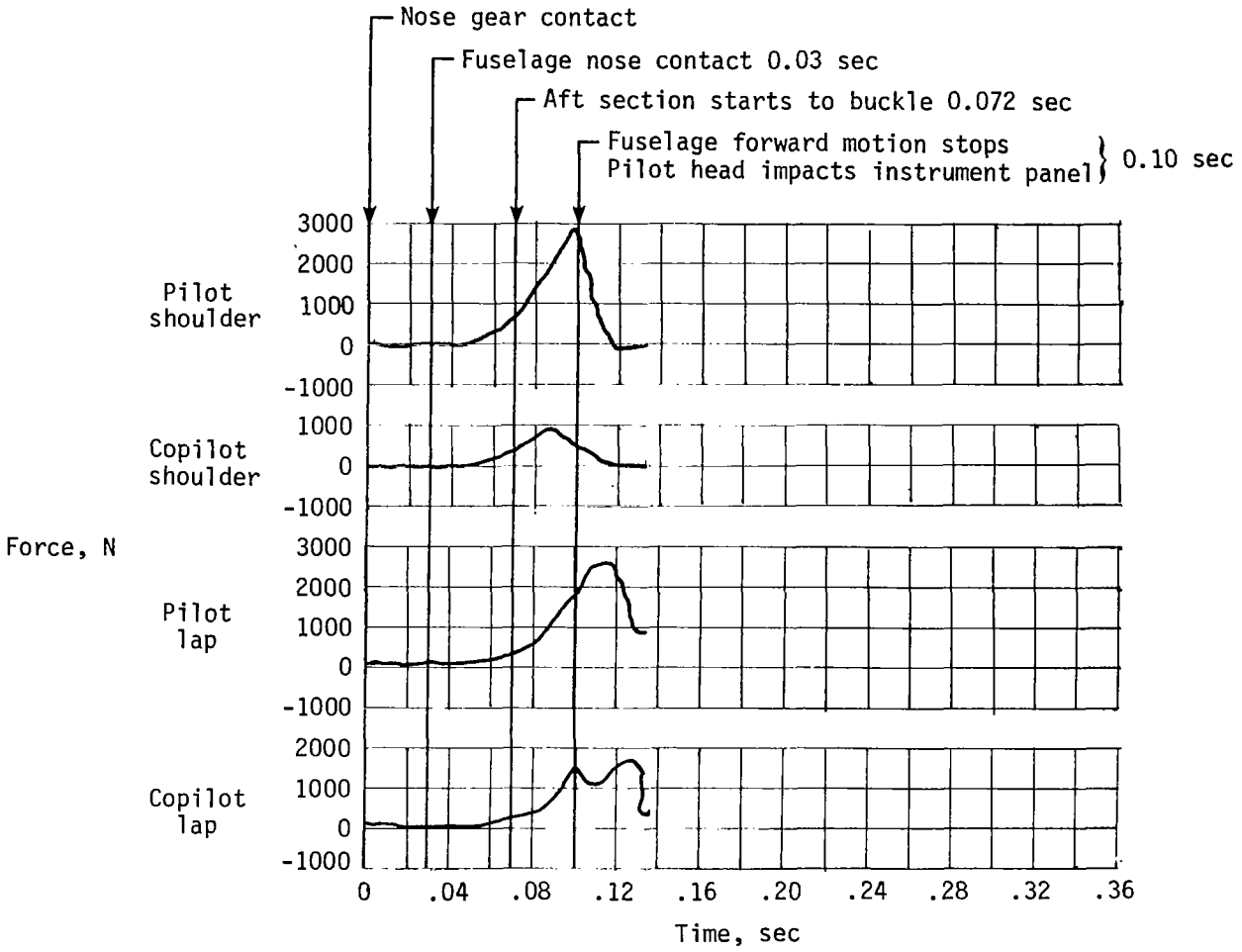

(c) Loads in restraint harness system.

Figure 25.- Concluded.

1. Report No.	2. Government Accession No.	3. Recipient's Catalog No.
NASA TP-1699		

4. Title and Subtitle	5. Report Date
CRASH TESTS OF FOUR IDENTICAL HIGH-WING SINGLE-ENGINE AIRPLANES	August 1980
	6. Performing Organization Code
7. Author(s)	8. Performing Organization Report No.
Victor L. Vaughan, Jr., and Robert J. Hayduk	L-13076
	10. Work Unit No.
9. Performing Organization Name and Address	505-41-33-01
NASA Langley Research Center Hampton, VA 23665	11. Contract or Grant No.
	13. Type of Report and Period Covered
12. Sponsoring Agency Name and Address	Technical Paper
National Aeronautics and Space Administration Washington, DC 20546	14. Sponsoring Agency Code

15. Supplementary Notes

Technical Film Supplement L-1265 available on request.

16. Abstract

Four identical four-place, high-wing, single-engine airplane specimens with nominal masses of 1043 kg were crash tested at the Langley Impact Dynamics Research Facility under controlled free-flight conditions. These tests were conducted with nominal velocities of 25 m/sec along the flight path at various flight-path angles, ground-contact pitch angles, and roll angles. Three of the airplane specimens were crashed on a concrete surface; one was crashed on soil.

Crash tests revealed that on a hard landing, the main landing gear absorbed about twice the energy for which the gear was designed but sprang back, tending to tip the airplane up to its nose. On concrete surfaces, the airplane impacted and remained in the impact attitude. On soil, the airplane flipped over on its back. The crash impact on the nose of the airplane, whether on soil or concrete, caused massive structural crushing of the forward fuselage. The livable volume was maintained in both the hard-landing and the nose-down specimens but was not maintained in the roll-impact and nose-down-on-soil specimens.

17. Key Words (Suggested by Author(s))		18. Distribution Statement
Airplane crash tests	Impact tests	Unclassified - Unlimited
Crash damage	Crash dynamics	
Crash worthiness		
General aviation		Subject Category 05

19. Security Classif. (of this report)	20. Security Classif. (of this page)	21. No. of Pages	22. Price
Unclassified	Unclassified	67	A04

For sale by the National Technical Information Service, Springfield, Virginia 22161

NASA-Langley, 1980

National Aeronautics and
Space Administration

Washington, D.C.
20546

Official Business
Penalty for Private Use, $300

THIRD-CLASS BULK RATE

Postage and Fees Paid
National Aeronautics and
Space Administration
NASA-451

U.S.MAIL

7 1 1U,A, 080180 S00903DS
DEPT OF THE AIR FORCE
AF WEAPONS LABORATORY
ATTN: TECHNICAL LIBRARY (SUL)
KIRTLAND AFB NM 87117

NASA

POSTMASTER: If Undeliverable (Section 158 Postal Manual) Do Not Return